MASTERARBEIT

Eclogite-blueschist-facies rocks of southern Sifnos, Cyclades, Greece

Jonas Weil Bakk.rer.nat.

Zur Erlangung des akademischen Grades

Master of Science (MSc)

Wien, 2010

CONTENT

1   ACKNOWLEDGEMENT

2   ABSTRACT

Occurrences of high-pressure/low-temperature eclogite/blueshist facies rocks in the southwest of Sifnos (Cyclades) are marked in the geological map by Davis (1966), but no information has been published concerning their geochemistry, petrology and structural position. These occurrences at the Fikiada Bay are the focus of this study.

The tectono-metamorphic evolution on Sifnos is dominated by regional high-pressure (HP) metamorphism during the Eocene, classically named (M1) in the Cycladic Blueschist Unit. Subsequently, the four major units of Sifnos were differently affected by retrograde equilibrations during the exhumation and/or the Oligo–Miocene medium pressure overprint (M2). The investigated rocks from the Fikiada Bay area formed during M1 but were overprinted by a brittle / ductile M2 event.

The HP rock assemblage of Fikiada bay represents a sequence of metamotphic basitic and acidic volcanites and sediments. They have been investigated in terms of their mineral assemblages, mineral chemistry and petrography and are compared to similar occurrences from the north of Sifnos, which have been described in detail by several authors. Lithologies comprise alternating garnet- rich, dark blueschists and Grt-gneisses, interbedded eclogites, massive Ep-Ab-Chl-fels and albite- ± carbonate- rich metasediments. These lithologies are embedded in highly strained calcite marbles with boudinaged lenses of dolomites. The commonly observed stretching lineation strikes NE-SW and records a consistent shear sense towards NE. Five episodes of mineral growth and/or deformation during the dominant HP-metamorphism can be distinguished in the studied area. These are compared to and correlated with the metamorphic history of northern Sifnos and other Cycladic islands. A greenschist-facies overprint is confined to local shear zones.

The HP rock assemblage is overprinted by brittle / ductile to brittle extensional structures. A system of conjugate high-angle brittle normal faults striking roughly NW-SE which interact with low-angle, brittle / ductile shear zones indicate NE-SW extension. SCC'-type foliation and synthetic Riedel shear zones indicate a SW-directed shear sense consistent with the S-directed M2 event in the Western Cyclades.

All structures are cut by younger, several meters thick cataclastic strike- slip- fault zones associated with proto- to ultracataclastic fault core zones. The fault cores and the pervasively jointed processes zones are associated with dolomitization of the originally mylonitic calcite marbles. Late volcanic dykes with a thickness of less than 30 cm intruded into these brittle fault zones.

ZUSAMMENFASSUNG

Vorkommen von Hochdruck/Niedrigtemperatur eklogit/blauschieferfaziellen Gesteinen im Südwesten von Sifnos in den Kykladen sind in der geologischen Karte von Davis (1966) verzeichnet, aber es wurden bisher keine Informationen über ihre Geochemie, Petrologie und strukturelle Position publiziert. Diese Vorkommen in der Bucht Fikiada sind das Thema dieser Studie.

Die tektono-metamorphe Entwicklung von Sifnos wird dominiert von einer regionalen Hochdruck (HP)-Metamorphose während des Eozäns, die in der Kykladischen Blauschiefer Einheit klassischerweise als (M1) bezeichnet wird. In Folge wurden die vier Haupteinheiten von Sifnos unterschiedlich stark von retrograden partiellen Gleichgewichts-Einstellungen während der Exhumation und/oder der Oligo-Miozänen Metamorphose (M2) bei mittlerem Druck überprägt. Die untersuchten Gesteine der Fikiada Bucht entstanden während M1, wurden aber von einem spröd-duktilen M2-Deformationsereignis überprägt.

Die HP-Gesteinseinheit der Fikiada Bucht stellt eine Sequenz aus metamorphen basischen und sauren Vulkaniten und Sedimenten dar. Diese werden in Bezug auf ihre mineralische Zusammensetzung, Mineralchemie und Petrographie untersucht und mit ähnlichen Vorkommen in Nord-Sifnos verglichen, die von einigen Autoren detailliert beschrieben wurden. Lithologien umfassen wechsellagernde granatreiche dunkle Blauschiefer und Granatgneise, eingelagerte Eklogite, massive Ep-Ab-Chl-Felse sowie Ab ± Karbonat- reiche Metasedimente. Diese Lithologien sind eingelagert in hoch deformierten kalzitischen Marmoren mit boudinierten Linsen von Dolomit. Die üblicherweise beobachtete Streckungslineation streicht NO-SW und erhält einen konsistenten Schersinn nach NO. Fünf Episoden von Mineralwachstum und/oder Deformation während der dominanten M2-Metamorphose können im Arbeitsgebiet unterschieden werden. Diese werden mit der metamorphen Geschichte von Nord-Sifnos und anderen Kykladischen Inseln verglichen und korreliert. Eine grünschieferfazielle Überprägung ist auf lokale Scherzonen beschränkt.

Die HP-Gesteinseinheit wird von spröd duktilen bis spröden extensionellen Strukturen überprägt. Ein System aus konjugierten steilen, spröden Abschiebungen die ungefähr NW-SO streichen, interagiert mit flachen spröd-duktilen Scherzonen und zeigt NO-SW-Extension an. SCC'-Gefüge und synthetische Riedelscherzonen zeigen einen SW-gerichteten Schersinn, konsistent mit dem S-gerichteten M2-Ereignis in den westlichen Kykladen. Alle Strukturen sind von jüngeren, mehrere Meter mächtigen kataklastischen Seitenverschiebungen zerschnitten, die mit proto- bis ultrakataklastischen Störungskernzonen assoziiert sind. Diese Kernzonen und pervasiv zerklüftete „prozesses zones" sind mit der Dolomitisierung des ursprünglichen mylonitischen Kalzitmarmors assoziiert. Spätere vulkanische Gänge mit einer Mächtigkeit < 30 cm sind in diese spröden Störungszonen intrudiert.

3   INTRODUCTION

The Aegean region is one of the classic and best investigated regions to study subduction systems with all the related features like exhumation of high-pressure/low- temperature (HP/LT) metamorphic rocks, back arc spreading, crustal thinning, plutonism and volcanism, active rifting and active seismicity. Much work has been done in many fields of study to accumulate geochemical, chronological data and petrological and structural observations, but also geophysical data that give insight in the deeper structure of the lithosphere, like gravimetry (e.g. Tirel 2004) and seismic profiles and maps (e.g. Bijwaard et al. 1998) and rates of plate motion (e.g. McClusky et al. 2000, 2003, van Hinsbergen et al 2005; Becker 2008). During this process, many geodynamic and kinematic models have been proposed, P-T conditions have been calculated and discussed to explain processes like exhumation of HP/LT metamorphic rocks or the generation of low angle normal faults, to name only two topics that are related to this work.

This study was accomplished in the framework of and funded by the ACCEL (Aegean Core Complexes along an Extended Lithosphere) - project (Austrian Science Fund). During this project, several diploma-theses and a PhD thesis have been mainly concerned with the investigation of extensional tectonics and related detachment shear zones on the islands of Serifos, Kea and Kythnos.

Fikiada bay was visited during an excursion of the University of Vienna to Sifnos leaded by K. Petrakakis, B. Grasemann in 2005. One intention was the investigation or verification of a normal fault, which, according to some authors, displaces the southeastern part of Sifnos to the south. A volcanic dyke was discovered, and samples of the eclogite- and blueschist-facies rocks were taken. Because no work has been published yet about this occurrence, this master thesis was initiated in 2008.

4   GEOLOGICAL SETTING

4.1   The Hellenides and the Aegean Sea

The Aegean region is a part of the Helenic Orogen that belongs in turn to the Alpine-Himalayan system, an orogenic belt, reaching from the mountain ranges around the Mediterranean all the way through Anatolia, Zagros and the Asian mountain ranges to the pacific. Sengör (1985) distinguishes two independent, but superimposed orogenic sequences that stretch between the Carpathians and the Pacific: The Cimmerides, formed between the early Carboniferous and the early Cretaceous by the subduction of Palaeotethys, and the Alpides, formed between the late Jurassic and the present by subduction of Neotethys and, locally, by the collision of continental fragments with Eurasia.

The paleogeography of the Tethyan Ocean is very complex and comprises alternations of ridges with shallow water carbonate platforms and troughs with pelagic sediments and volcano-sedimentary formations, including mafic rocks and oceanic crust.

A summary of the paleogeographic evolution is given e.g. by Stampfli et al. (2002). Fig. 1 gives an overview of the Tethyan Ocean and its sub-basins.

Fig. 1: Paleogeographic map of the world in the lower Cretaceous (Aptian) by Stampfli (2002). The Vardar- and the Pindos basin were successively subducted to the north during the Alpine Orogeny.

The Hellenides formed due to the collision of the northward moving terranes with the Eurasian plate and the subduction of the oceanic crust, sediments and/or continental fragments of the Neotethys (Papanikolaou 2007). The classic subdivision of this process is given by V. Jacobshagen (1986), dividing the orogeny in four cycles:

(1) the Cimmeric Cycle, Dogger,   (2) the Eohellenic Cycle, early Cretaceous,

(3) the Mesohellenic Cycle, Eocene, and   (4) the Neohellenic Cycle, Miocene.

Fig.2: Geological map of Greece by Voit (2008) after V. Jacobshagen (1986).

The Hellenides are classically subdivided in four tectonic units:

From north to south are these: (1) the Internal Hellenides, including e.g. Rhodopes, Pontides, the Vardar-Izmir-Ankara-zone and the Pelagonian-Lycian zone, (2) the Central Hellenides, also called Pindos Oceanic Unit, including the Cycladic Blueschist Unit and the Menderes Massif (3) the External Hellenides, including the nappe sequence on the Greek mainland and on Crete, and (4) the Foreland of the Pre-Apulian zone.

The timing and tectonic evolution of the orogenic processes is described below.

10

4.2   The Cycladic Blueschist Unit

The Pindos Oceanic Unit involves oceanic crust and continental basement-cover sequences, which have been juxtaposed in an accretionary complex that formed mainly during the Eocene. The Cycladic Blueschist Unit reaches from the peninsula of Euboea and Attica in the west over the Cycladic islands and can be connected to the crystalline of the Menderes Massif in the east, including the islands of Ikaria, Fourni and Samos. In the Cyclades, occurrences of blueschist-facies rocks are reported from Amorgos, Andros, Ios, Kythnos, Milos, Tinos, Syros, Sifnos, northern Serifos, and southeastern Naxos (van der Maar and Jansen, 1983).

This Unit is made up of marbles, gneisses and schists that can be seen as the metamorphic equivalent to the sediments, volcanics and oceanic crust of the Pindos-oceanic basin which underwent high pressure / low temperature metamorphism. In Attica and Euboea, the tectonic contact of these crystalline rocks and the superposed unmetamorphic sedimentary rocks of the Pelagonian Nappe is exposed. In the Menderes Massif, the geometry and characteristic of the orogenic building is well exposed and can be studied in a coherent picture. This picture is much more complicated to infer from the Cycladic islands, because most of the Aegean is submerged and only punctual insight to the overall system is available.

In the Cycladic Blueschist Unit, three main tectonic units are distinguished:

The Basal Unit is made up of Carboniferous continental basement (ortho- and paragneisses), metapelites and meta- bauxite bearing marbles, that are derived from Permo-Mesozoic sediments.

The Intermediate Units are characterized by thinner marbles, metapelites, sequences with mainly mafic volcanics, and metamorphic flysch-sediments. Schliestedt and Okrusch (1988) interpreted them as a Permo-Carboniferous to late Cretaceous passive-margin sequence. Mocek (2001) investigated the geochemistry of the meta-vulcanites, using immobile trace elements and REE to characterize their protolith nature. He suggests that the Intermediate Unit was derived from an island arc environment and earlier (ca. 250 Ma) subduction zones must have been active in the Tethyan Ocean. Sifnos is made up entirely by rocks of this unit.

While the Basal and Intermediate Unit were involved in the subduction processes and experienced high strain and high pressure metamorphic conditions, the rocks of the Upper Unit are very low grade metamorphic.

The Upper Unit (ophiolitic melange) is made up by basal metamorphous olistostromes and mélanges, containing ophiolitic material and Permo-Triassic limestones, greenschists,

intrusions and crystalline and granitoid slices. A partially preserved ophiolite sequence consists of serpentinites and marks the suture between the Pindos Oceanic Unit and the overlying Pelagonian-Lycian nappe-sequence. The tectonic contact between these two units is well exposed in the south of the Menderes Massif. Highly strained carpholite-bearing rocks in the basal thrust sheets of the Lycian nappes indicate HP - very low T metamorphism and document that this Unit has also been affected by Eocene metamorphism (Oberhänsli et al. 2001).

In the Cyclades, relics of the Pelagonian–Lycian Unit are found as tectonic klippen e.g. on Mykonos and Naxos. They represent the former hanging wall of shear zones during the exhumation of the Cycladic Blueschist.

4.3   Geodynamic setting

Carboniferous metamorphism like in the basement rocks of the Basal Unit is sometimes referred to as (M0). The "Cimmeric cycle" is relevant in the northern part of Greece and Turkey, leading to the formation of the Rhodopes and Pontides (e.g. Papanikolaou 2007), and will not be discussed here.

The evolution for HP/LT metamorphic rocks of the Cycladic Blueschist Unit for the Aegean region can be described in three steps:

1. Subduction with the sinking plate,

2. First exhumation within the subduction channel (compressional regime)

3. Post-orogenic exhumation below low-angle normal faults (extensional regime)

The Alpine Orogeny in the Hellenides comprises large scale nappe stacking and development of fold-and-thrust sequences during the subduction of the Neotethyan Ocean, incorporating Mesozoic sediments and vulcanics, ophiolites and elements of the older, Cimmeric continent. Papanikolaou investigated the timing of tectonic emplacement of ophiolites in the Hellenides and distinguished tectonostratigraphically four oceanic and five continental terranes (see **Fig.3**, with the Pindos Oceanic Unit named H2, green, Papanikolaou et al. 2004). He found that the tectonic emplacement of ophiolitic bodies over adjacent continental crust and sediments was generally south directed and that the timing becomes younger from north to south, following the general model of northward subduction. Material of the Tethyan basins was accumulated in accretionary wedges and brought to great depth with the subducting plate. Younging of HP metamorphism in a southerly direction

(from the Vardar-Izmir-Ankara suture zone in the north to the external HP belt on Crete in the south) also indicates the southward retreating of the subduction (Ring and Layer, 2003).

Fig. 1. Terrane map of the Hellenides (after Papanikolaou, 1997, modified).
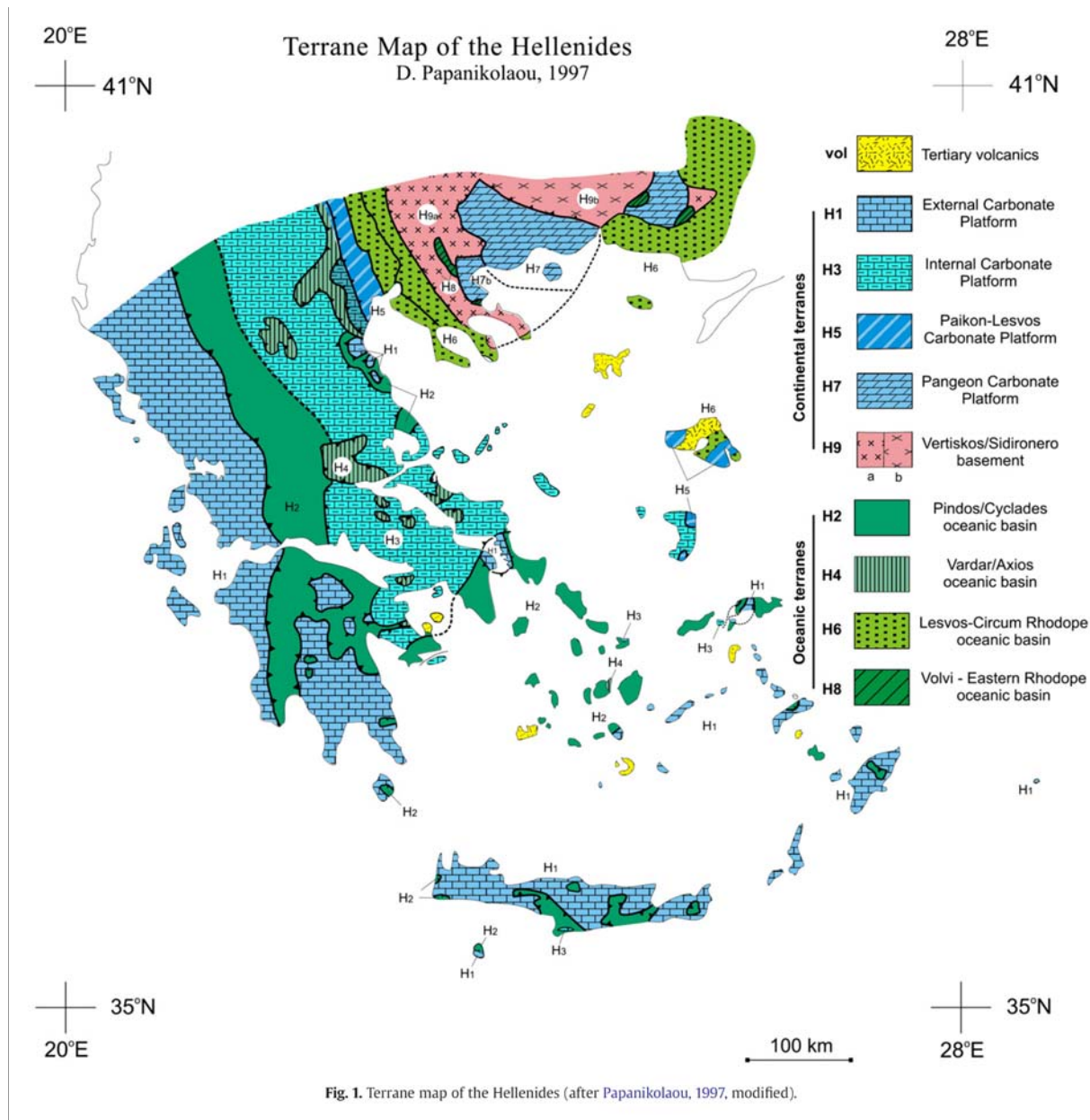
Fig.3: Terrane map of the Hellenides. From Papanikolaou et al. (2004), inferred from obductet ophiolites. Pindos Oceanic Unit with Cycladic Blueschist Unit named H2, in green

At least in Oligocene, the overall tectonic regime in the Aegean region changed, with the establishment of an extensional setting due to orogenic collapse and slab retreat (e.g. Gautier et al., 2001, Jolivet, 2010). The recent Aegean Sea is a back arc basin, related to the presently active subduction zone at the Hellenic Trench. Back arc spreading with regional scale extension lead to widespread crustal thinning: Today, the Moho lies relatively flat at

13

around 25 km in most parts of the Aegean Sea, as gravimetry (Tirel 2004) and seismic tomography (Vigner 2002) indicate.
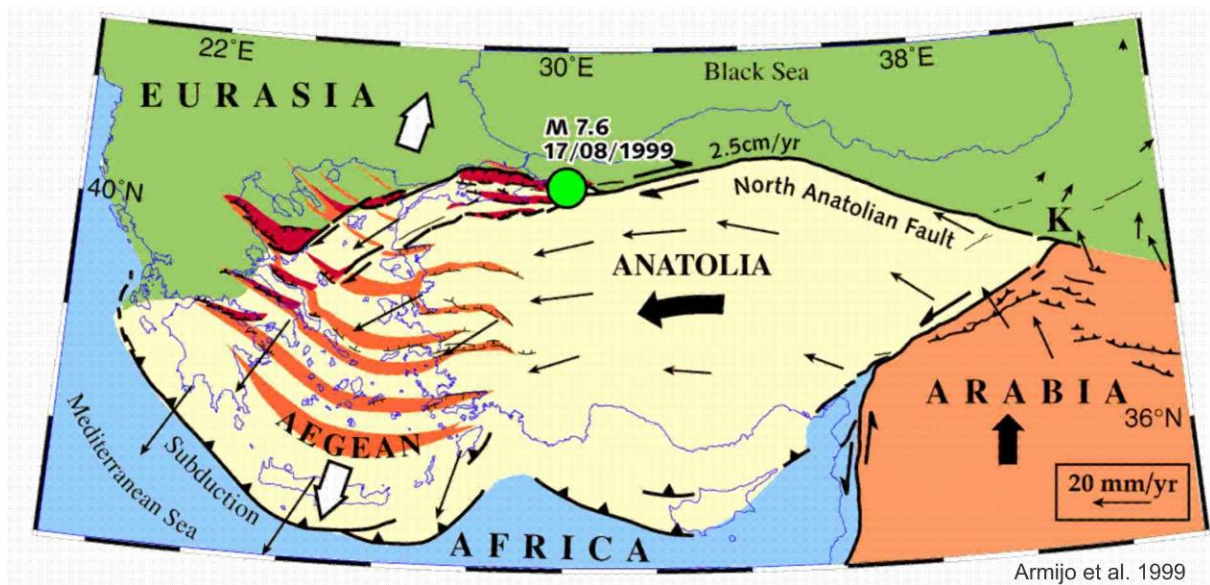
Fig.4: Extension in the Aegean region, caused by back arc spreading and the sinistral north Anatolian fault, related to the plate collision of Arabia and Eurasia and the rotation of the Anatolian plate. From Armijo et al. (1999)

The observation of low-angle normal faults and the relation to exhumation of Cycladic metamorphic core complexes (Forster and Lister, 2009 and references cited therein), e.g. on Ios, Naxos (Lister et al. 1984, Avigad et al. 1997), Tinos (Avigad and Garfunkel, 1989; Katzir et al. 1996, Mehl et al. 2005), Andros (Huet et al 2009), Ios (Forster and Lister, 1999, Huet et al. 2009) or Serifos (Grasemann and Petrakakis 2007) has been a popular topic in recent times, with ongoing discussions of different mechanical models for the evolution of such structures (e.g. using the initial low-angle fault geometry (Wernicke 1985) or the rolling-hinge model (Buick 1988). Rice (2009) points out the applicability of the model proposed by Chéry (2001), developed for the Gulf of Corinth, in the Western Cyclades, that also explains the abundant outcrop examples of conjugate high-angle fault systems interacting with creep on low-angled shear zones .

Crustal extension is accommodated by large scale detachment systems from Oligocene to Miocene. The kinematics in the upper crust show top-to-NE movement in the Eastern Cyclades (Andros, Tinos, Naxos), dated to ca. 28 Ma (Oligocene) on Tinos. Jolivet et al. (2009) propose the "North Cycladic Detachment System", a series of distinct detachments cropping out on the islands of Andros, Tinos and Mykonos, which they interpret as one single major detachment-structure that reactivates the Vardar Suture zone.

14

Top-to-southwest movement is observed on several islands of the western Cyclades (Kea, Kythnos, Serifos), dated to 21-13 Ma (lower Miocene) on Kea (Rice et al. 2009, Iglseder et al. 2008).
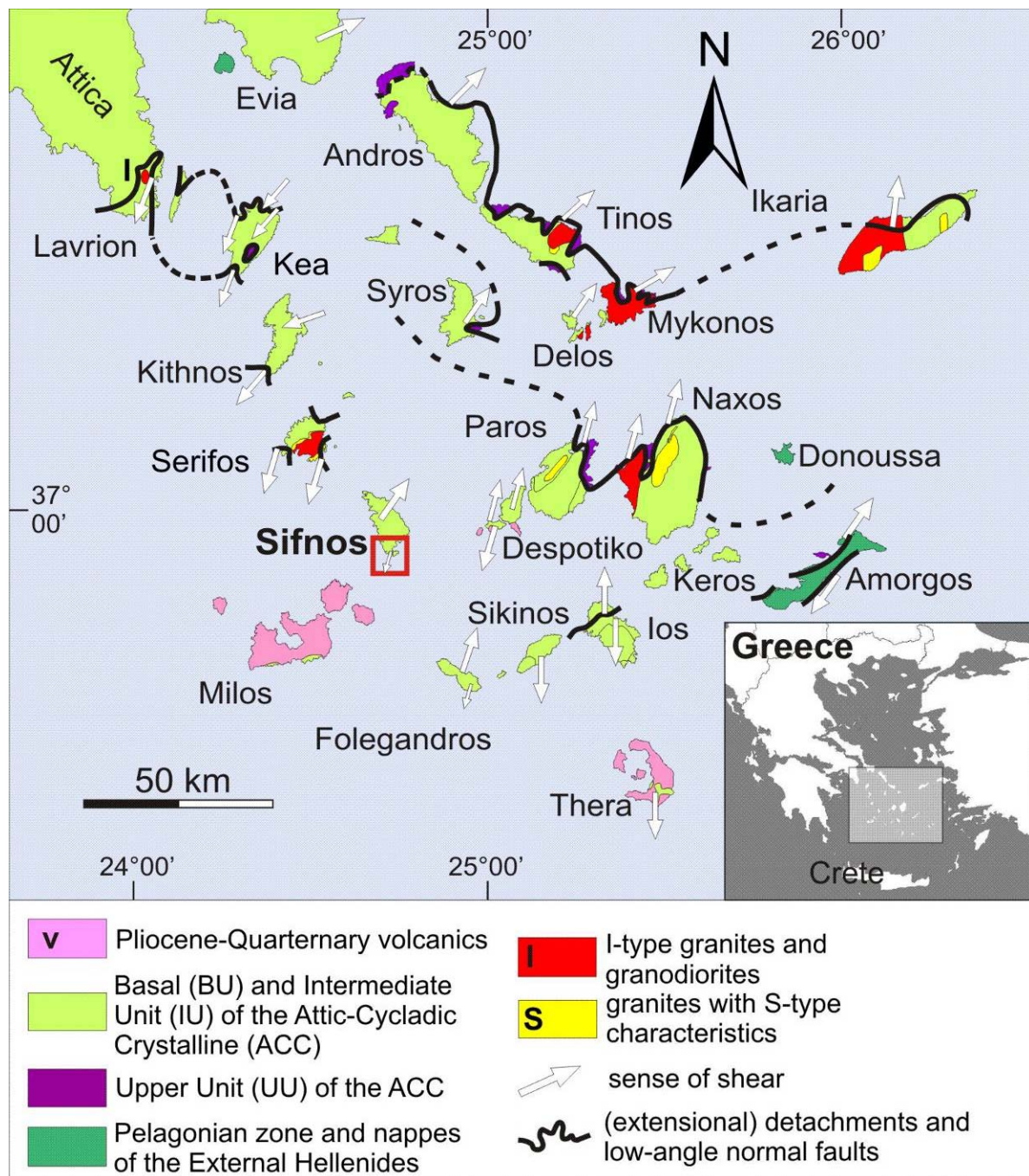
Fig.5: Detachment systems in the Cyclades (modified after Iglseder et al., 2009).

Lithologies associated with the Cycladic Upper Unit are often associated with tectonic contacts on low angle detachment shear zones, for example on Andros, Tinos, Paros and Naxos, where also isolated occurrences of the Pelagonian Zone can be found. The southern islands (Milos, Thira) are dominated by Pliocene to recent volcanic activity. Kinematics of displacement directions show bilateral symmetry: On the northern and the eastern Cyclades, the reported movement is mainly NNE-directed, while SSW-directed kinematics are found on several islands of the Western Cyclades.

Extension is still active today, for example in the Gulf of Corinth, where an active graben-system accommodates ca. 15 mm/y extension (Skourtsous and Kranis 2009), and caused several destructive earthquakes in historic time.

In the South Aegean Volcanic Arc (between the Saronic Gulf and Nisyros), active volcanism can be observed on he islands of Aegina, Antiparos, Kimolos, Kos, Methana, Milos, Santorini and Nisyros (Fytikas et al., 1984). Small volcanic dykes have also been discovered in the working area of this study at Fikiada bay.
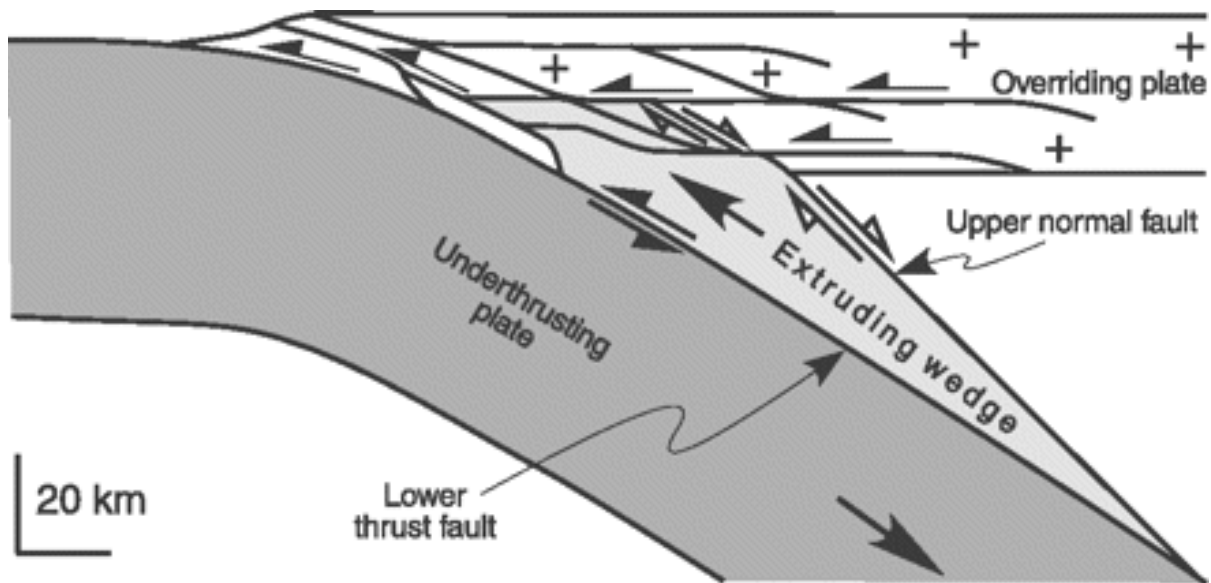
4.4   Exhumation models

The exhumation of HP/LT metamorphic rocks has been the scope of many studies, and several mechanical models have been developed to explain how they can reach the surface. These models include mechanisms in a compressional regime like underplating and tectonics in accretionary wedges (Platt 1986, 1993) "extrusion wedges", (Ring and Layer 2003, Ring and Glodny 2010), upflow in a subduction channel (e.g. "corner flow model" of Cowan and Silling, 1978, Cloos and Shreve 1987, 1988; Platt, 1993, Gerya et al. 2002; Jolivet et al. 2003; Yamato et al. 2007), in extensional regimes (Wernicke 1981, 1992; Lister et al. 1984; Gautier and Brun 1994a; Brun and Sokoutis 2007) or due to erosion (Ring et al. 1999a). The critical factor to preserve the eclogite- and blueschist facies mineral assemblages is a mechanism to avoid a retrograde, thermal overprint along the exhumation path. General agreement is that exhumation of HP/LT- facies rocks begins already during active subduction, and a "cooling mechanism" must be available during their exhumation. It seems that in most cases, several mechanisms interact or play a role at different stages of the exhumation, dependent on regional characteristics.

Some authors tried to combine available data of the Aegean to fit them in an overall picture. For example, Jolivet and Brun (2008) developed a synthetic tectonical map and N-S directed cross-section of the Aegean region based on available geophysical, plate kinematic, petrological and structural data.
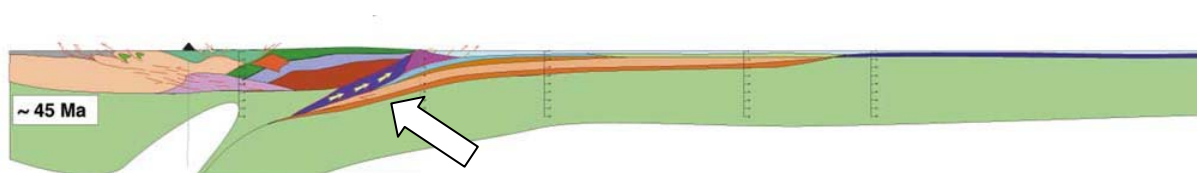
Fig.6: Schematic cross section (N-S-directed) of the Aegean during Eocene, as an example for the model of Jolivet and Brun (2008). In this stage, the exhumation of the Cycladic Blueschist Unit (purple) in the still active subduction zone is indicated by yellow arrows.

16

They suggest one continuous northward subduction of the African plate for the last 70 Ma (in the sense of van Hinsbergen et al. 2005 but in contrast to Papanikolaou (2004), who suggested a second one for the units involved in this model).

Fig.7: Schematic sketch of Ring (2010): A mechanical model is proposed for the exhumation of crustal material during ongoing subduction (convergent setting). The extruding wedge is confined by a thrust fault at the base and a normal fault at the top. In the middle crust, this wedge is sliced up by thrusts in the overriding plate.

4.5   Metamorphic evolution

As described above, the Cycladic Blueschist Unit is derived from sediments, volcanics and oceanic as well as continental crustal material of the Pindos basin. These rocks were involved in the subduction-accretion system during the Cenozoic and experienced blueschist- to eclogite facies HP-metamorphism. A good overview of P-T-paths obtained for various rock units on various cycladic islands is given in Ring et al. (2010) (see **Fig. 8**).

Although the timing is different between individual regions, the shapes of these P-T paths are similar and document pronounced isobaric cooling during decompression. In the next chapter, the available chronology- and P-T- data for Sifnos will be discussed in detail.

Classically (e.g. Okrusch and Bröcker), the Eocene HP-metamorphism is referred to as (M1). A medium pressure overprint has been interpreted as a distinct Barrovian type overprint (e.g. Okrusch and Bröcker, 1990, Schliestedt and Matthews, 1987) with medium to low pressure and greenschist-, locally up to amphibolite-facies conditions (see below). The nature of this temperature- pronounced metamorphism has been a subject of controversy discussion, because it is not pervasive throughout the Cyclades. Some Aegean islands are dominated

by a greenschist facies overprint (e.g. Andros, Ios, Kea, Kythnos, Paros, Tinos, Serifos and Syros), but several units on various islands throughout the Cyclades are effected only moderately, if at all. Generally, overprinting is more pronounced in large shear zones that acted as fluid pathways, related to the back arc extension. At the example of Sifnos, the characteristic of this retrograde overprint will be discussed below.
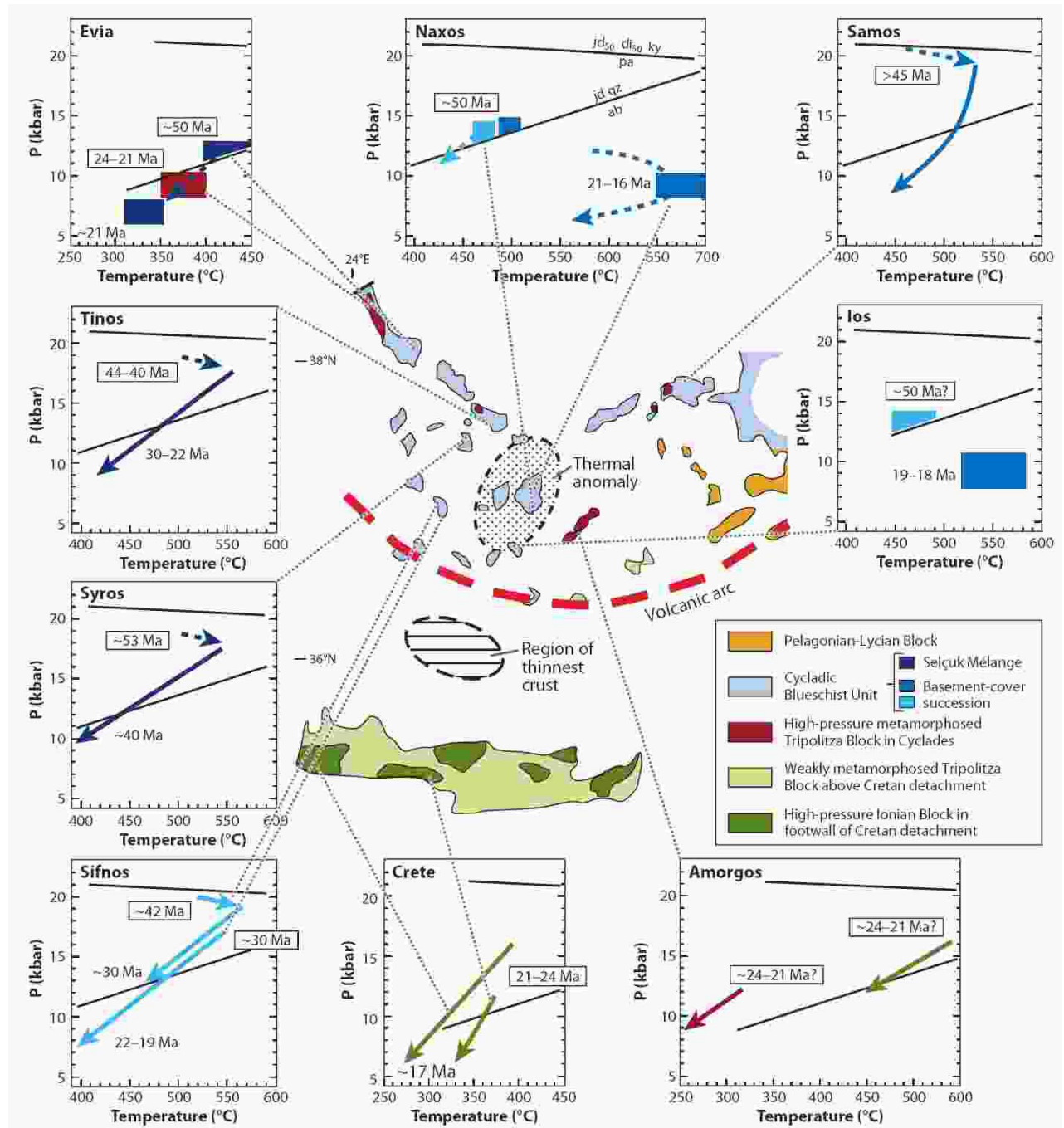
Fig.8: Overview of P-T-paths, published for various islands in the Aegean, especially in the Cycladic Blueschist Unit (light blue) (from Ring et al., 2010)

18

A thermal pulse during early Miocene, probably related to extensional deformation, is observed on Paros and Naxos, where temperatures of 650 – 700 °C were reached at 8 - 10 kbar (Buick and Holland, 1989, Buick, 1991). Before, temperatures had cooled from the Eocene HP-metamorphism to 400 – 480 °C at >12 kbar (Avigad, 1998). This thermal anomaly is described in Ring et al. (2010) and marked in **Fig.8**.

5   SIFNOS ISLAND

5.1   General geology

As mentioned above, the island of Sifnos is made up entirely of rocks of the Intermediate Unit, part of the Cycladic Blueschist Unit. Based on the geological map of Sifnos by Davis (1966), four lithological units are commonly distinguished. This schema is established in literature and has been adapted and interpreted by many authors (e.g. Okrusch et al. 1978; Matthews & Schliestedt 1984, Schliestedt & Matthews 1987; Avigad & Garfunkel, 1988; Trotet et al., 2001a,b).

From structural top to bottom:

(1) The Upper Marble Unit (UMU), a 300 m thick complex of calcitic and dolomitic marbles with lenses of quartzite, eclogites and blueschists, forms the northernmost part of the island.

(2) The Blueschist Unit (BU), which covers a big area in the north, consists of well preserved eclogite- and blueschist- facies rocks. Coherent interlayered quartzites, acidic gneiss, metabasites, metasediments and metagrauwackes form a 900 m thick pile.

(3) The Main Marble Unit (MMU) occupies most of central and southern Sifnos and is dominated by calcitic marble with horizons and lenses of dolomite. There also occur conglomerates with components of marble and metabasite. Intercalated metabasitic layers reach up to 100 m thickness and occur today as greenschists. According to this subdivision, the well preserved blueschist assemblages from southern Sifnos belong to this unit

(4) The Greenschist Unit (GU) is described as the structurally deepest unit and exposed mainly in the eastern and central part of the island. It consists mainly of metasediments and metabasites with relictic eclogite- and blueschist-facies assemblages and a graduated greenschist-facies retrograde overprint.

The overall dipping in these units is toward N. The contacts are mainly tectonic, but the degree of displacement accommodated along these lithological contacts is still subject to ongoing discussion: For example Trotet et al (2001a) see the contact between MMU and BU as a major low angle detachment (first proposed by Avigad, 1993). Their interpretation and the related map are given in chapter 10 (discussion). During this study, no field evidence for such a shear zone was found.
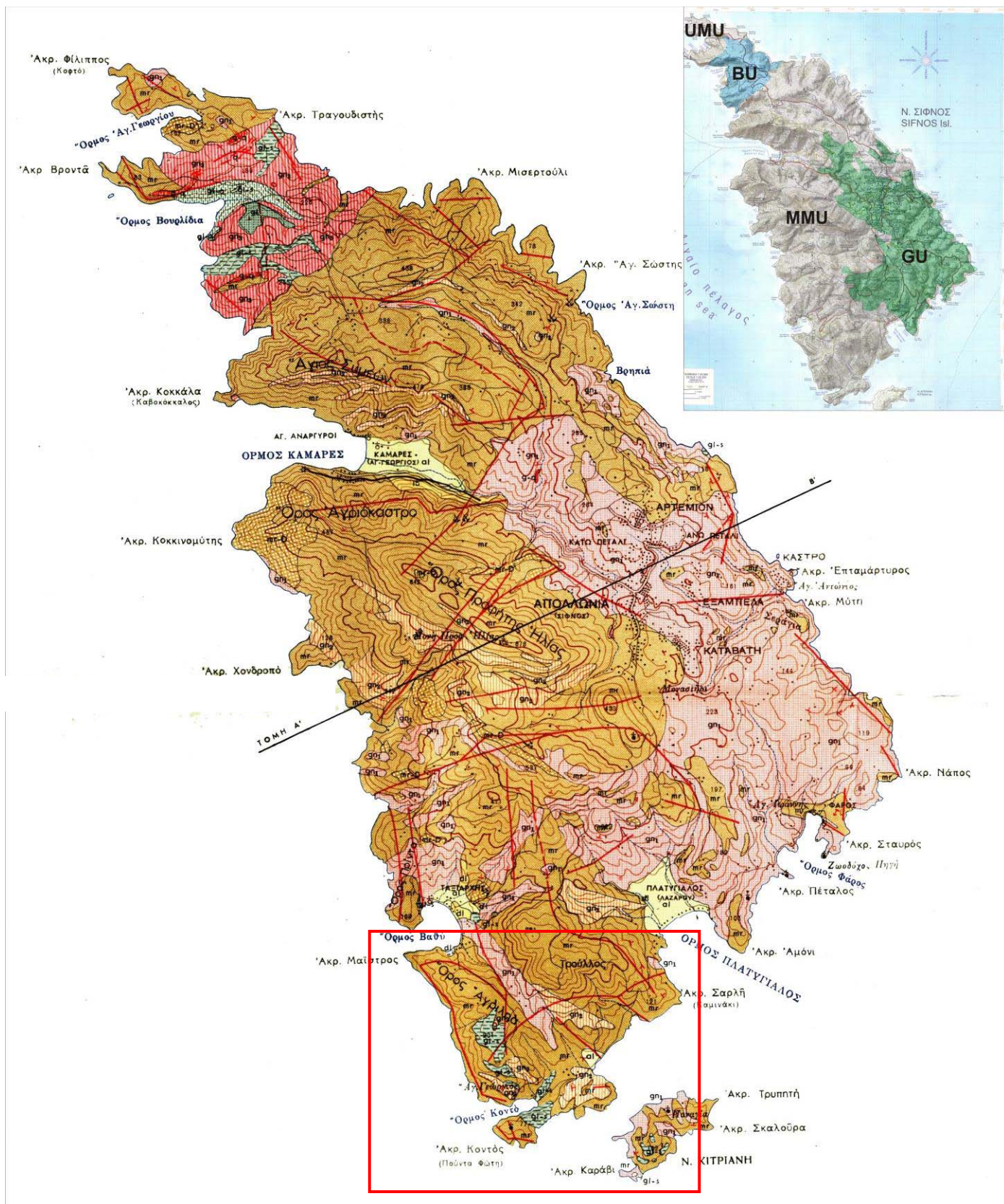
Fig.9: Geological map of Sifnos by Davis (1966), with schematical overview of the four units:

UMU = Upper Marble Unit, BU = Blueschist Unit, MMU = Main Marble Unit, GU = Greenschist Unit

The studied area in the south, with explanation of the lithologies distinguished in this map, is given in the next chapter.

In all of these units, the eclogite-blueschist-facies HP-metamorphism can be recognized, i.e. all these units experienced an analogous (prograde) metamorphic history (e.g. Lister and Raouzaios, 1996) until parts were differently affected by a retrograde overprint.

Several authors used rocks of the BU in northern Sifnos for geochronological investigations:

Altherr et al. (1979) used the Rb–Sr- and the K–Ar system to investigate phengites and paragonites from eclogites, Jd-gneisses, Grt-Jd-Gln- and Grt-Ep-Gln-gneisses and Chl-Act-felses from the BU and Ab-gneisses from the GU. The closing temperatures in white mica for the Rb–Sr-system are at about 500 to 550 and at least 360°C for the K–Ar-system (450 to 500°C after Villa 1990). The dates from the best preserved rocks of the BU gave concordant ages of around 42 Ma and are thought to indicate eclogite-blueschist-facies metamorphic peak conditions. The phengites from the GU gave ages between 21 and 24 Ma.

Wijbrans et al. (1990) also used single grain K-Ar analyses of phengite to investigate eclogites, micaschists and impure marbles of the BU, impure marbles and interlayered blueschist of the MMU, and impure marbles and Ab-gneiss of the GU. They found similar ages for the BU (between 41 and 42 Ma), slightly lower for the GU (ca. 19 Ma) and values between 30 and 36 Ma for the MMU. Wijbrans (1990) interpreted these younger dates in the GU as an overprint of the M2-event, and the gradually decreasing trend from BU to GU was seen as a more severely overprint in this intermediate unit.

The effect of the so-called M2-event in Sifnos has been an issue debated by several authors. While HP/LT-assemblages are well preserved in the BU and around Fikiada bay, they can be found only relictic in the GU that has been pervasively overprinted under greenschist facies conditions. In the interjacent marble unit, intercalations of greenschist facies mafic rocks as well as lenses of blueschists are observed. Generally, the greenschist-facies overprint is more distinct along lithological contacts and localized shear zones (own observations and e.g. Trotet et al. 2001a). There are different interpretations of this graduated greenschist-facies overprint in rock units that occur relatively close to each other (see below)

5.2   Metamorphic conditions

Numerous PT-calculations have been published for Sifnos and are used as a base for interpretations. Conventional thermobarometry as well as phase equilibria approaches have been used to estimate metamorphic peak conditions and the P–T paths of eclogite- and blueschist-facies rocks.

Schliestedt, (1986) and Schliestedt and Okrusch (1988) used garnet-pyroxene equilibria to derive temperatures of 470 to 520 °C and the stability fields of jadeite and paragonite to estimate pressures between 13 and 21 kbar.

Matthews and Schliestedt (1984, revised Matthews 1988) estimated P-T conditions of greenschist-facies rocks of the GU using oxygen isotope studies and mineral equilibria, indicating temperatures of 400-500°C and pressures of 5-7 kbar.

Similar values for peak conditions were obtained by Ridley (1984) and Evans (1986).

Avigad et al. (1993) used multi-equilibrium approaches to calculate pressures above 12 kbar at temperatures of 480-520°C for eclogitic relics. Metabasic rocks consisting of glaucophane-crossite, albite and epidote equilibrated at pressures of 8-10 kbar and similar temperatures (Ep-Ab-blueschist facies).

These published estimates are based on the calculation of breakdown reactions, which limit the P-T stability fields of multivariant parageneses and lead to large stability fields. For this reason, they do not allow to draw a constrained P /T- path, especially not in the later retrograde state of exhumation (to resolve the question of the different greenschist-facies overprint).

P–T diagrams modeled for specific bulk compositions (so called pseudosections) have been widely used to constrain the evolution of different rock types. This approach has the advantage that the bulk rock composition or an observed equilibrated assemblage can be used and thermobarometric data may be inferred from both compositional isopleths and isomodes. Trotet et al. (2001b) used multi-equilibrium approaches, involving several end members and solid-solution models for chlorite, phengite and garnet to estimate the stability P-T conditions of different parageneses, assuming local equilibria based on textural criteria. Their resulting P-T paths are shown in **Fig 10**. Schmädicke and Will (2003) determined the HP-peak conditions at 550 to 600° C and 2 kbar and produced phase diagrams for observed retrograde assemblages, defining successions of partial equilibration states to infer P-T paths for blueschists and greenschists (see **Fig. 51** in chapter 10).

To account for the observed ferric iron content of the blueschists, Groppo et al. (2009) modeled P–T isochemical diagrams (pseudosections) for the oxidized N(K)CFMASHO system and used solid solution models involving Fe^{+3}-end-members. Resulting P–T conditions show two distinct HP events with conditions of 2.0 GPa / 450 - 500 °C and 1 GPa/ 525–565 °C.

Lister and Raouzaios modeled published $^{40}Ar/^{39}Ar$ apparent age spectra for white micas (from Wijbrands 1990, 1993) to estimate cooling rates and PT-paths for blueschists and greenschist ("Argon geospeedometry"). Their results are given in **Fig 10**.
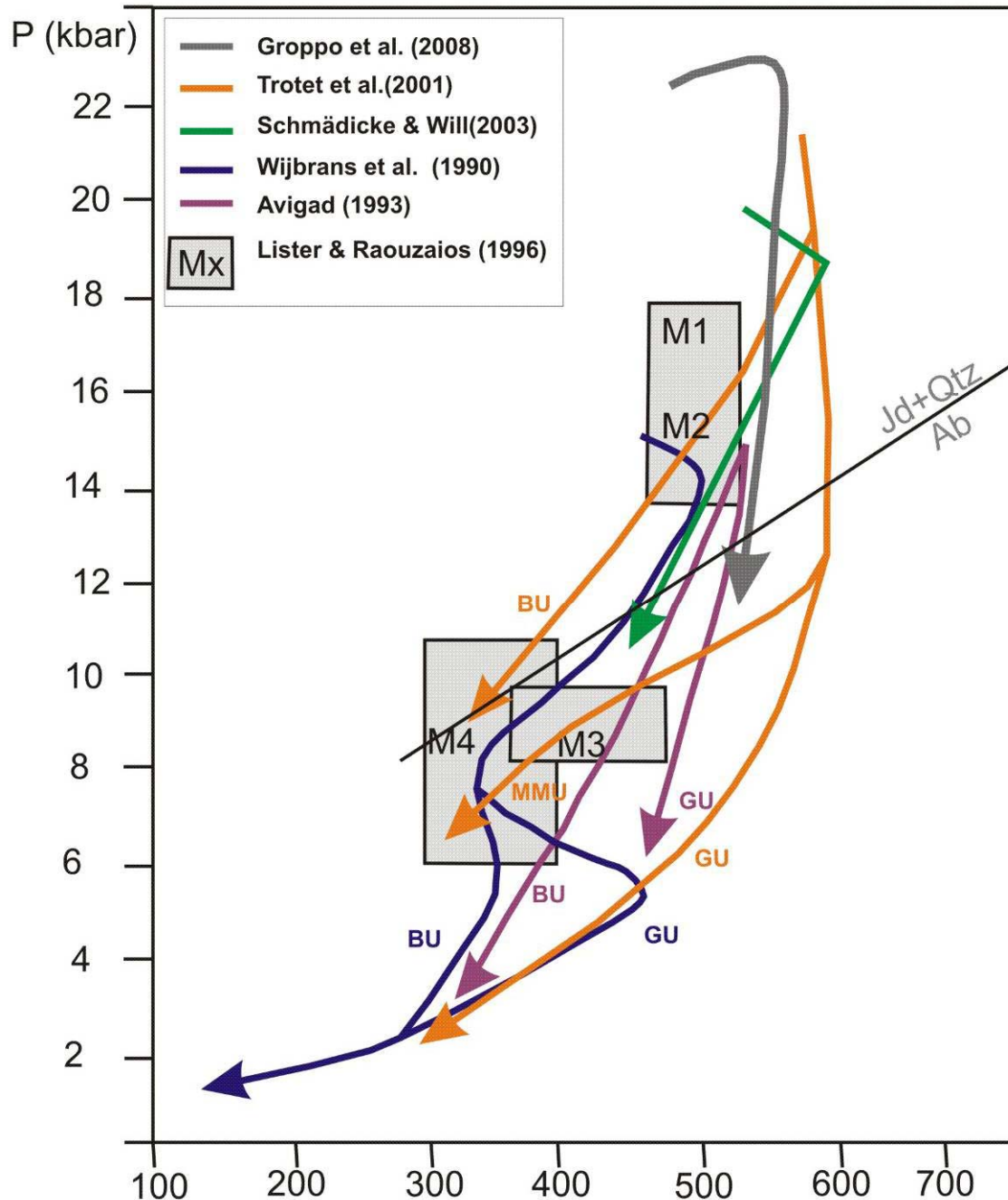
Fig.10: Examples of published PT-trajectories. For further explanation see text.

Fig 10 shows various published PT-trajectories. Especially the later studies, using multi-equilibriums approaches and pseudosections, come to different paths for the PT-history of

different rock units. Generally, samples that show a stronger retrograde overprint (like rocks from the GU) give resulting PT-paths with more pronounced segments of isothermal decompression, while samples of well preserved eclogite show a more typical "blueschist-path" (like those derived for e.g. the franciscian blueschists, Ernst 1993), with coeval decompression and rapid cooling, and no big loop to higher temperatures.

Most authors acknowledge that a PT-path can not be drawn just by linking some calculated points or domains, and that especially episodes of syntectonic mineral growth are hard to resolve. Excursions from smooth, clockwise PT-loops are drawn by some authors, e.g. Forster and Lister (2005) propose several "thermal pulses" during the high pressure metamorphism, based on their reassessment of $^{40}Ar/^{39}Ar$-data. They interpret these thermal pulses in their geodynamic model of "several distinct tectono-metamorphic slices" (Forster and Lister, 2005). However, the origin of the heat during these metamorphic processes remains an open question.

5.3   Previous interpretations of metamorphic evolution

The so called M1- metamorphism can of course not be seen as one single event. Observed metamorphic assemblages do in most cases not reflect the pressure maximum or the peak conditions, but different stages of later, more or less pervasive retrograde re-equilibrations during ongoing metamorphism and the exhumation. Obviously, blueschist- and greenschist facies rocks both underwent HP metamorphism under similar conditions, but were affected to a different degree by retrograde processes during exhumation.

Matthews and Schliestedt (1984) suggested pervasive fluid infiltration as the main reason for the overprint of the GU, while the blueschists and eclogites were sealed by the main marble that acted as an impermeable layer. Wijbrans et al. (1990) assumed that a temperature increase at the base of the structural pile caused the overprint.

Another hypothesis is that blueschist- and greenschist-facies rocks were derived from different structural levels and experienced a different exhumation path and therefore different PT-history, and that their adjacent occurring is an effect of tectonics during extensional (Miocene) processes. Avigad (1993) suggested that blueschist and greenschist- facies rocks, i.e. the main marble unit and the GU, were juxtaposed by a low-angle detachment fault subsequent to the Oligocene-Miocene greenschist-facies overprint.

Trotet et al (2001b) suggest major ductile shear zones to be responsible different PT-paths for the units. They note that the degree of retrogression as well as the ages obtained by Ar-

Ar-chronology decrease from structural high (BU) to lower levels (GU), and attribute this to the cooling effect of a superposed shear zone that was more effective on top during the exhumation of the whole lithostratigraphic pile, while Lister and Raouzaios (1996) suggested thrust tectonics during the exhumation as a mechanism to preserve the HP-rocks and juxtapose the two different units. These different interpretations will be discussed in the last chapter.

6 SOUTHERN SIFNOS AND FIKIADA BAY

6.1 Working area and mapping

In the geological map of Davis (1966), occurrences of glaucophane schists (signature: gl-s, i.e. Gln-Ep-Msc-Grt-schists) are marked between the village of Vathy and Fikiada bay in the very south of Sifnos (see **Fig. 11).** In detail, blueschists have been mapped at one location near Vathy, along the trail to Fikiada at a hill called Spilia i Siniore (all local names from topographic map of ANAVASI 1:25 000, 2002), and in the northeast and the south of Fikiada bay. In addition, beds of gneiss and schist- gneiss inside the marbles (gn_2) and gneiss, schist and amphibolite (gn_1, i.e. Msc-Ep-Chl-gneiss etc. alternating frequently with schist and amphibolite) have been distinguished. (gn_1) is here the lithology typical for the Greenschist Unit.
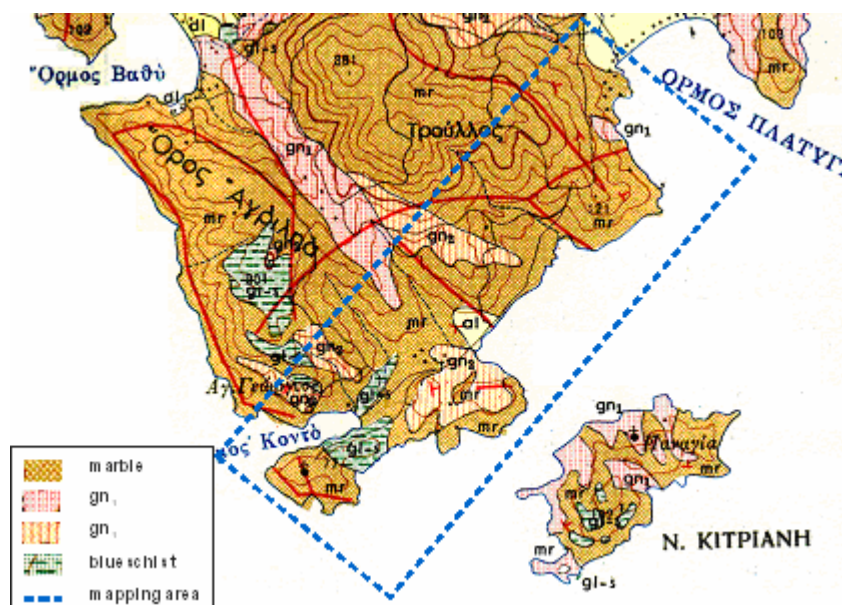
Fig. 11: Southern Sifnos, geological map of Davis (1966). In blue the area of field investigations during this study. Refer to text for explanations of lithologies.

Leitner (1999) mapped the southeastern part of the island in the course of his diploma thesis. He distinguished greenschist, micaschist, jadeite-gneiss, blueschist and occurrences of serpentinite near Vathy. HP-assemblages at Fikiada bay are confirmed, and several more

outcrop-areas are marked. He reports the best preserved blueschists from *Stavrou Petali*, but samples from the well preserved outcrops around Fikiady bay were not investigated.

Fig. 12: Mapped area in Google Earth (Terrain view, north directed)

Fig. 13: a) Layer of greenschist in hills south of Platy Gialos, **a)** in Quickbird satellite image
b) in geological map

According to the classic subdivision of Sifnos, the south of the island belongs to the MMU, lithostratigrafically above the GU and below the BU. In this sense, the blueschist-facies rocks of Fikiada bay (and Vathy) represent large, boudinaged layers or lenses inside the Main Marble Unit. A new geological map has been created for the area in the south of Vathy and Platy Gialos. It is based on field work in September 2008 and the interpretation of the two existing maps of Davis (1966) and Leitner (1999) as well as

27
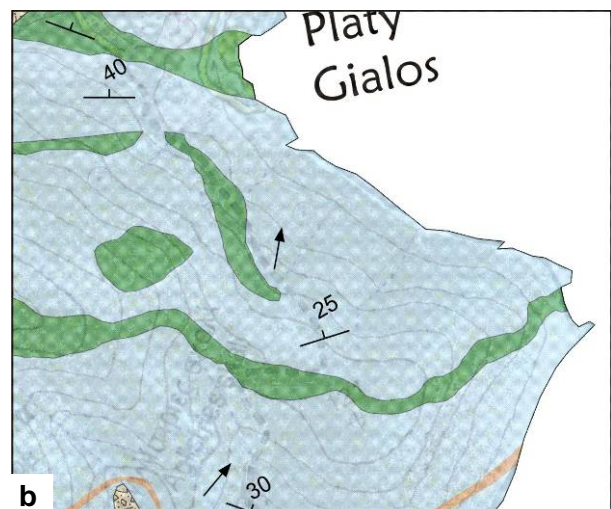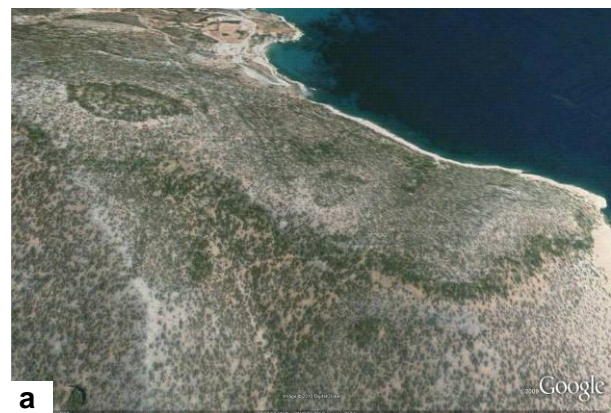
Quickbird satellite images in Google Earth with a resolution of approximately 50 cm. The mapped area is marked in **Fig. 11**. Especially the border of marble and schists can be recognized and traced through the terrain in the satellite image, due to the relief resulting from different weathering properties and differences in color and the covering vegetation (see **Fig. 13**). It has been observed in the field that schists, superposed by karstified marbles, act as aquitardes and provide more favorable conditions for trees and scrubs in the generally dry environment. The combination of field observations (lithological information and orientation of structural elements) and georeferenced satellite-images provides a good tool to depict geological information in a high resolution and accuracy. Nevertheless, contradicting information in the two existing maps in terms of the mineralogy of silicate rocks can not be dissolved. Therefore, the silicate rocks in the new map are only distinguished where this is based on the authors own observations.

The software package ArcGIS 9.2 has been used for management, interpretation and preparation of the acquired data and to create a geological map with two layouts: One regional map, covering the whole area and a more detailed map of the southernmost area with the best preserved blueschist-facies rocks (see Appendix).

Orientations of foliations, lineations, fold geometries and fault planes have been measured throughout the working area. The data were visualized and analyzed using the software Tectonics FP.

6.2 Lithostratigraphy and structural settings around Fikiada bay

Fresh outcrops of Silicate rocks can be found N' and S' at the coast of Fikiada bay and at *Tourkavlako,* along the southern cliffs of the little peninsula (*Pounda tou Foti*).

The HP rock assemblage of Fikiada bay comprises dark, garnet-rich blueschists with mylonitic fabrics and large garnet-porphyroclasts, alternating with cm to m thick layers of light colored garnet and glaucophane-bearing, quartz-rich gneiss. Eclogites occur as rare boudins in the blueschists, with diameters from 5 to 30 cm, accompanied by extensive quartz veining. Associated with these veins are clusters of idiomorphic epidote-crystals, reaching several cm in length. Brown lenses of massive Fe- and Mn- carbonate, identified as siderite and ankerite with secondary limonite by Leitner (1999) are common, and interpreted as concretions that formed during diagenesis.

Massive, very coarse grained Ep-Ab-Chl-fels forms layers with up to 5 m thickness. Metasediments comprise light carbonate-rich gneisses as well as metapelites and quartzites.

Fig. 14 shows the outcrop of the investigated HP-rocks at the south of Fikiada bay, which has been surveyed in detail and where most of the samples were taken. Although the compositional layering is well developed, a detailed general lithostratigraphic profile can not be described due to the intense overprint of brittle tectonics with tilting and shifting of blocks.

	Carbonate-rich gneiss		Blueschist		Dolomitized marble		Quaternary debris		Blocks
	light-coloredGarnet gneiss		Ep-Ab-Chl-fels		Volc. Dyke + hydroth. alter.		Normal fault		
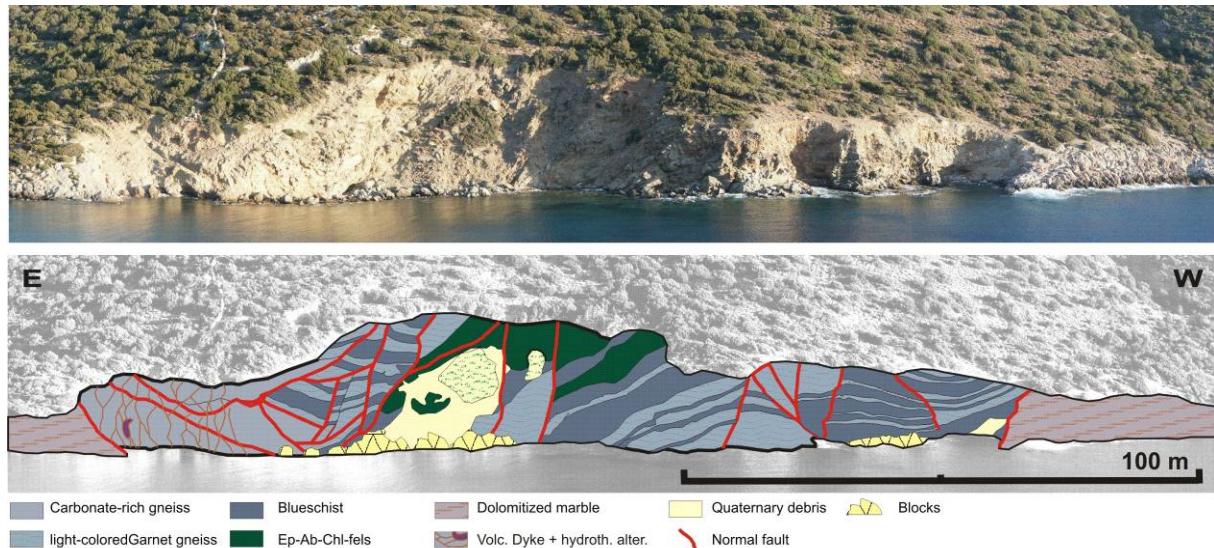
Fig. 14: Outcrop of silicate rocks at the southern coast of Fikiada bay
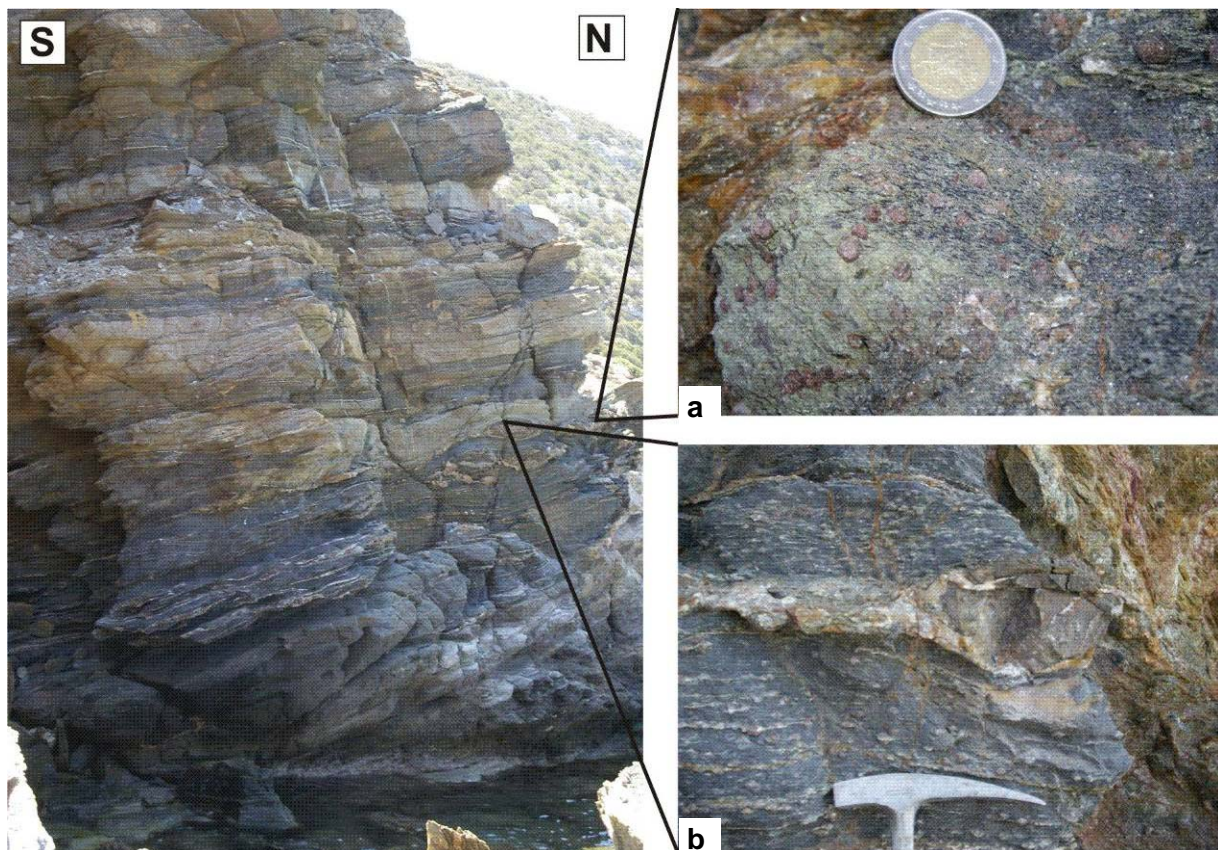
Fig. 15: Intercalations of blueschist and light-colored Grt-gneiss, with S-parallel Qtz veining and boudins of **a)** Eclogite **b)** Fe-Mn carbonate (siderite and ankerite)

All lithologies show a more or less developed, foliation-parallel compositional layering. Rootless isoclinal folding of this layering is common with fold axes trending roughly NW-SE. Hinges are overprinted by the dominant foliation. This foliation is well developed and defined by white mica, glaucophane and epidote, and mostly dips to N to E. The main pervasive stretching lineation is shallow and plunging roughly to NE. Delta- and sigmaclasts (dolomitic boudins in marble, eclogite-boudins and garnet-porphyroblasts in blueschist and gneiss) as well as SCC'- fabrics in the blueschist-facies fabrics indicate consistent top to NE-kinematics.

These lithologies are superposed by highly strained calcite marbles with colors from pure white over grey and yellow to reddish. A well developed foliation and lamination is common. Along the way to Platy Gialos, the grainsize shows variations with more coarse grained domains, and bluish shades can also be observed. Dolomitic marbles occur in several horizons, especially superposing the investigated schists and gneisses. They can occur as fine, mm to dm thick layers, commonly folded, or as boudins, cm to tens of m in length.

Intercal although no bigger outcrops of fresh rock could be observed in the field. These rocks record mylonitic structures with isoclinal folds and thinning of the layers to a few centimeters. The extensive neoblastic growth of albite and chlorite and a foliation, defined by white mica, chlorite and epidote, parallel to the axial planes, overprint these folds. These schistous layers are often affected by brittle / ductile to brittle deformation structures, which is ascribed to their mineral ations of greenschists with thin layers of light albite-rich, garnet-bearing gneiss can be observed in the marble sequence. They occur in tectonostratigraphic higher positions than the blueschist-facies assemblages at Fikiada bay. Layer thicknesses may reach from 1 m to 10 m or more, compositions, making them a less competent material than the adjacent marbles and therefore a favored zone of strain localization.
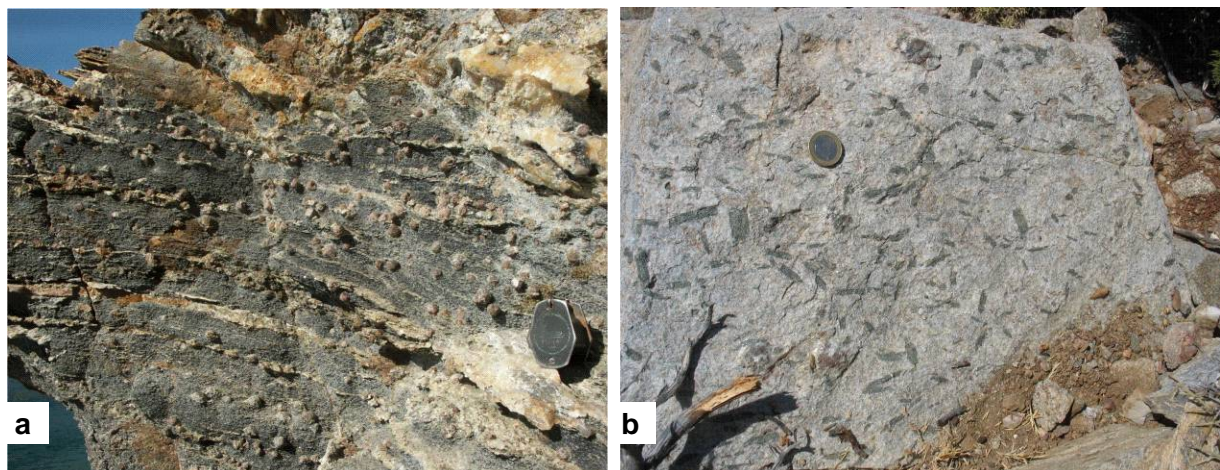
Fig. 16: a) Blueschist, typical mylonitic fabric with Grt-porphyroclasts **b)** Blueschist, foliation plane with S-parallel, but therein disoriented growing Gln-porphyroblasts up to 5 cm in length
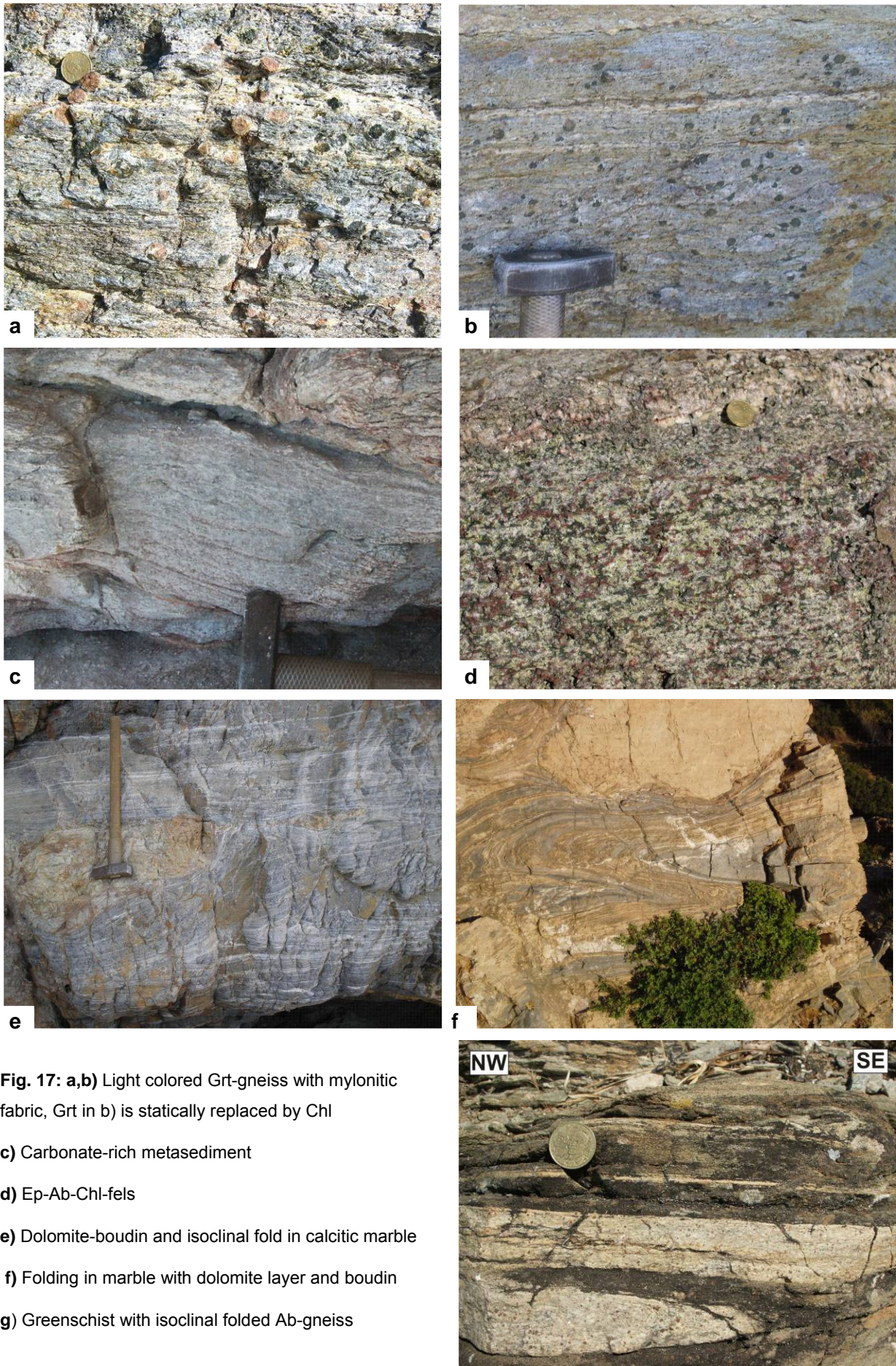
Fig. 17: a,b) Light colored Grt-gneiss with mylonitic fabric, Grt in b) is statically replaced by Chl

c) Carbonate-rich metasediment

d) Ep-Ab-Chl-fels

e) Dolomite-boudin and isoclinal fold in calcitic marble

f) Folding in marble with dolomite layer and boudin

g) Greenschist with isoclinal folded Ab-gneiss

Horizons of calcitic meta-conglomerate with layer- thicknesses of up to three meters were observed. Components consisting mainly of carbonate and rare meta-vulcanite are embedded in a mylonitic matrix and elongated and flattened, so that they indicate the finite strain these layers experienced (compare Ring and Kumerics 2008). Sigmaclasts in the north-eastern horizon (see map) can be used as shear sense indicators and show a movement of top to NE.
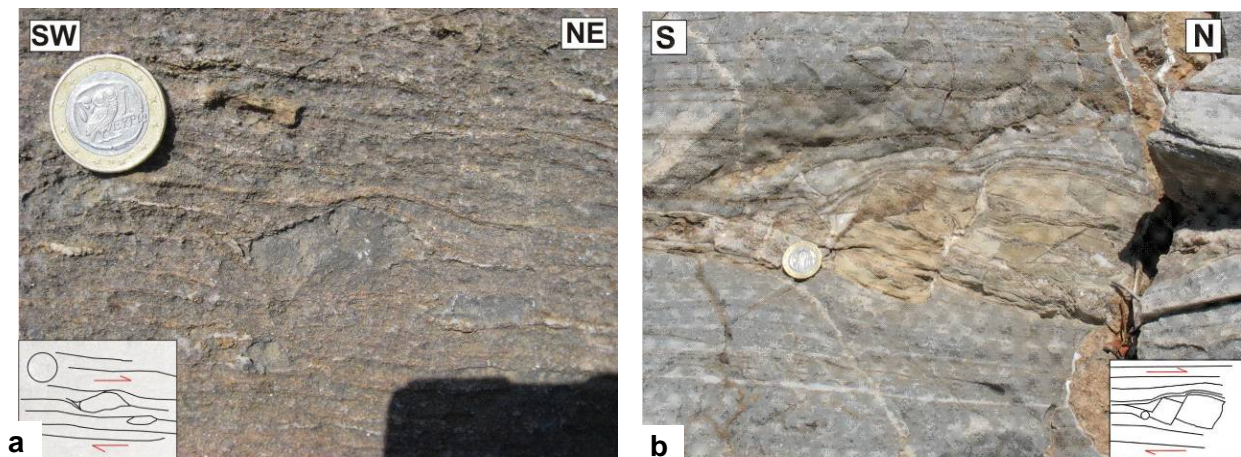
Fig. 18: Shear sense indicators: **a)** sigmaclast in meta-conglomerate   **b)** dolomite-boudin in calcitic marble

The marbles with intercalated greenschists and metaconglomerates show a general dipping to NE between Fikiada bay and Platy Gialos. Axes of flat lying, isoclinal folds in marble and greenschist strike roughly NW-SE. The HP/LT facies-rocks are located in a tectonostratigraphic low position of the marble-unit that forms the southern part of Sifnos. Their "root" or lower boundary is not exposed, so their thickness can only be estimated, but must exceed at least 50 m.

6.3 Late extensional deformation structures

The HP rock assemblage is overprinted by brittle / ductile to brittle extensional structures. S-parallel, ductile shear bands are associated with extensive chloritization and growth of Fe-hydroxides and formed under low greenschist-facies conditions.
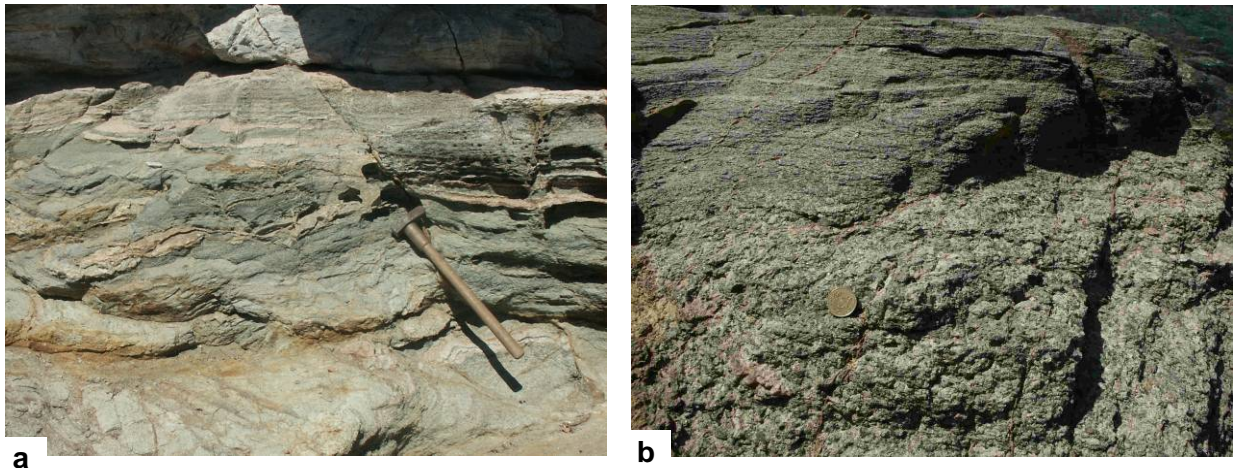
Fig. 19: a, b) S-parallel greenschist-facies shear zone, overprinting Ep-Ab-Chl-fels

All outcrops of HP-rocks are fragmented by a conjugate system of high-angle brittle normal faults, striking roughly NW-SE (stereoplots of the observed structures are given in **Fig. 20**). From the measured orientations of fault planes, lineations and shear sense indicators, the paleostress-directions were calculated using the software Tectonics FP. Resulting orientations are σ_1 = 139/74 and σ_3 = 031/06, indicating NNE-SSW extension.

✳ P- or T-Axes
⬤ P-Axes
☐ B-Axes
▲ T-Axes

Mean vector
P: 139 / 74 76%
B: 303 / 12 61%
T: 031 / 06 82%
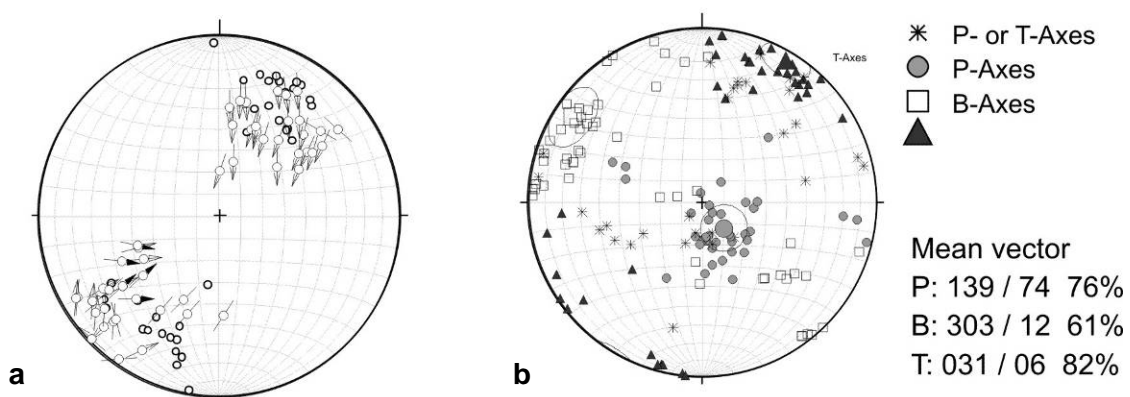
Fig. 20: a) Stereoplot (Angelier-plot) of high angle normal faults: Fault planes, lineation and slip direction
b) calculated orientation of stress directions (P-T-axes, P = σ_1, B = σ_2, T = σ_3)

A major, undulating low-angle, brittle / ductile shear zone is localized at the lithological boundary of silicate rocks and the overlying marbles, and corresponds with the conjugated high angle system. SCC'-type foliations in the low angle fault zone and synthetic Riedel shears indicate a SW-directed shear sense, consistent with the S-directed M2 event in the Western Cyclades.
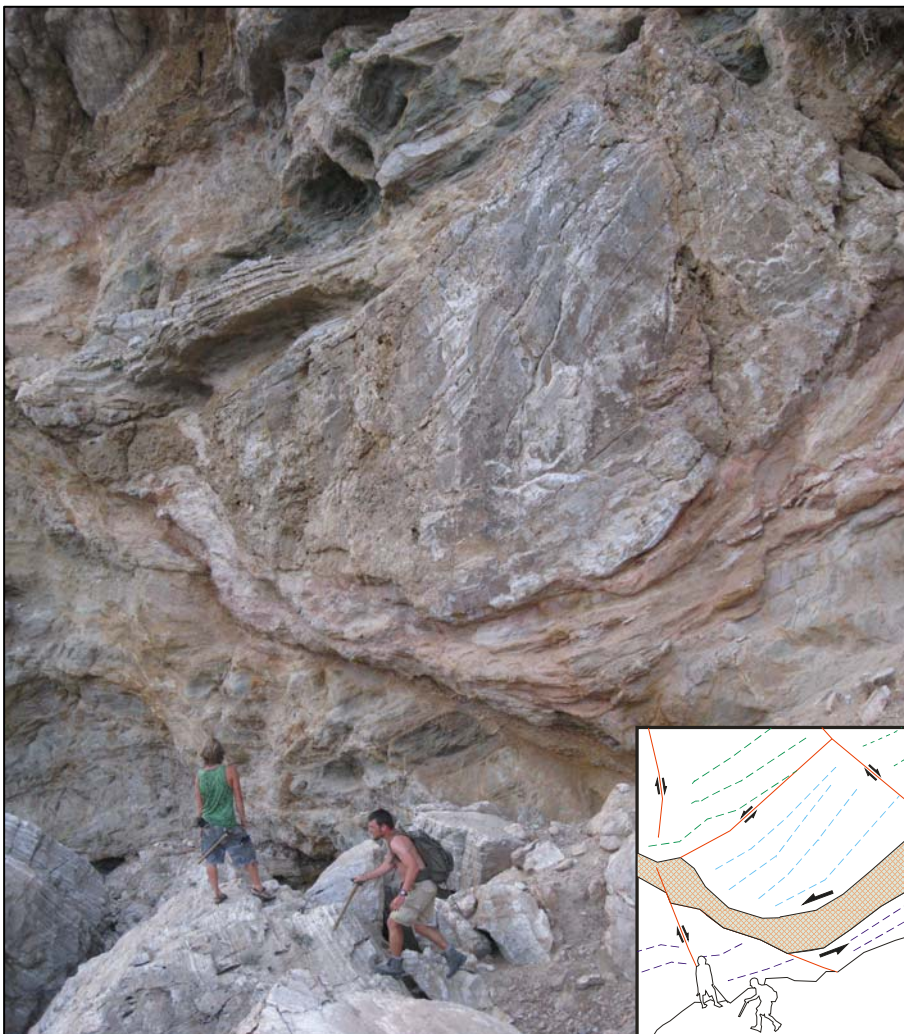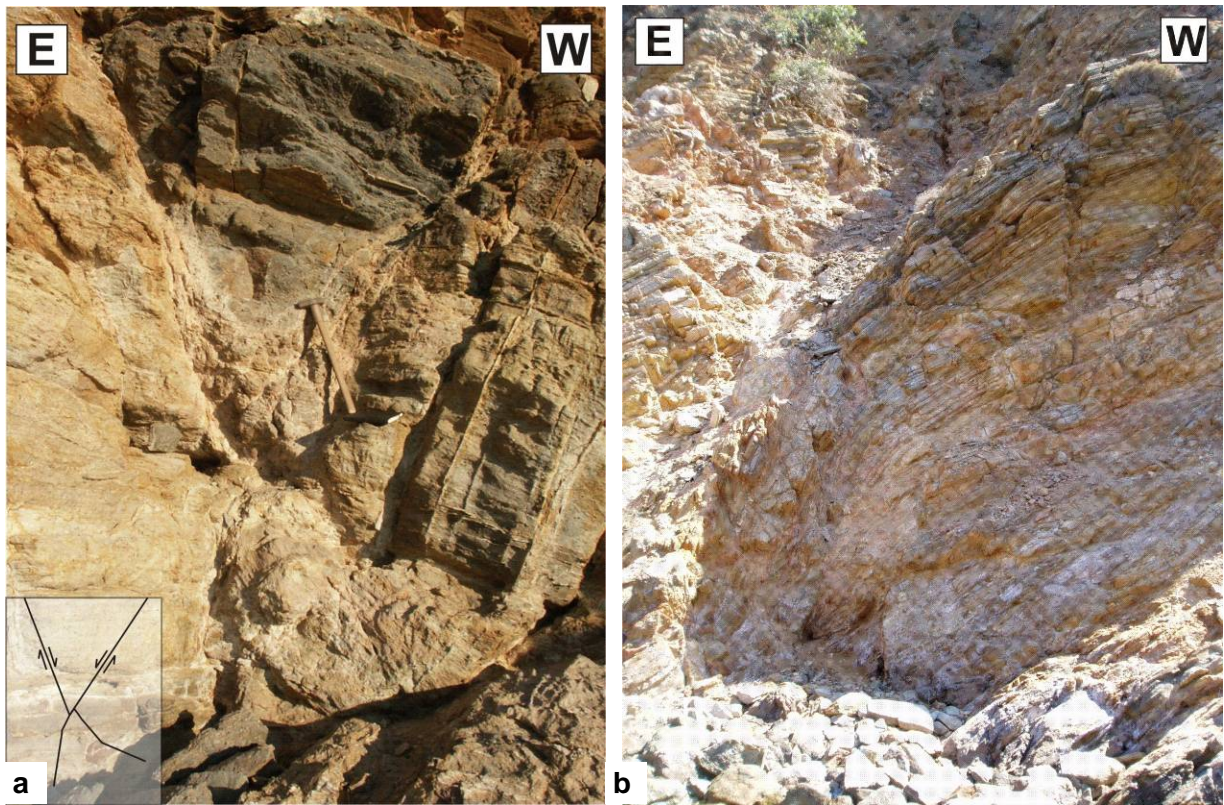
Fig. 21: a) conjugated
system of high-angle
normal faults

b) fault drag along a
brittle-ductile high
angle fault

c) interacting system of
high-angle and low-
angle faults

Fig. 22: Low angle normal fault, with riedel-shear in marble of hanging wall and SCC'-fabric indicating top to SW-kinematics
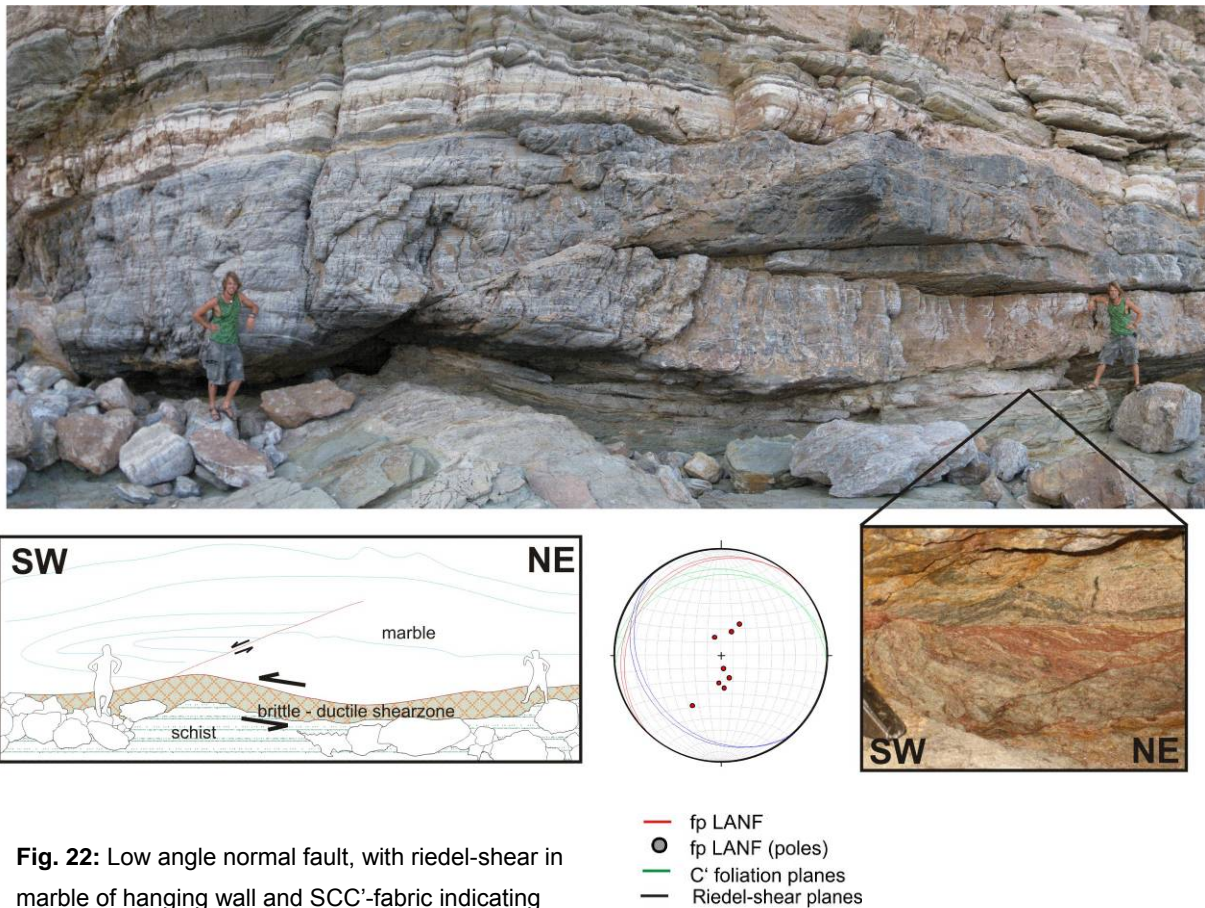
c s interacting system is best to observe in the approximately 20 – 30 m high cliffs at the southern side of the peninsula (*Pounda tou Foti*), where it is exposed in a spectacular way. Blocks large as houses are rotated between meter–wide high angle normal faults in these walls, and the low-angle shear zone undulates between them, mostly displaced by the normal faults, but although deflecting or sometimes confining them.

Fig. 23: Ca. 30 m long slickenside of a SSW directed normal fault, southern coast of *Tourkavlako*

Along the outcrops of silicate rocks and surrounding marbles, the brittle faults are associated with extensive growth of travertine. The marbles in the studied area are intensely karstified, and the contact to the underlying schists and gneisses confines these karst systems to the bottom. While brittle deformation in competent, massive carbonate rocks can lead to a better permeability through newly developed cracks and joints, faults in schistous rocks are commonly sealed. So the CO_2-rich and Ca^{2+}-saturated fluids are brought to the atmosphere along this contact zone, where CO_2 devolatilizes and flowstones of travertine can form.

Some of these sinters have been cut by later, brittle faults, indicating that these faults have been active in relatively recent time.
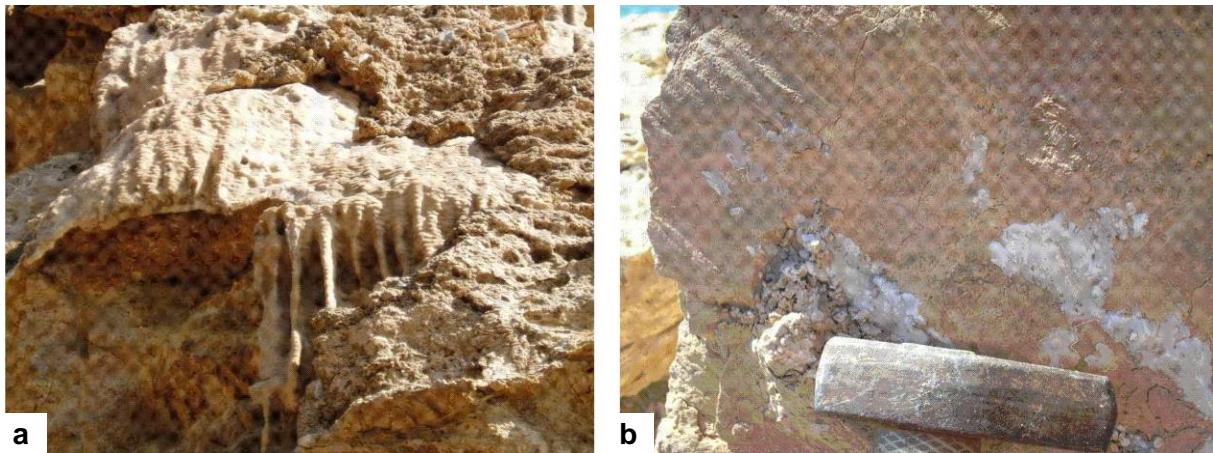
Fig. 24: a) Travertine along brittle normal fault at outcrop south of Fikiada bay. **b)** slickenside on sheared travertine

The youngest observed structures are several meters thick, cataclastic strike-slip-fault zones with proto- to ultracataclastic fault core zones. This fault system is associated with an extensive alteration by hydrothermal fluids. In the marble, the fault cores and the pervasively jointed processes zones are associated with dolomitization of the originally mylonitic, laminated calcite marbles. The fluid traces the more fine grained and impure layers, and therefore the dolomitization follows the foliation. This results in conspicuous structures on the rock surface due to higher resistance of dolomite during weathering processes.

Leitner (1999) describes similar structures and fault zones associated with Mg-rich fluids. He mentions that the *Kontos*-trench, a gully trending SSW from the bay of Vathy, is confined in the west by a major fault with sinistral slip direction, juxtaposing blueschists/gneisses and marbles. Striking directions and similar observations concerning the involved lithologies and fluids allow drawing a major strike-slip-fault up to the bay of Vathy (see map).
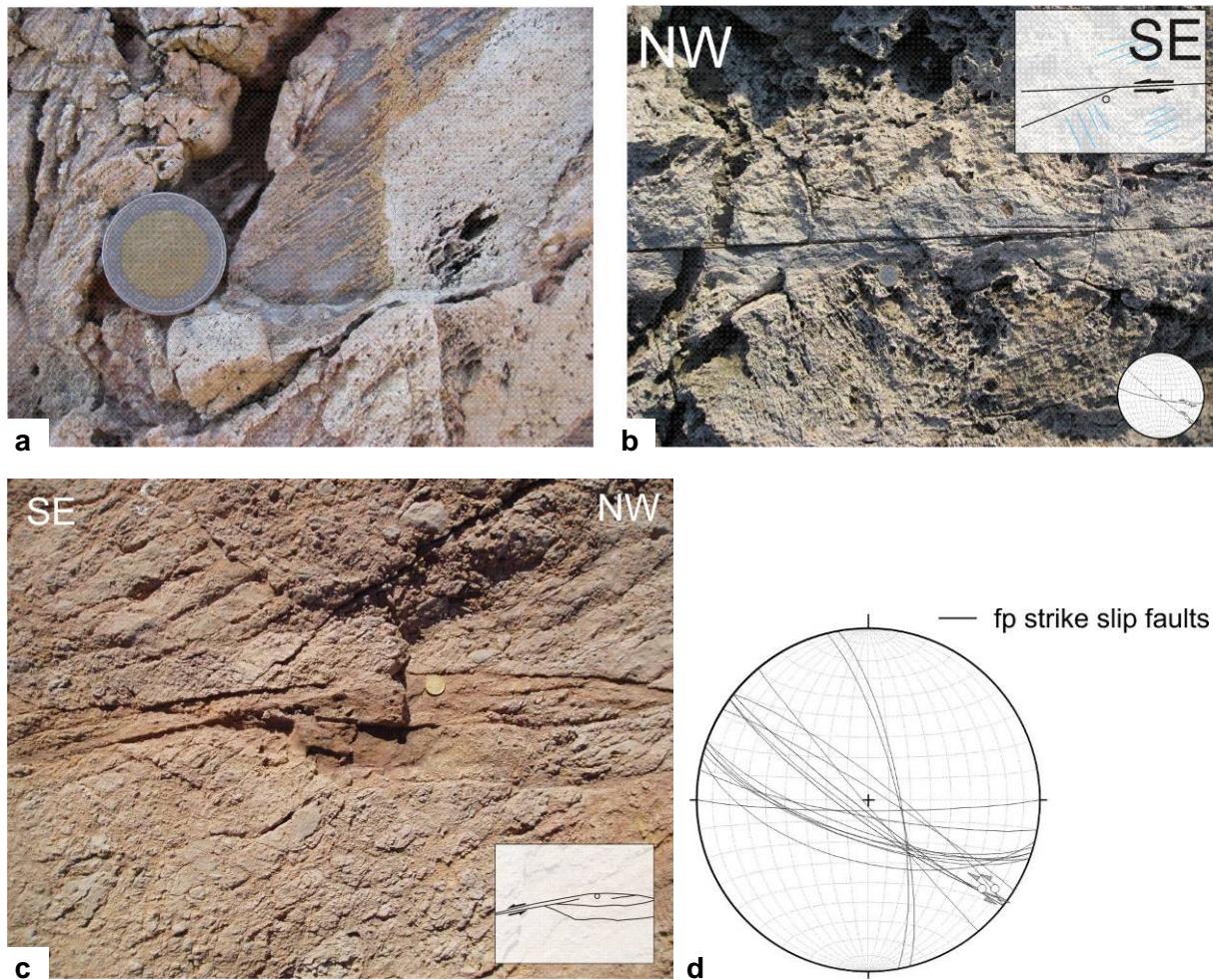
Fig. 25: Dolomitization along cataclastic strike-slip fault system: **a)** laminated, calcitic marble is dolomitized along foliation planes **b)** Young fault plane in cataclastic material (rotated components), with associated dolomitization along the fault. Riedel shear indicates sinistral shear sense. **c)** Ultracataclastic processing zone **d)** stereoplots of measured fault planes

Late volcanic dykes with a thickness of less than 30 cm intruded into these brittle fault zones. All surrounded rocks are strongly altered. The high angle - low angle fault system is cut by veins of quartz, Fe- bearing carbonate and/or hydrothermal Fe- mineralizations. In some small veins (< 5 mm), cutting through quartz, flaky, metallic gleaming minerals show a hexagonal pattern. Under the microscope, these have been identified as so called epitaxic crystals, consisting of intergrown magnetite and rutile, generated as exsolution product of ilmenite (first described by Pelikan 1902). These volcanic and hydrothermal systems are thought to be related to the young volcanism of Milos, the volcanic island approximately 20 km to the southwest.
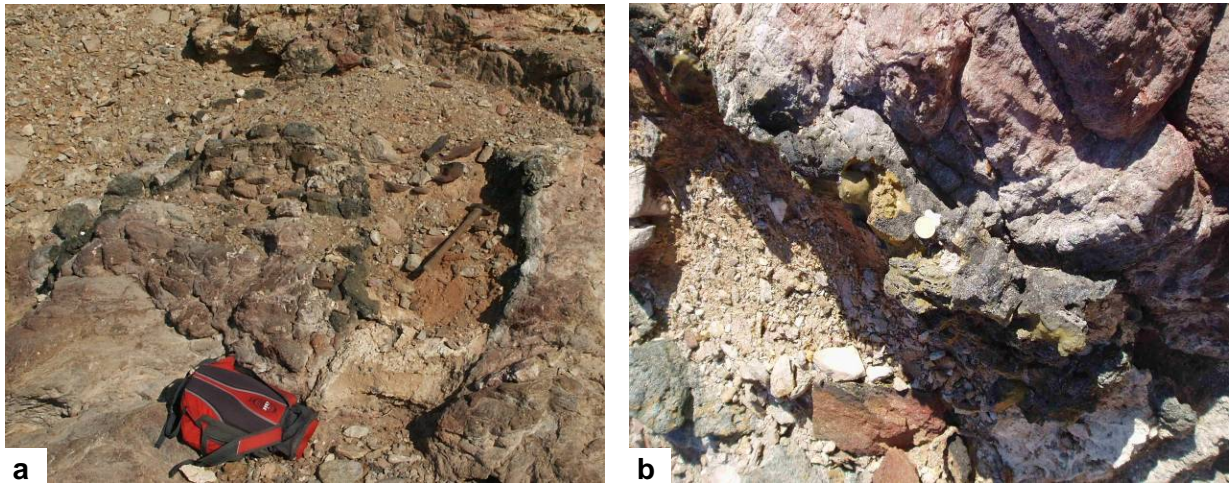
Fig. 26: a, b) Volcanic intrusion

6.4   Conclusion of structural field observations

As a result of the field observations, four main phases of deformation with syntectonic or intertectonic mineral growth can be distinguished for the area of Fikiada bay:

1: Macroscopically, the first phase of deformation is characterized by isoclinal folding and flattening of the layers (the assumption that this layering is of metamorphic origin will be discussed in the next chapter). This phase of deformation is postdated by the extensive porphyroblastic growth of Grt, Gln, Ep and white mica.

2: The development of the dominant foliation and lineation under blueschist-facies conditions. Hinges of isoclinal folds are overprinted by this foliation. Large porphyroblasts act as clasts. Observed fabrics suggest a movement top-to-the-NE.

These phases (1 and 2) can be addressed to the classical M1-high pressure metamorphism and will be discussed below in detail.

3: Extensional shear zones and the development of the interacting system of high-angle faults and south-directed low-angle faults under low greenschist-facies to brittle conditions. This can be interpreted as the local effect of the extensional M2-event.

4: The brittle, cataclastic sinistral strike-slip fault system overprints all other structures, and is postdated only by the intruded volcanic dyke, that does not show any signs of brittle deformation.

38

7 PETROGRAPHY AND PETROLOGY

7.1 Methods

41 rock samples were taken during the fieldwork in September 2008, mostly from the outcrops along Fikiada bay and the peninsula *Pounda tou Foti*, and some samples from outcrops along the way to Platy Gialos. Six samples from an earlier excursion (University of Vienna leaded by Petrakakis, Grasemann in 2005) were although subject to investigation (sample list and locations in Appendix). From these samples, 43 thin section (thickness of ca. 20 µm) where produced for microscopic analyses, using a LEICA DM 4500 p polarizing Microscope with a DCF 420 camera. In the following, mineral abbreviations according to Kretz (1983) will be used.

7.2 Petrographical and microstructural observations

Matthews & Schliestedt (1980) and Schliestedt & Matthews (1987) interpreted the very similar HP-rocks from northern Sifnos (Vroulidia bay) as a volcano-sedimentary sequence. Characteristic metamorphic assemblages of metabasites, meta-acidic rocks and metasediments are given in Schliestedt (1984), see **Fig. 27**.

From the filed observations, following lithologies were distinguished in the working area:

- Blueschist (BS) and intercalated

- light-colored Grt-Gneiss (LGG)

- Eclogite (lenses up to 20 cm)

- Ep-Ab-Chl- Fels

- Carbonate-rich metasediments

- Marble (with intercalations of meta-

  conglomerate and dolomite)

- Greenschist with cm-thick layers of Ab-gneiss,

  occurring in the marble

Table 1. Characteristic metamorphic assemblages in north and central Sifnos (after Schliestedt 1980; Okrusch et al. 1978 and this work)

A. *High-pressure metamorphic assemblages[a] – Blueschist unit, northern Sifnos*

Metabasites

Glaucophanites (□) (± Q, Ru)	Gl – Ep – Gt – Pg – Omph
	Gl – Ep – Ctd – Ph
	Gl – Ep – Gt – Pg – Ph ± Ctd
Eclogites (o) (± Q, Sph, Ru, Ap)	Omph – Gt – Ph – Ep ± Gl
	Omph – Gt – Ep ± Gl
Omphacitites (◊) (± Q, Sph)	Omph – Ph – Ep – Gt – Gl
Actinolithe-bearing Metabasites (*) (± Q, Ap, Ca)	Act – Ep – Ph – Omph ± Gt
	Act – Ep – Gl – Gt – Ph ± Omph

Meta-acidic rocks

Jadeite gneisses (o) (± Ph, Ru)	Jad – Q – Gl – Pg – Gt ± Ep

Metasediments (Δ)

Marbles	D – Cc
	D – Ph – Q
	Cc – Ep – Ph – Q ± Gl ± Chl C Omph
Quartzites	Q – Ct; Q – Gl; Q – Omph – Ep
	Q – deerite-Mt – Gt-aegirine-Augit-crossite
Metapelites	Gt – Gl – Q – Ph – Ep

B. *Greenschist facies rocks of central (and south) Sifnos[a]* (X)

Albite gneisses (± Gl)	Q – Ab – Ph – Chl – Cc – Ep - ± Act
Greenschists	Ep – Chl – Ab – Ph – Cc – ± Act ± Q

* Symbols:

Q	= quartz	Ph	= phengite	Gt	= garnet
Pg	= paragonite	Omph	= omphacite	Ep	= epidote
Ctd	= chloritoide	Gl	= glaucophane	Act	= actinolithe
Jad	= jadeite	Mt	= magnetite	D	= dolomite
Cc	= calcite	Chl	= chlorite	Ru	= rutile
Sph	= sphene	Ap	= apatite		

Fig. 27: Lithologies and characteristic metamorphic assemblages in north and central Sifnos (from Schliestedt 1984, table 1, after Schliestedt 1980 and Okrusch et al. 1978).

Blueschist and Light-colored Grt-gneiss

As described above, BS and LGG occur in intercalated layers of several dm to m thickness. They show a very similar fabric.

In the blueschists, the matrix is built up by Gln (>30% vol. per cent), Phn, Pg, Ab, Qtz and Rt, with a well developed foliation defined by Gln and the micas. LGG have more Qtz, Ab, mica and Ep and less Gln. Accessory phases are Ttn, Ap, Rt and Mag. Large porphyroblastic crystals of Grt, Ep and Carbonate deflect this foliation. Grt-crystals have diameters up to 30 mm and are characterized by an extreme poikiloblastic habit. Their complex inclusion pattern is described below. They act as porphyroclasts and mostly deflect the dominant foliation, but in some samples, crystals appear elongate and spindle-shaped, confined by ductile shear bands with white mica and Qtz-ribbons up to 5 cm long, suggesting a late phase of syntectonic growth. Especially in the vicinity of large Grt-porphyroblasts, shear bands are common. SCC'-fabrics carried by Gln and mica indicate a shear sense of top to NE.

Late veins along small shear zones are associated with fluid intrusions and retrograde growth of Chl, Ab, Phn, Carbonates and Fe-hydroxides and overprint the dominant foliation.

The large Grt-porphyroblasts form a monocrystall network (so-called dyctionitic growth), growing over an earlier fabric oblique to the main foliation. Similar Grt-structures have been described by Stöckhert et al. (1997) from eclogites of the Tauern Window, Eastern Alps. The pattern of the inclusions reflects a compositional layering with domains of massive Grt and domains very rich in Qtz. Grt grows interstitially among Qtz- grains, forming approximately 10 to 30 µm wide seams, mimicking the original high angle grain boundaries. Triple points with angles of 120° suggest static crystallization of this relictic Qtz-fabric, typical for a so called foam structure (Underwood, 1970). The grain boundaries of Qtz are nearly normal to the borders of massive Grt, a geometry that is typical for fabrics of Qtz and mica, dominated by the low angle grain boundaries of mica (Vernon, 2004, A practical guide to rock microstructures). Stöckhert (1997) observed similar fabrics and suggested that massive Grt has replaced former mica layers. This is also true for the here investigated samples, as examples of the LGG (sample 010A) indicate impressively (see **Fig.30 a,b,c**): Grt has grown over a strongly foliated fabric of mainly Qtz and white mica. This happened under static conditions, the overgrown foliation is not bent or wrapped in the growing Grt. During a subsequent deformation, the Grt rotated, but in the strain-shadows, the original orientation of the overgrown mica-layers was preserved. They form a direct extension of the "massive" Grt-domains. Stöckhert pronounces the extreme low probability of nucleation indicated by the

size and distribution of Grt (comparable to the here investigated samples), and that the growing Grt must have been supplied with its chemical components by grain boundary diffusion.
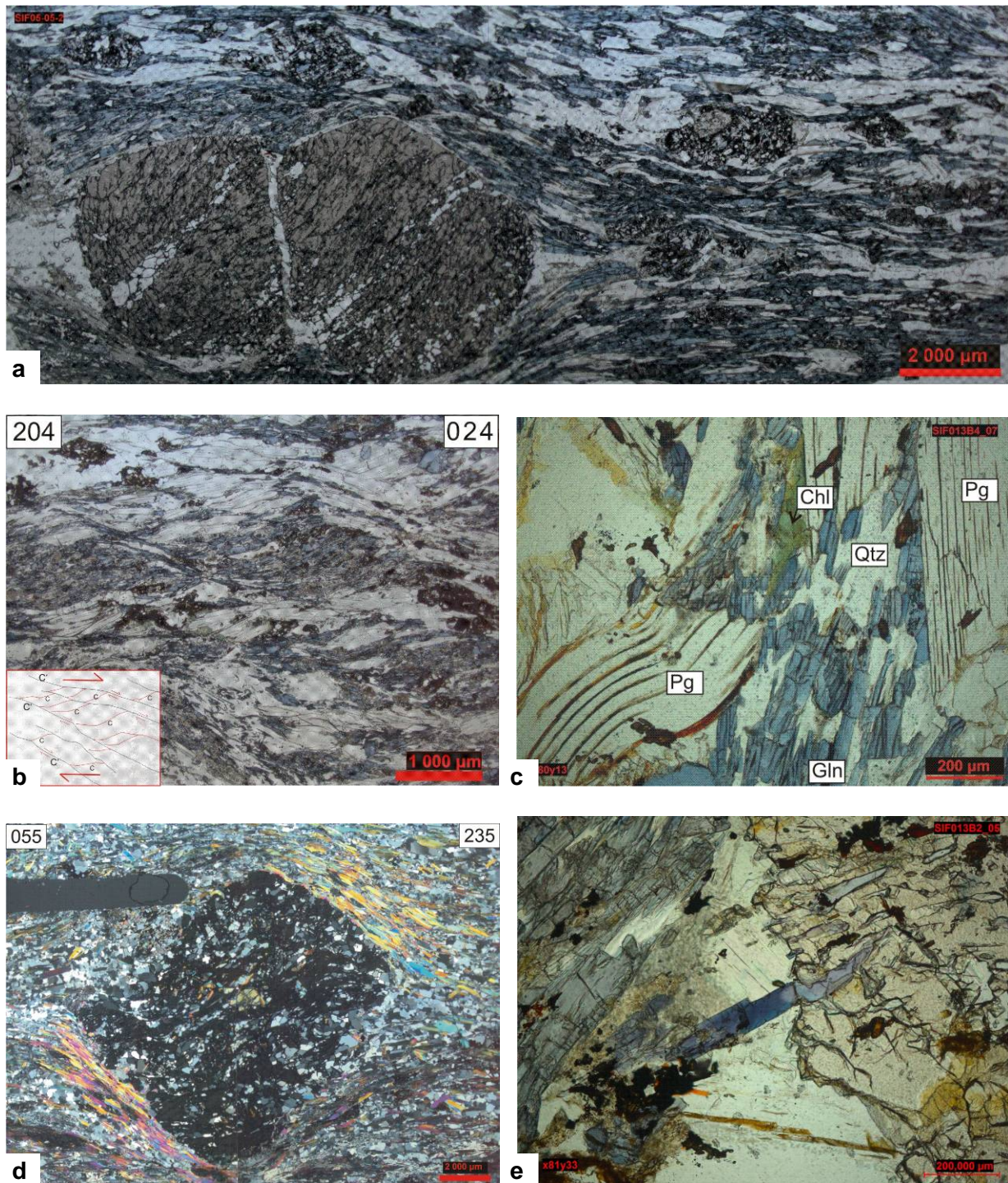
Fig. 28: Photomicrgraphs of blueschist-samples: **a)** intergrown Grt-porphyroblasts with internal fabric deflect main foliation. Relictic pseudomorphs after Arg act as clasts.   **b)** SCC'-fabric in blueschist, indicating top-to-NE-kinamtics   **c)** porphyroblastic Pg with Gln growing in strainshadow, kinked and with Fe-hydroxides growing between c-planes. Retrograde Chl   **d)** inter- to syntectonic Grt, indicating top-to-NE-kinematics (xPL)   **e)** Grt gowing over Na-amphibole. Intense bluish color indicates more crossitic composition (compare BSE-image, **Fig38 b**)

41

The composite layering preserved in the Grt-blasts is observed in all samples and can therefore be interpreted as a penetrative fabric, resulting from earlier folding and the establishment of a crenulation cleavage, with Qtz-rich domains representing the microlithon- and massive Grt-domains the cleavage domains. In sample (SIF014), an inclusion pattern of massive Grt, Qtz-rich domains and an earlier, folded foliation is conserved very well by a completely statically crystallized Grt-porphyroblasts (**Fig. 29**). The strain shadows of the Grt and the surrounding foliation were created much later and have nothing to do with the internal pattern. Especially the domains of massive Grt (former cleavage domains) record an earlier mineral assemblage: Inclusions consist of needle-shaped Gln and Rt, Jd, Ctd, Ep, Phn, Pg and sparse quartz. In LGG, inclusions in Grt mostly consist of Qtz, Ep and relictic Jd or pseudomorphs of Ab and Pg after Jd. Small crystals of magnetite have been identified with the EMP and indicate a high oxygen fugacity for this HP-assemblage. Integrated in the overgrown layering, nearly inclusion-free, massive Grt domains with diameters up to 1 mm and idiomorphic shapes are interpreted as relics of an older Grt-generation.

Fig. 29: Poikiloblastic Grt in light Grt-gneiss, conserving an earlier folding structure.
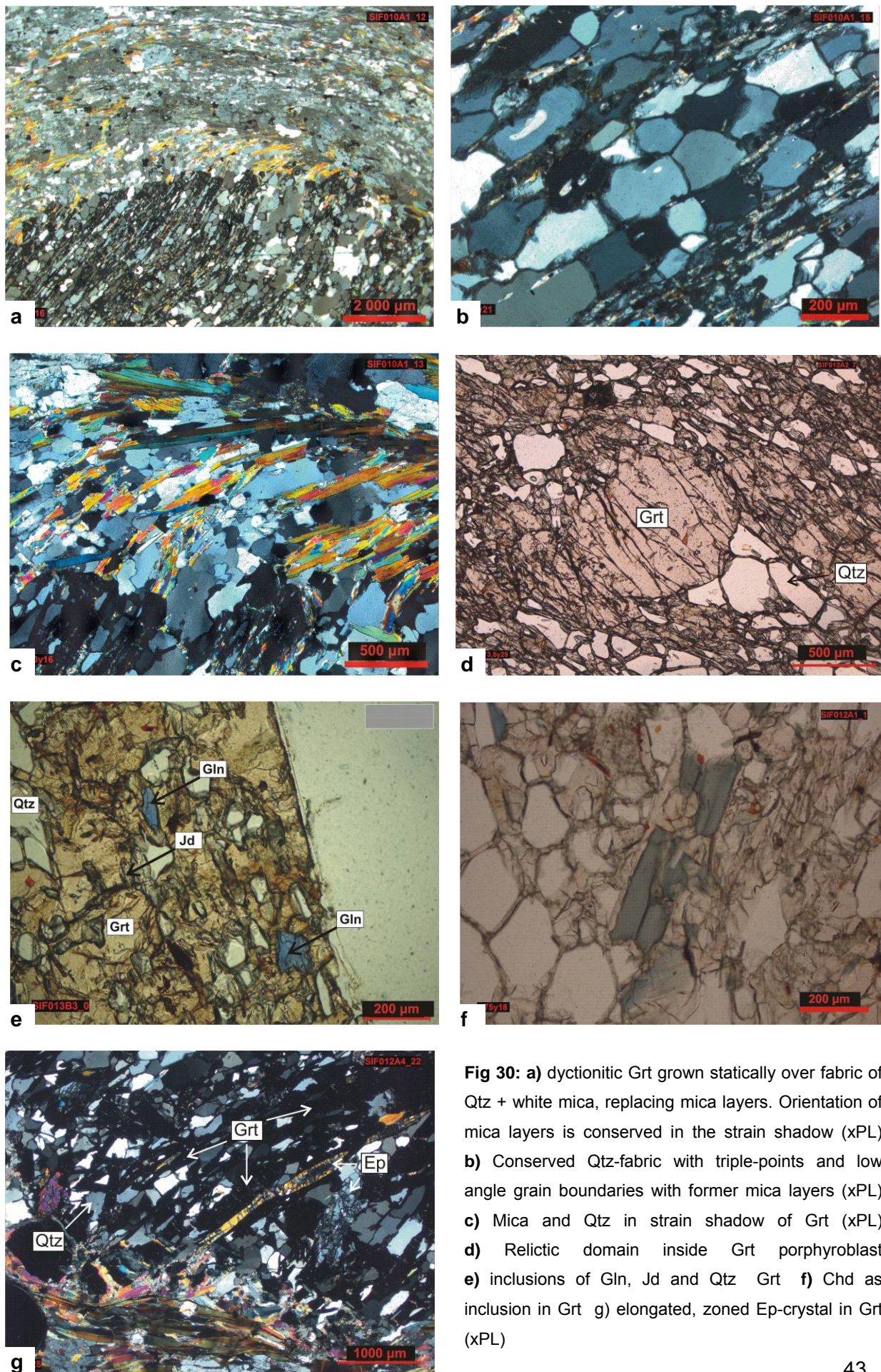
Fig 30: a) dyctionitic Grt grown statically over fabric of Qtz + white mica, replacing mica layers. Orientation of mica layers is conserved in the strain shadow (xPL) **b)** Conserved Qtz-fabric with triple-points and low angle grain boundaries with former mica layers (xPL) **c)** Mica and Qtz in strain shadow of Grt (xPL) **d)** Relictic domain inside Grt porphyroblast **e)** inclusions of Gln, Jd and Qtz Grt **f)** Chd as inclusion in Grt g) elongated, zoned Ep-crystal in Grt (xPL)

43

At least three different structural positions of white mica, both Pg and Ph, can be distinguished: 1. Inclusions in Grt are both Phn and Pg and define the relictic foliation. 2. Porphyroblastic, but mostly foliation parallel large crystals can be bent and contain veins of Cal and Fe-hydroxides parallel to the c-planes. Grains are partly resorbed and act as porphyroclasts to the dominant foliation. 3. Later, smaller grained Pg and Ph grow S-parallel in the dominant foliation, the strain shadows of Grt and Ep porphyroblasts and in shear bands. In samples of LGG, the retrograde breakdown of Pg can be observed, with old large Pg crystals and Phn being gradually resorbed and replaced or enclosed by statically growing Ab, new Msc and Chl or opaque Fe-ore-minerals.

Besides the inclusions of Ep in Grt, that can also show chemical zoning, large (up to 5 mm long) porphyroblastic Ep crystals are common. Elongate crystals show foliation-parallel orientation and act as porphyroclasts to the dominant foliation. Ep is more abundant in LGG and shows typically compositional zoning (decreasing interference colors due to decreasing Fe-content from core to rim).

A common feature in BS, and more abundant in LGG, are elongated, rhombic Cal-crystals up to 5 mm in length with Fe-hydroxides tracing the cleavage planes. They show stable grain boundaries with Grt, act as porphyroclasts to the dominant (blueschist-facies) foliation and are therefore interpreted as pseudomorphs after Aragonite. The observed Fe-minerals seem to be the product of Fe-rich fluids, that have been associated with the re-crystallization of Aragonite to Calcite. Another explanation could be primary Fe-contents, as they can be found in crusts of Fe-hydroxides around small grains of calcitic sediments. During the re-crystallization, these Fe-impurities would accumulate along crystallographic planes.

In contrast to the high-temperature Qtz fabric conserved by overgrowing Grt, Qtz microstructures in the strain shadows of Grt or Ep (ribbons)and the matrix have irregular grain shapes and lobate or sutured grain boundaries. Patchy extinction, subgrain rotation and LPO-patterns can be observed. This indicates ductile deformation by dislocation creep and temperatures of approximately 350°C, documenting the influence of differential stress at a relatively late and cool stage. The preferred orientation of the c-axes in Qtz of the matrix and in S-parallel veins indicates shear sense of top to NE (consistent with the higher tempered SCC' fabrics described before) and a strong coaxial flattening during this deformation.
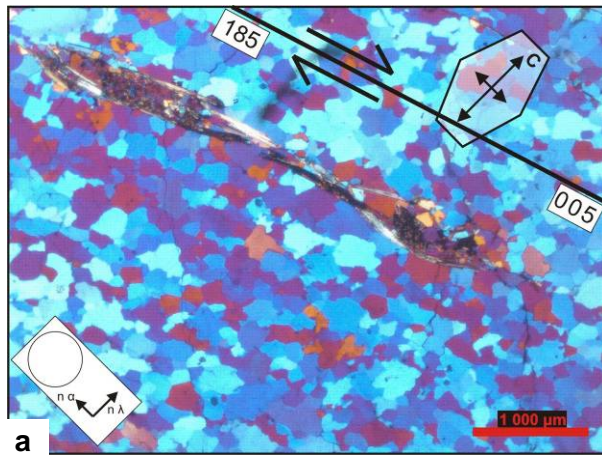
Fig. 31: a) LPO-pattern (xPL with tint plate) in dynamic re-crystallazed Qtz-vein, indicating top-to-N kinematics and a strong coaxial flattening **c,d)** Pg and Phn replaced by Ab, Msc and Chl and opaque Fe-phase (a: parallel nichols, b: xPL) **c)** relictic pseudomorph Cal replacing Arg, with Fe-ore-minerals tracing the cleavage planes **d)** Ep-Ab-Chl-fels: foliation 1, defined by Gln-inclusions in Ep-porphyroblast, and foliation 2, deflected by this Ep
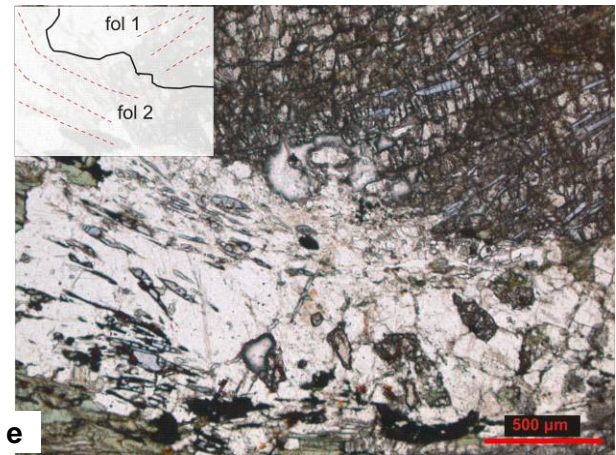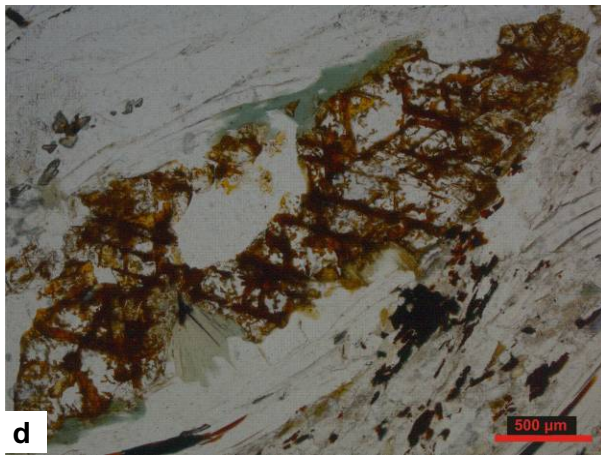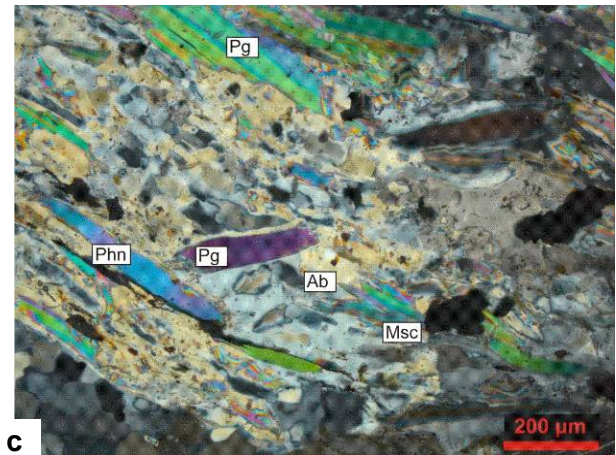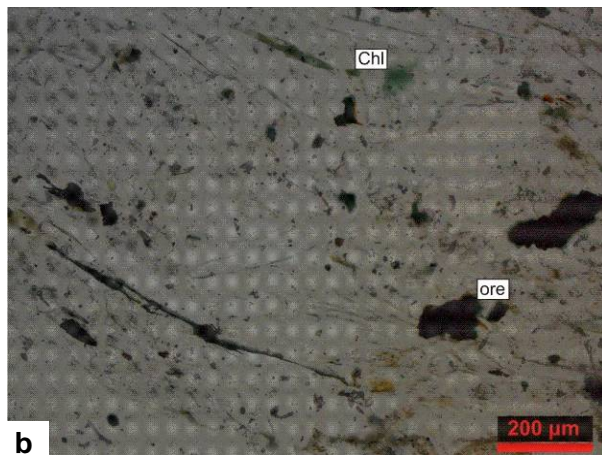
Ep- Ab- Chl- Fels

These very coarse grained, massive greenish rocks are composed of Ab, Ep, Chl, Phn and Gln have a characteristic felsic fabric. Under the microscope, a completely static crystallized fabric of Ab, Chl and Ep that has overgrown older deformation structures becomes visible. Two relictic foliations can be observed: The oldest fabric element is a well developed foliation, defined by small crystals of Gln and Ep. It can be found in porphyroblastic Ep.

These Ep-porphyroblasts deflect a second foliation, defined by Gln and Phn. Idiomorphic Grt is conserved only in relics and mostly replaced by pseudomorphs of statically grown Chl. These relics also deflected the second conserved foliation. Ep- crystals reach more than 20 mm in diameter and show a well developed chemical zoning (decrease of Fe from core to rim), that can be observed as a decrease of interference colors. This zoning is partly gradually, but partly very distinct: Three different structural types can be distinguished: The large, porphyroblastic crystals (type 2) are very rich in fine grained inclusions and grow over the first relictic foliation, but deflect the second one. In these porphyroblasts, relictic domains can be observed (type 1). Smaller, elongated to round grains of Ep can also be found as inclusions as well in Ab and Grt. Around the porphyroblasts of type 2, rims of a later generation can be observed (type 3), typically with a sharp boundary and a contrast in interference-color (higher order see **Fig. 32 d**, characteristic for a higher Fe-content). These rims are more massive and bear lesser inclusions than type 2, but grow over the second foliation. They are statically intergrown with Chl and Ab and define the dominant patchy, felsic fabric. Accessory phases are Ttn, Ap, Rt and Mag.
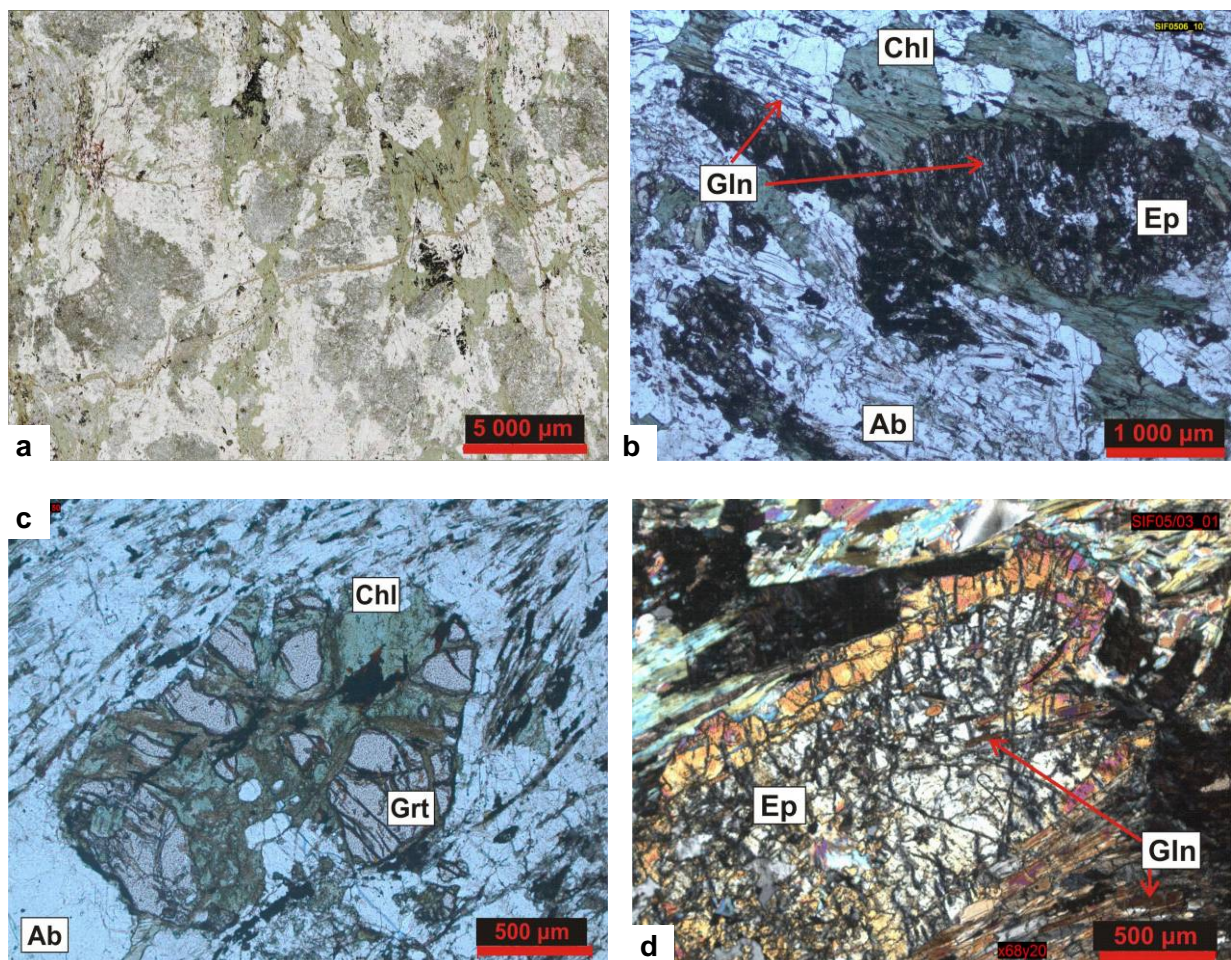
Fig. 32: a) static crystallized fabric of Ep-Ab-Chl-fels   **b)** "felsic" Ep-Ab-Chl fabric growing over Gln+Phn foliation   **c)** Grt resorbed and statically replaced by Chl   **d)** zoned Ep-porphyroblast, with relictic foliation 1 defined by Gln-inclusions (xPL)

46

Eclogite

As mentioned above, eclogites occur only as relictic lenses inside the blueschists. These lenses are surrounded by Qtz-veins, strongly aligned Gln and especially at the margins accompanied by growth of large white-mica-crystals that can also be found along vein-like structures cutting through the massive fabric of pyroxene and Grt. Smaller crystals of white mica can also be found in this massive fabric, growing stable next to Pyroxene and Grt. Compositions are described in the next chapter (mineral chemistry).

The massive eclogite-fabric is made up typically of a compact matrix of greenish Pyroxene and smaller amounts of Phn and Gln, and idiomorphic Grt-crystals up to 10 mm in diameter. Compared to the eclogites of Vroulidia bay in the north, the lighter greenish color of the pyroxenes is suspicious, and a foliation can be observed only at the margins at the transition to blueschist. Gln occurs as inclusion in Grt, in the matrix and in later veins. Some idiomorphic Gln-crystals show a chemical zoning, indicated by their change in color (more intense blue to the rim due to a more crossitic composition). The Grt-crystals bear inclusions, but are more massive and do not conserve patterns like the large porphyroblasts in blueschist and light-colored Grt-gneiss. As inclusions were found: Gln, Jd, Ph, Pg, Qtz and Ep.

In the same structural position like the lenses of eclogite and Fe-carbonates embedded in the blueschist, clusters of idiomorphic greenish crystals, up to 5 cm in length, and Qtz can be found. In the thin section, the green needle-shaped crystals have been identified as Zoisite. Long idiomorphic crystals are broken and boudinaged in a matrix of dynamic re-crystallized Qtz (see **Fig. 33**).
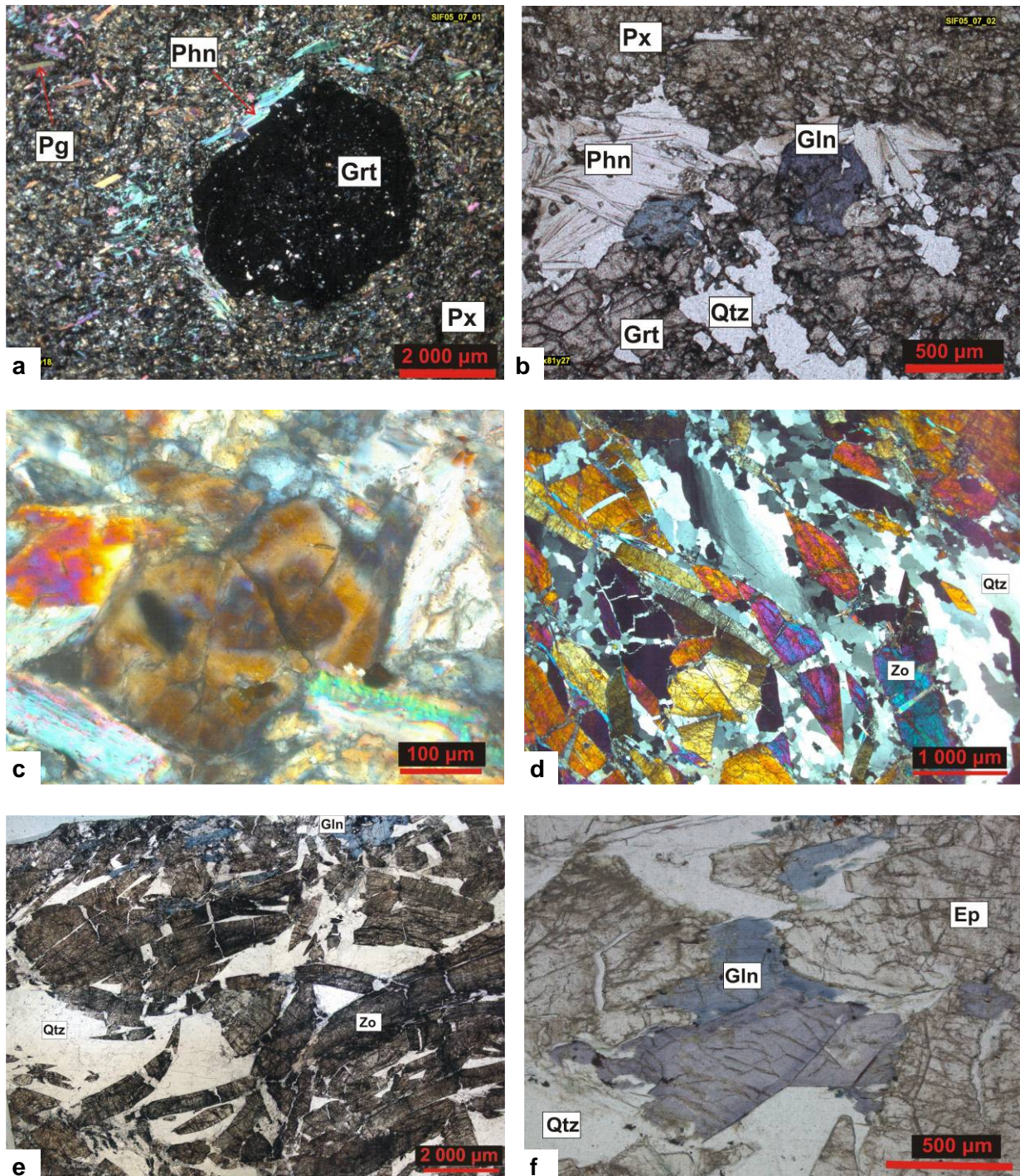
Fig 33 a) fabric of eclogite, xPL **b)** Stable association of Grt, Gln, Phn, Jd and Qtz **c)** zoned Jd-crystal, together with Phn in eclogite-fabric (xPL) **d,e)** Brittle deformation of idiomorphic, zoned Zo-crystals in matrix of ductile deforming Qtz (c: xPL, d: pPL) **f)** zoned Gln, intergrown with Ep. (pictures b,c and d from Ep-rich lens in blueschist)

Marbles

The marbles are bearing varying amounts of white mica, Qtz, Fs, Chl and Dol. Coarser- and finer-grained layers can be observed. Laminated marbles with yellow, greenish or bluish colors have mostly coarse grained, static re-crystallized fabrics, but laminations, flat lying,

48

rootless isoclinal folds and boudinaged dolomitic layers document the earlier deformation, and a stretching lineation can be observed commonly.
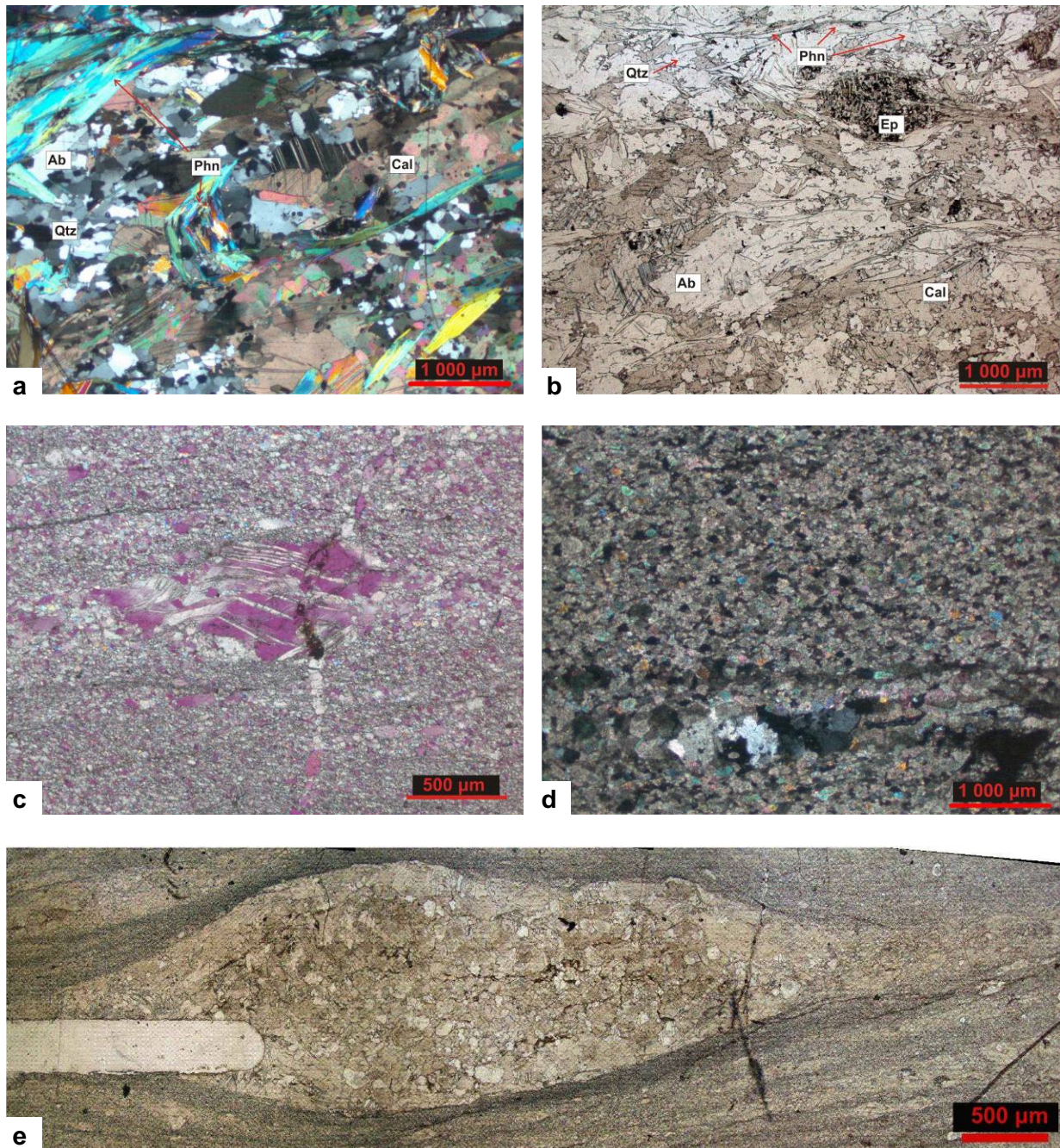
Fig 34: Carbonate-rich metasediments, **a)** relictic fold in microlithon-domain (xPL)   **b)** Fabric with relictic Ep-porphyroblast   **c)** Porphyroclasts in mylonitic marble   **d)** mylonitic dolomite, DOL   **e)** dolomitic boudin in calcitic mylonitic

Especially near the contact to the underlying assemblage of silicate HP rocks, mylonitic structures with porphyroclasts of dolomite, Qtz and larger calcitic grains are common. Younger veins of coarse grained calcite cut through these fabrics.

Carbonate- rich metasediments

These light colored rocks have massive to gneisseous fabrics, and consist mainly of static crystallized Ab, Cal, Qtz and white mica, with relictic porphyroblastic crystals of Ep.

The foliation is defined by white mica, that also defines a compositional layering between layers of Qtz, Ab and Cal. Relictic folds, defined of mica can be found in these layers (microlithon-domains).

Greenschist and Ab-gneiss

Greenschists and therein occurring thin layers of Ab-gneiss intercalated in the marble sequence have been sampled along the way to Fikiada bay to compare them to the silicate rocks in the main working area. Cm-thick layers of light Ab-gneiss are embedded in greenschists of more mafic composition, consisting of Chl, Ab, Msc, Ep, Ca-amphibole, Qtz and relictic Grt. Light layers contain Ab, Qtz, Msc, Grt and Ep. Gln occurs in both lithologies as small, needle-shaped inclusion, overgrown by Ab, Chl and Ph. It defines a strong, relictic foliation. The distinct compositional layering is apparently a result of isoclinal folding and subsequent thinning of the layers. Parallel to the layering and axial planes, a foliation is defined by mica, Ep and Gln, overprinting the isoclinal folds (best documented in thin sections of sample SIF017A2, taken from the hinge of a folded layer of Ab-gneiss, see **Fig. 17 g**, chapter 7).

Grt occurs in idiomorphic porphyroblasts, well preserved and only marginally chloritized in the light, Ab-rich layers, while it is almost completely replaced by Chl only within 1 cm distance in the adjacent, more mafic greenschist-layers. Grt crystals have diameters up to 3 mm and show inclusion patterns similar to those observed in blueschists and light Grt-gneiss, although the porphyroblasts are much smaller in size. Inclusions consist of mainly Qtz and Ep, and neither Jd nor Ab could be observed as inclusion in the investigated samples. Varying angles of overgrown inclusion trails to the foliation of the matrix indicate a rotation, postdating the static poikiloblastic growth of Grt. Ca-amphiboles are mostly aligned in the dominant foliation, that is defined by Chl and white mica, but also disorientated crystals can be found. Ep occurs in small, granular crystals trough out the fabric, overgrown by Grt, Phn, Ab and a second generation of larger, needle shaped Ep-crystals. A zoning pattern with typically decrease of Fe from core to rim is common.
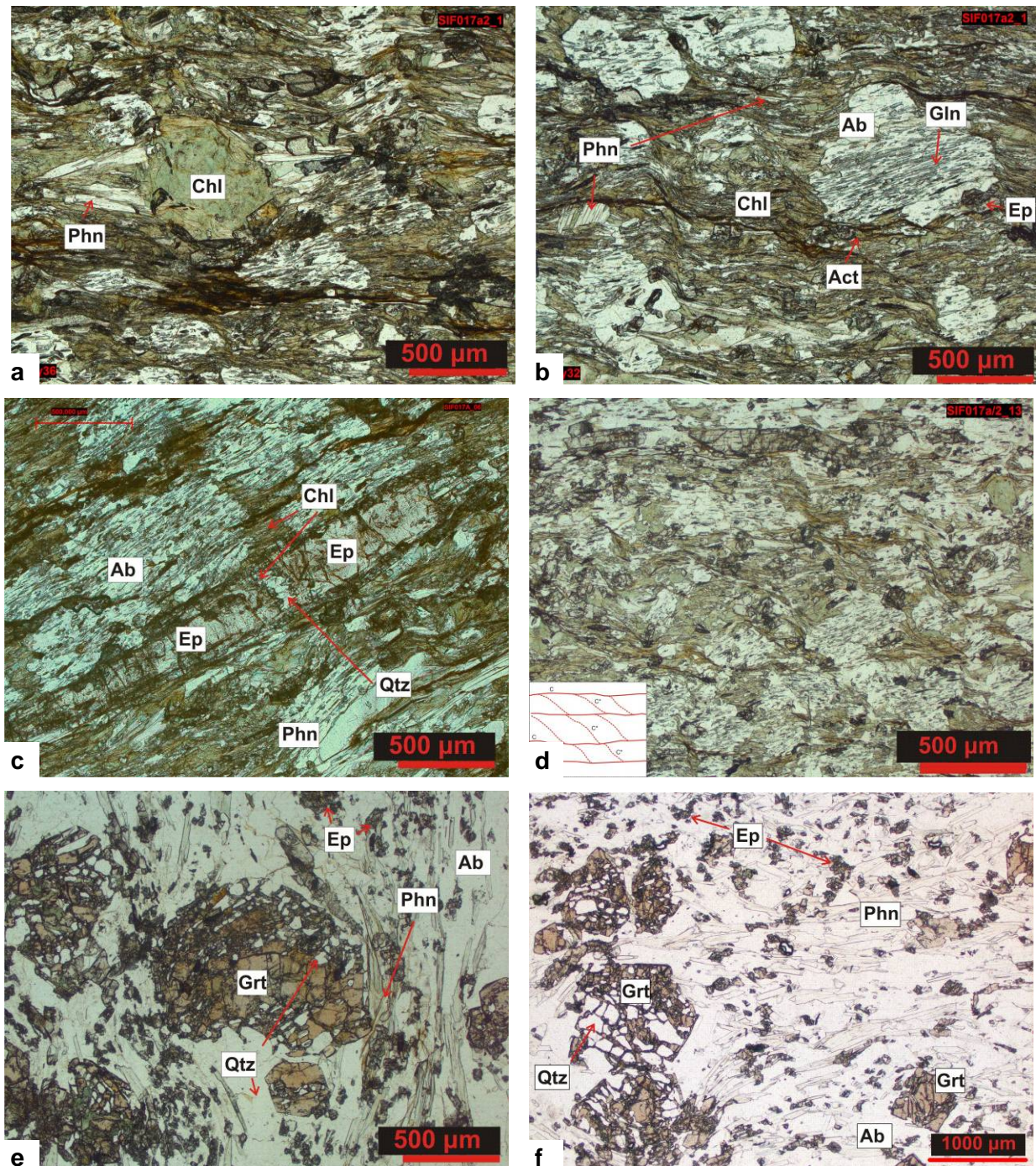
Fig. 35: a) greenschist: Grt completely replaced by static crystallized Chl **b)** static crystallized Ab with overgrown foliation of Gln **c)** boudinaged Ep-crystal and Ab-clasts with syntaxial growing Chl, Phn and Qtz **d)** asymmetric crenulation cleavage overprinting Ab-blastesis and foliation **e,f)** Grt in Ab-gneiss layer in greenschist, with relictic foliation (defined by Qtz-inclusions) Grt with

White mica is of phengite- composition (see next chapter) and occurs as old, large porphyroclast as well as in the main foliation (stable grain boundaries with Grt, Ep, and Ca-Amphibole) and as later crystals intergrown with Chl. The old foliation defined by Ep, Gln and Msc is pervasively overgrown by patchy Ab and Chl. These Ab-porphyroblasts with

51

diameters up to 3 mm are then affected by younger deformation processes, where they act as porphyroclasts. Long, needle-shaped Ep-crystals are boudinaged with Chl, Phn and Qtz growing from the necks during this deformation and the development of the associated foliation.

Even later, another tectonic event generated an asymmetric crenulation cleavage that is inflected by Ab-crystals, with syntectonic growing Chl, Msc and Fe-hydroxides. This might indicate a late folding of the rock unit.

Rocks of greenschist-facies shear zones

Some samples where taken out of late, ductile shear zones in blueschist and Ep-Ab-Chl-fels. Macroscopically, a strong influence of fluids and alteration (brown to reddish colors) was observed. In the sample of former Ep-Ab-Chl-fels, the static fabric is totally overprinted. Ep breaks down and occurs only relictic, while Ab-blasts act as clasts and are accompanied by growth of Chl and carbonate in the strain shadows. Fe-hydroxides grow in shear bands, and large, idiomorphic crystals of Mag and other opaque Fe-phases overgrow the fabric.

On outcrop scale, a stronger retrograde overprint and stronger influence of fluids associated with growth of Mag and Cal (e.g. sample SIF011) towards the overlying marble and the large shear zone at the lithological contact can be observed. Better preserved blueschist was found at lithostratigraphic lower positions. In the retrograde overprinted and altered blueschist and gneiss near the shear zones, Grt, Gln and Ep are found only relictic, and the rocks consist mainly of Ab, Chl, Qtz, Carbonate and opaque Fe-phases.
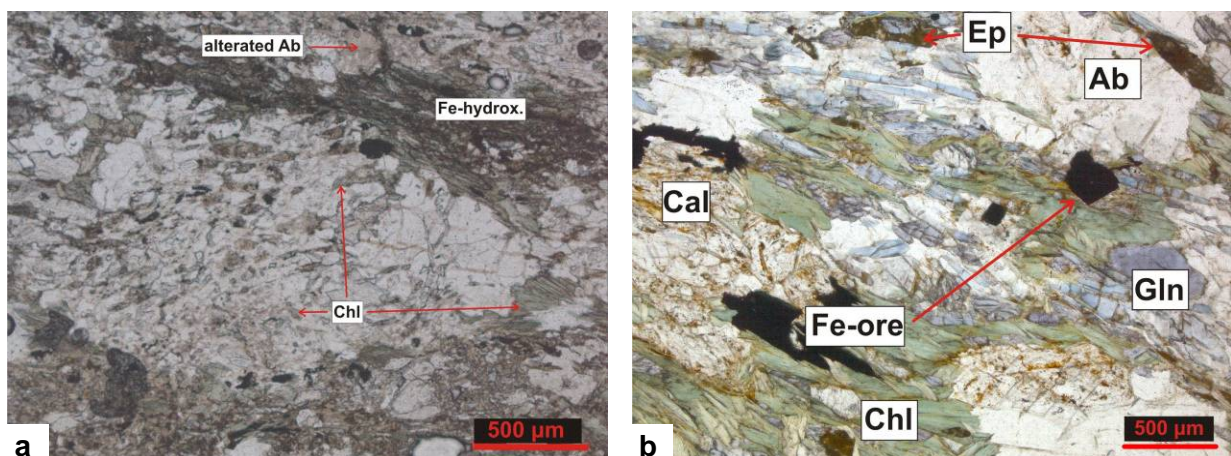
Fig 36: a) Ab-porphyroclast in sample from margin of brittle-ductile shear zone Gln-inclusions replaced by Chl, Fe-hydroxide and altered Ab (yellowish color) indicate hydrothermal fluid activity **b)** retrograde overprint in BS near shear zone: breakdown of Gln, extensive growth of Chl, Cal and opaque Fe-phases

7.3 Summary: Deformation- and mineral growth events

Various phases of deformation and mineral growth can be distinguished and correlated in the investigated samples. The observed fabrics of course depend on the structural position of the samples, and not all phases can be observed in all samples. It is also obvious that the bulk composition and the effect of later deformation processes play the most important roles in the re-equilibration of mineral assemblages.

Forster and Lister (2005) distinguished four distinct episodes of metamorphic mineral growth during the classical "M1 – metamorphic event" for the Cycladic Blueschist Unit (described on p. 525-527). These defined episodes are in good agreement to the observations in the studied area, and therefore this proposed nomenclature was used in this work to address the microstructurally observed phases accordingly (M1 split up in M_{1A} to M_{1D} –episodes).

M_{1A} : The first episode of mineral growth reported in this work is characterized by the growth of Gln and Lws, associated with a strong foliation and lineation. This episode represents the preserved prograde part of the PT-path.

M_{1B} : This episode includes the eclogite-facies with growth of Jd and Omp. The development of eclogite-facies shear zones and subsequent recumbent folding of eclogite-facies fabrics (foliations and lineations) is reported (nice examples are the eclogites of Vroulidia bay, northern Sifnos). Forster and Lister (2005) pronounce that locally, M_{1A} –fabrics are preserved, and they do not show an eclogite-facies overprint. M_{1C}- porphyroblasts grow directly over M_{1A}- fabrics in some places. They conclude that "metamorphic mineral parageneses were not pervasively developed throughout the rock mass during M_{1B} times" and eclogite-facies equilibrium was not obtained everywhere.

In the investigated samples from southern Sifnos, the earliest fabrics are preserved in the large porphyroblasts (Grt in BS and LGG, Ep in Ep-Chl-Ab-Fels): A well developed foliation (and lineation?) with mineral assemblages of the eclogite-blueschist-facies:

Grt + Gln + Ep + Phn + Pg + Jd/Omp ± Chd + Qtz

Lws could not be detected, but because the earliest mineral assemblages are conserved only relictic or as pseudomorphs, $M1_A$/$M1_B$ can not be precisely separated in the working area. The described recumbent folding of the foliation in late M_{1B} could explain the crenulation cleavage and the folded fabric conserved in later Grt-porphyroblasts (e.g. sample SIF014B). The macroscopic isoclinal folding and metamorphic layering predates the

following episodes and is overprinted by the dominant foliation, and might therefore be seen as an effect of this early folding.

M_{1C}: This phase of intense static, porphyroblastic growth, followed by the development of an intense foliation is characteristic throughout the Cyclades.

All investigated lithologies around Fikiada bay record this episode, large porphyroblasts of Grt, Ep, Gln, Fe-carbonate, Phn and Pg are dominant characteristics in some lithologies. Obviously, most of this phase of extensive mineral growth was characterized by static conditions, strikingly indicated by the dyctionitic growth of Grt. But the subsequent deformation already starts in a late stage of porphyroblastic growth, documented by the adjustment of Gln, Ep and Fe-carbonates to the dominant foliation and by examples of sigma-shaped Grt and mica- crystals in BS and LGG.

M_{1D}: This phase is characterized by "transitional blueschist-greenschist facies metamorphism" (Forster and Lister, 2005, p. 527), with mineral assemblages typical for the Ep-Ab-blueschist facies of Evans (1990), that is also described by Okrusch & Matthes (2005). Under these conditions, one characteristic is the stability of Chl together Gln+Ep+Ab+Phn+Pg+Qtz or Gln+Ep+Ab+Phn+Ca-amphibole in metabasites.

This episode of metamorphism is most evident in the Ep-Ab-Chl-fels, responsible for the development of the dominant static fabric. In blueschist and LGG, the pseudomorphic replacement of Grt by statically growing Chl document this phase. The bulk composition is crucial for the intensity of re-crystallization: While Gln in blueschists and eclogites is not much affected, it is more strongly resorbed in LGG and Ep-Ab-Chl-fels. In the greenschist with the cm-thick Ab-layers, Grt is well preserved in Qtz-Ab-rich layers, while it is completely resorbed in the typical greenschist layers.

The effects of retrograde overprinting or a possible later metamorphic event are not pervasively observed. In the vicinity of lithological contacts and the greenschist- facies to brittle high- and low angle faults, chloritization and growth of late Msc is common, accompanied by extensive fluid activity and growth of Mag and Fe-hydroxides. The greenschist layers in the marble show a higher degree of retrogression. This may be assigned to their rheology (high amount of Chl and white mica, therefore less competent during deformation processes than the adjacent marbles), so that strain localization led to a stronger tectonic impact on these rocks during exhumation and accordingly a more pervasive re-equilibration. The asymmetric crenulation cleavage observed in the greenschist layers might indicate a late event of folding. Leitner (1999) reports similar fabrics and

macroscopically observed folds in the same layer of greenschist, 2 km northeast, with fold axes trending to 302/05. This orientation is consistent with the orientation of the observed C'-planes (**Fig. 35 d**), dipping to ca. 035/70.

In the extensional shear zones, deformation took place under low temperatures and no equilibrium was obtained.

8 MICROPROBE INVESTIGATION AND MINERAL CHEMISTRY

8.1 Instrumental methods

Seven representative samples were selected to prepare ten thin sections (thickness ca. 45 µm) for pointed geochemical analyses, using the Microprobe CAMECA SX 100 at the Department of Lithospheric Research, University of Vienna. A beam current of 20 nA and a voltage of 15 kV were used. For minerals with a significant formal content of Na or OH (i.e. white mica, amphiboles, pyroxene, chlorite, chloritoide, feldspar), a defocused ion beam was used (spot width ca. 5 µm compared to 1-2 µm focused). For calibration, standards of augite, albite, orthoclase, jadeite and almandine were used.

Mineral formula of garnet, amphibole, white mica, albite, chloritoide, epidote, chlorite and magnetite were calculated using the latest version of MINSORT software (Petrakakis and Dietrich, 1985). Representative analyses, used models of formula calculation and estimations of ferrous/ferric iron ratios are given below.

8.2 Mineral compositions

Amphiboles

Sodic Amphiboles

Representative EMP-analyses of sodic amphiboles are given in **Tab. 1**. Fe^{II+}/Fe^{III+}-ratios and structural formula ($A_{0-1}B_2C_5\ T_8OH_2O_{23)}$ have been calculated on the base of 15 cations exclusive of K.

The relatively high ratios of ferric to ferrous iron resulting from this calculation conforms to the observation of magnetite in the matrix as well as in the relictic assemblage ($M_{1A}/\ M_{1B}$) conserved in garnet.

In the blueschist, four different microstructural positions (structural types) of sodic amphiboles can be distinguished:

1. inclusions in Grt
2. cores of zoned crystals in the matrix,
3. rims of zoned crystals in the matrix and
4. crystals in shear bands with Chl, Cal and Phn.

Type 1 and type 2 are interpreted as relics of (M$_{1A}$/ M$_{1B}$). They do not show differences in chemical composition. In the XMg vs. XFe^{III} – diagram after Leake (1978), they plot around the border of the glaucophane and the ferro-glaucophane field (see fig x).

Type 3 represents the M$_{1C}$ –episode, and crystals are characterized by slightly increased XMg and a wider range of XFe^{III}.

Sodic amp of Type 4 plot in the ferro-glaucophane- and crossite-field, the total Fe-content is significantly higher than in Type 1 and 2. This difference in composition can be recognized in BSE-images as well as in a difference in color under the polarizing microscope (more intense blue with more crossitic composition).

The border between core-domains (type 2) and Fe-rich parts of the crystal is mostly not distinct along a crystallographic boundary, but in many cases an undulating transition zone, suggesting that the difference in chemical composition is caused by metasomatic processes. This is evidenced by elongate crystals of Gln, partially overgrown by Grt (see **Fig. 28 e** and **38 b**), that show a different composition inside and outside the Grt.

	light colored Grt-gneiss		blueschist			eclogite	Ep-Ab-Chl-fels		greenschist
Title:	inclusion	matrix	inclusion + core	shearzone	rim		inclusion	matrix	actinolite
	Mean 12pt	Mean 26pt	Mean 22pt	Mean12p	Mean11pt	Mean 10pt	Mean 6pt	Mean 9pt	Mean 10pt
SiO2	54.63	55.90	56.64	55.12	55.74	56.31	57.36	57.50	54.73
TiO2	0.070	0.022	0.017	0.022	0.016	0.04	0.04	0.02	0.01
Al2O3	8.32	9.90	10.57	8.27	8.92	9.24	10.44	10.57	2.05
Fe2O3	6.27	3.32	1.02	4.19	3.45	3.16	1.38	1.00	1.97
FeO	15.99	13.99	14.42	16.83	15.62	14.34	11.31	11.57	10.56
MgO	4.84	6.48	7.19	5.36	6.16	6.80	8.80	8.91	15.66
CaO	0.47	0.347	0.25	0.25	0.22	0.22	0.33	0.32	11.92
Na2O	6.87	7.00	6.84	6.68	6.78	6.93	7.03	6.97	0.70
Total	96.94	96.69	96.88	96.40	96.61	96.87	96.65	96.87	97.67
Si	7.903	7.954	7.999	7.998	8.000	8.005	8.014	8.016	7.811
Al_IV	0.097	0.046	0.001	0.002	0.000	0.000	0.000	0.000	0.189
Al_VI	1.322	1.613	1.759	1.413	1.508	1.549	1.719	1.736	0.155
Fe_3+	0.682	0.355	0.108	0.457	0.372	0.338	0.145	0.104	0.211
Mg	1.044	1.375	1.514	1.160	1.317	1.441	1.832	1.851	3.333
Fe_2+	1.934	1.654	1.617	1.968	1.801	1.668	1.299	1.304	1.260
Fe_2+	0.000	0.010	0.087	0.074	0.074	0.037	0.022	0.045	0.000
Ca	0.072	0.053	0.037	0.039	0.033	0.034	0.049	0.048	1.822
Na	1.927	1.931	1.874	1.879	1.886	1.910	1.904	1.885	0.178
T(8)	8.000	8.000	8.000	8.000	8.000	8.005	8.008	8.002	8
C(5)	5.000	5.000	5.000	5.000	5.000	5.000	5.000	5.000	4.995
B(2)	2.000	2.000	2.000	2.000	2.000	1.997	1.996	1.998	2
A(0-1)	0.004	0.003	0.003	0.005	0.003	0.005	0.004	0.006	0.028
Xmg	0.351	0.452	0.471	0.362	0.413	0.458	0.581	0.578	0.726

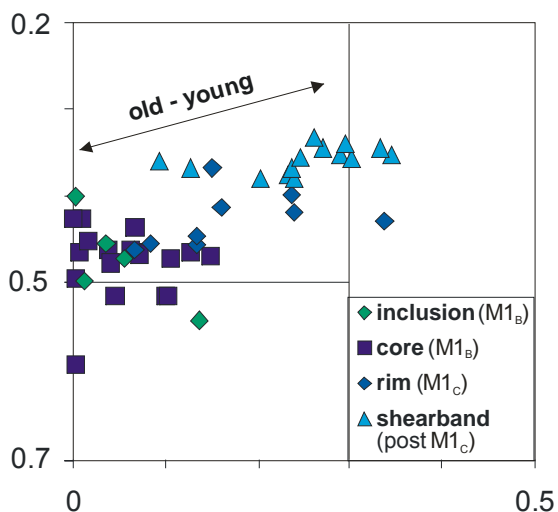**Tab. 1:** Representative analyses (mean values) of amphiboles. Formula calculation based on 23 Oxygens, Fe3+ estimated based on model Cations – K = 15

Nomenclature of Sodic Amphibole
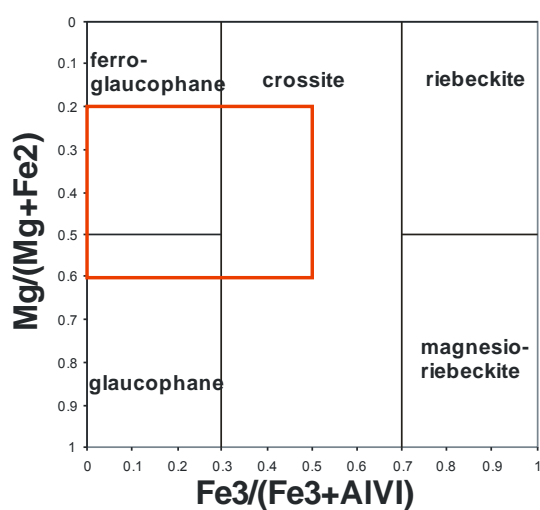
SIF013B - blueschist

SIF012A - light colored Grt-gneiss
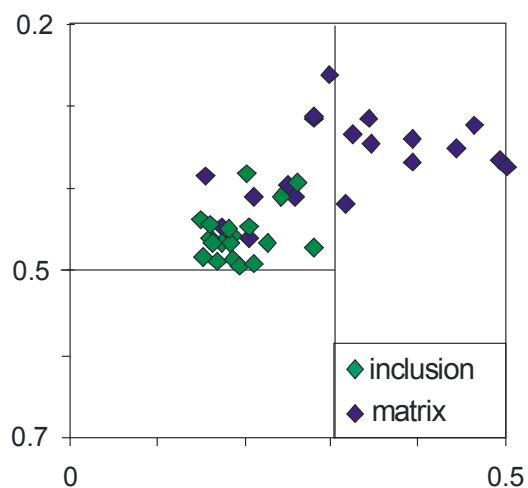
SIF05/03: Ep-Ab-Chl-fels
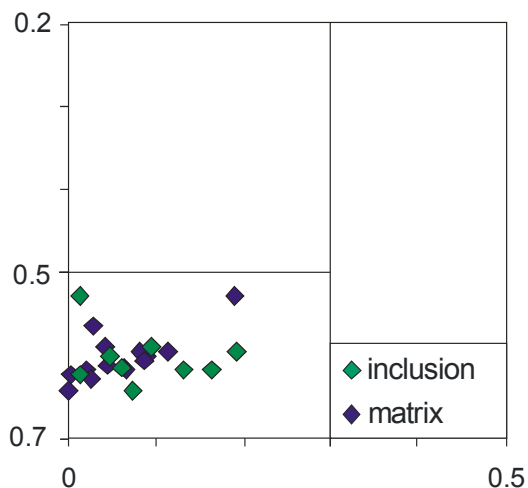
SIF05/07: Eclogite
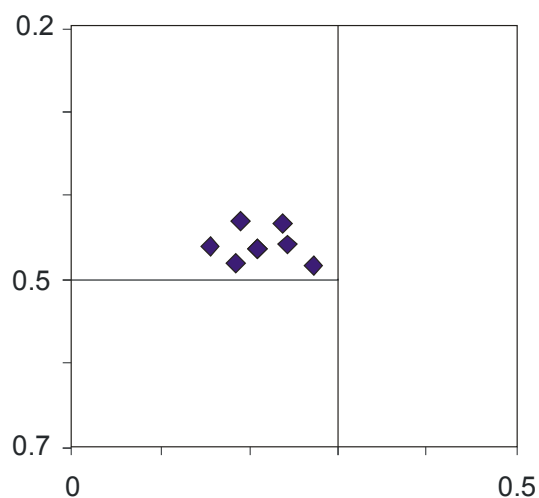
Fig. 37: Classification diagram of sodic amphiboles according to Leake (1978), compositions of four lithologies plotted.
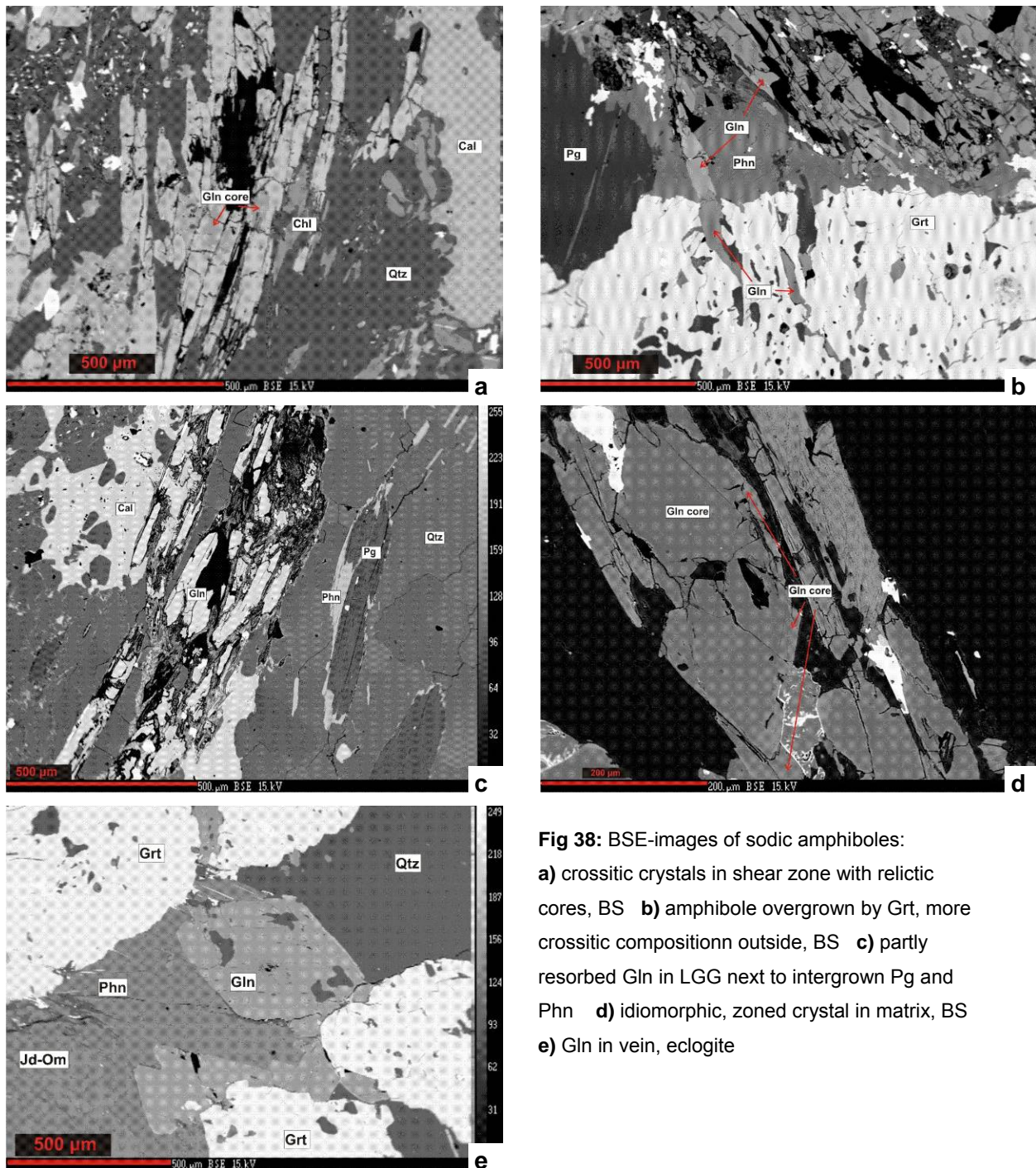
Fig 38: BSE-images of sodic amphiboles: **a)** crossitic crystals in shear zone with relictic cores, BS **b)** amphibole overgrown by Grt, more crossitic compositionn outside, BS **c)** partly resorbed Gln in LGG next to intergrown Pg and Phn **d)** idiomorphic, zoned crystal in matrix, BS **e)** Gln in vein, eclogite

In the LGG, a similar pattern can be observed: Compositions of inclusions in Grt plot in the ferro-glaucophane field, while the partially resorbed crystals in the matrix trend to the crossite-field. Sodic amphiboles in Ep-Ab-Chl-fels do not show significant differences in composition of structural types (inclusions in Ep (foliation 1) and crystals in foliation 2). They have real glaucophane- composition, with X_{Mg} higher than 50 %. In the eclogites, calculated compositions plot in the ferro-glaucophane field.

Calcic amphiboles

The calcic amphiboles, analyzed in the sample of greenschist, plot in the actinolite-field in the nomenclature of calcic amphiboles according to Leake (1978). Representative analyses are given in **Tab. 1**.
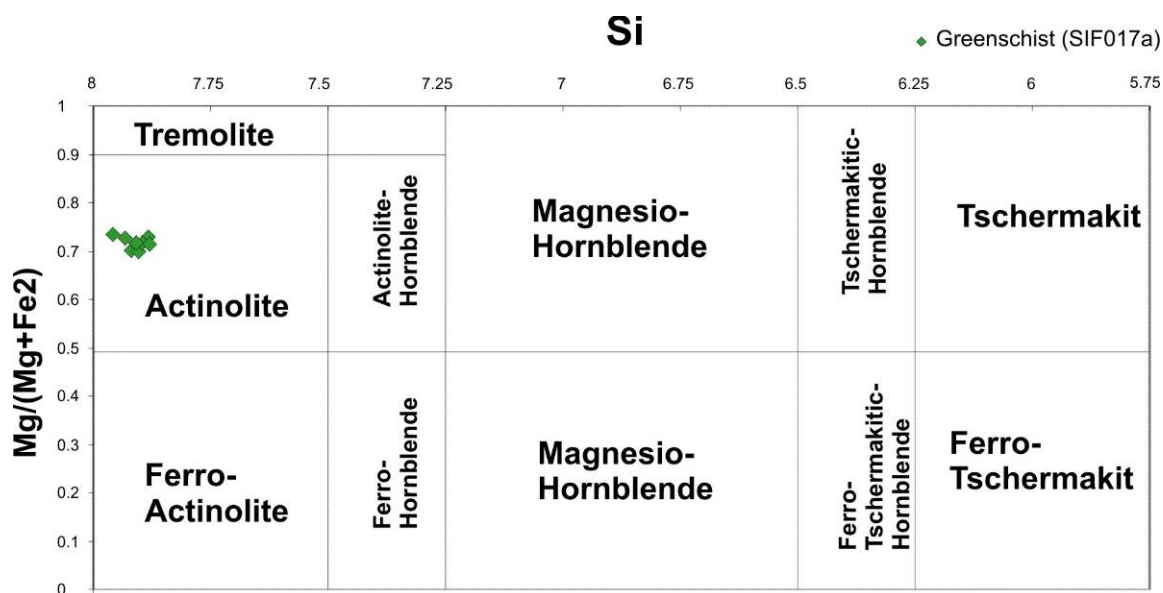
Fig 39: Classification diagram of calcic amphiboles according to Leake (1978). Compositions of calcic amphiboles plot in the actinolite field.

Garnet

Representative EMP-analyses of Grt are given in **Tab. 2**. Structural formula of Garnet ($T_3M_2C_3O_{12}$) have been calculated on the base of 12 oxygens, Fe^{3+} estimated by iteration of Fe_2O_3/FeO-ratio until M = 2.

Microsructures of Grt have been described above. Grt in blueschist and LGG are generally low in Ca. The optical investigation allowed the distinction of different structural elements in the large poikiloblasts on blueschists and light Grt-gneisses (massive and network-like domains and relictic "grains" preserved inside the large monocrystals). Those Grt- crystals were analyzed in detail in five thin sections of samples SIF012A and SIF013A and B, using BSE-images and point analyses along profiles and at points of special interest. Nevertheless, a significant difference in chemical composition of the relictic domains could not be observed.

Results are plotted in the triangle pyrope – almandine + spessartine - grossular.

The large dyctionitic crystals show a trend of decreasing Sps and increasing Grs from core to rim, with a Grs-component between 15 and 33 % in LGG and between 18 and 28 % in BS. Relictic parts plot in the area of core-composition.
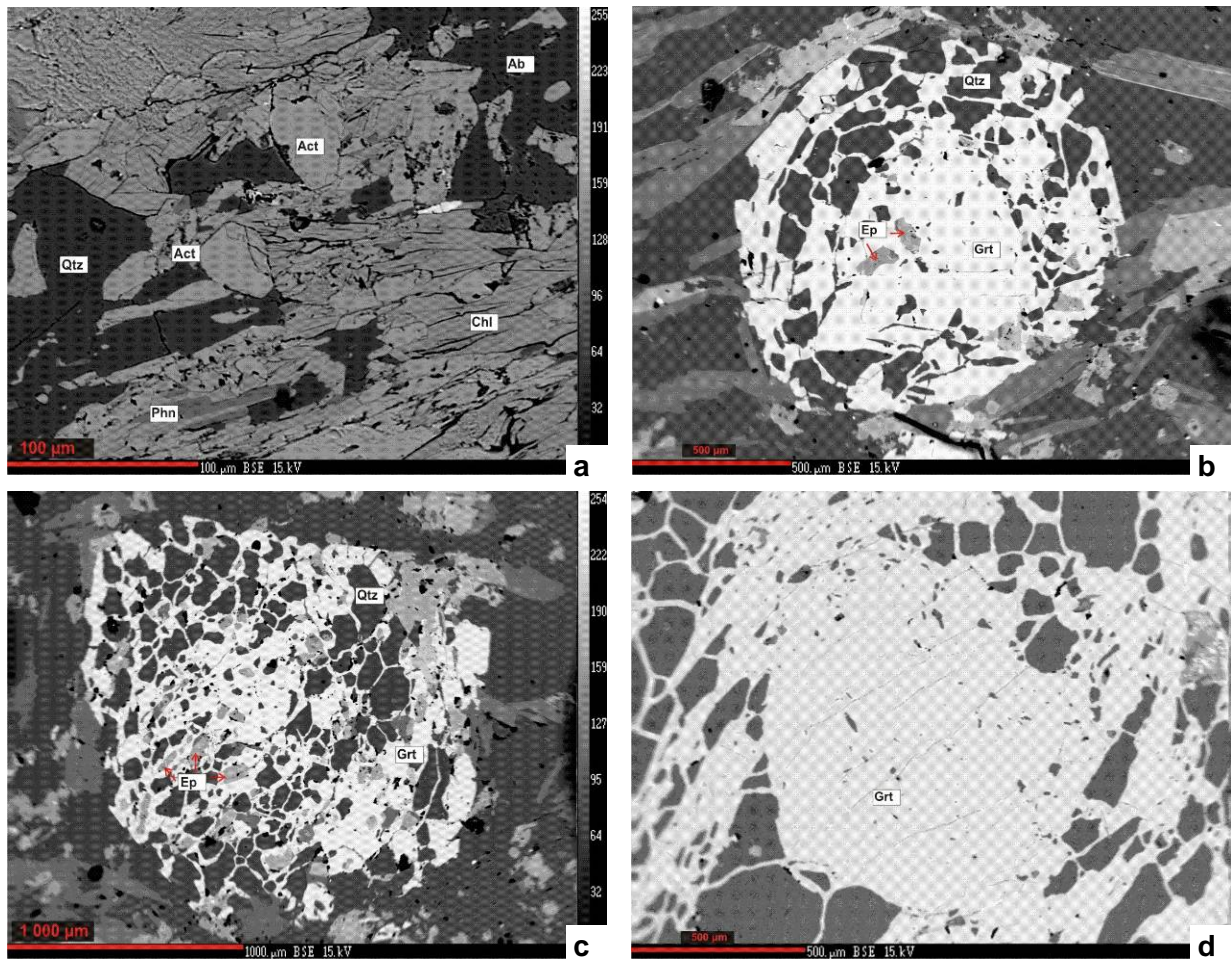
Fig. 40: BSE-pictures of **a)** actinolite, greenschist   **b,c)** Grt with Ep and Qtz inclusions, Ab-gneiss (greenschist) **d)** relictic domain in Grt-porphyroblast, BS

Grt preserved in the Ab-gneiss layers in the greenschist also show a trend to higher Grs-, but in addition to higher Pyr- component from core to rim.

Grt in eclogite does not show this trend: Only a slight decrease of Sps- and increase of Pyr - component was measured, but analyses plot mostly in the area of core-composition of blueschist-Grt. Only locally at the very margin, an increase of Grs-component is evident. Grs-component lies between 15 and 20 %.

 In the Ep-Ab-Chl-fels, relictic Grt has compositions similar to the Grt in eclogites, with Grs-components between 15 and 20 %.
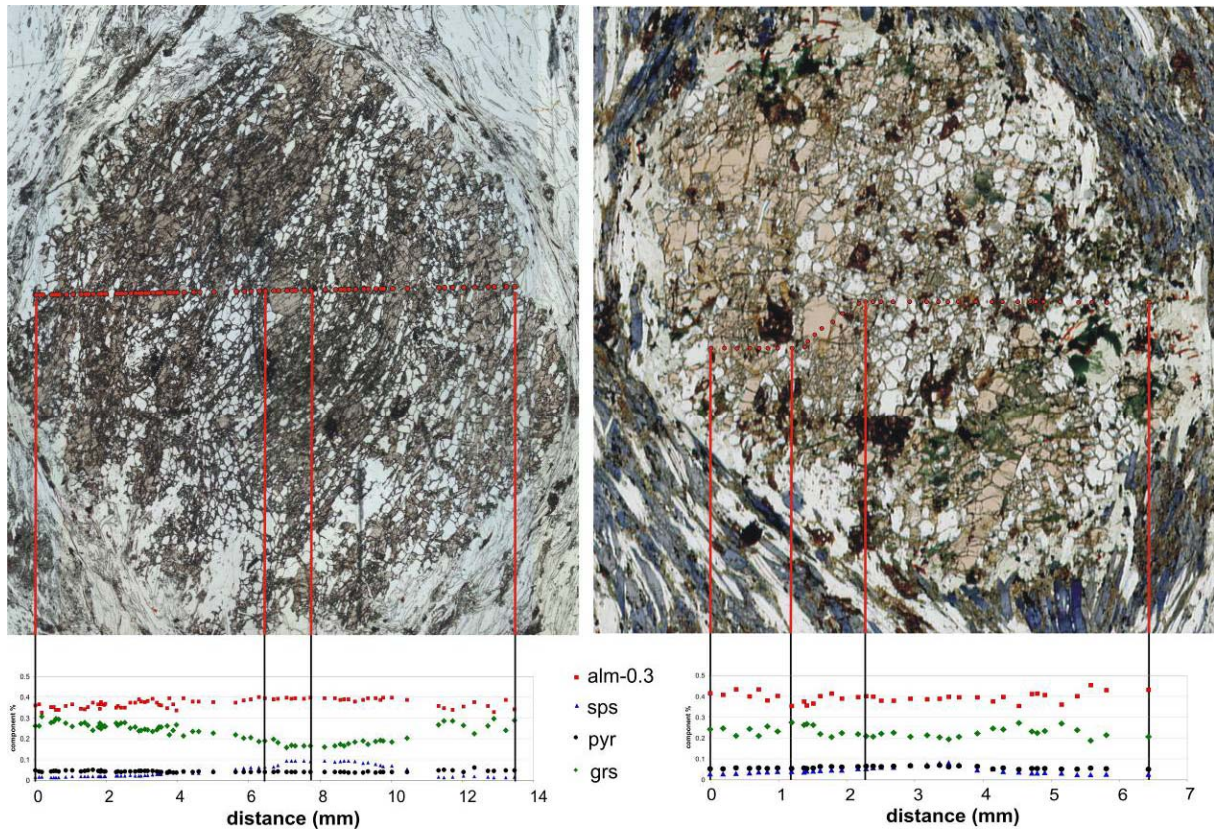
Fig. 41: Calculated compositions of garnet, % component of pyrope, almadine -0.3, spessartine and grossular plottet along two profiles of Grt in LGG (left) and BS (right). A trend of decreasing Sps and increasing Grs from core to rim can be observed.
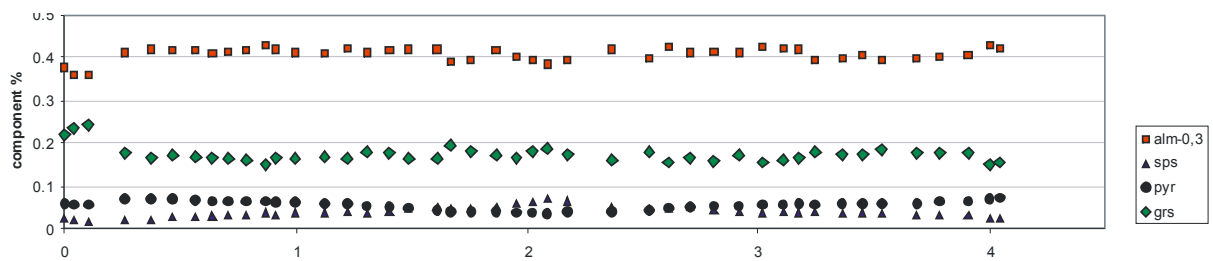
Fig. 42: Profile of Grt in eclogite, showing a slight decrease of sps and increase of pyr from core to rim, and lower alm and higher grs at the margin
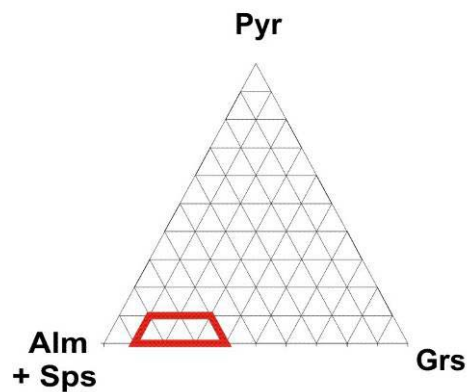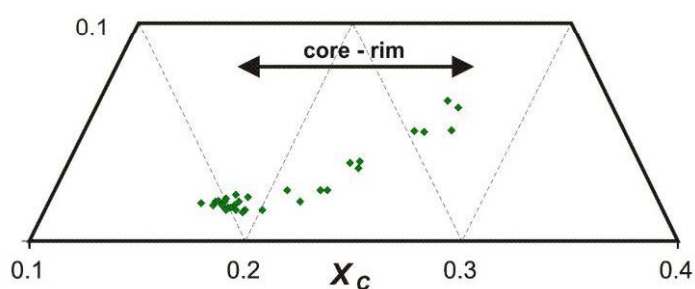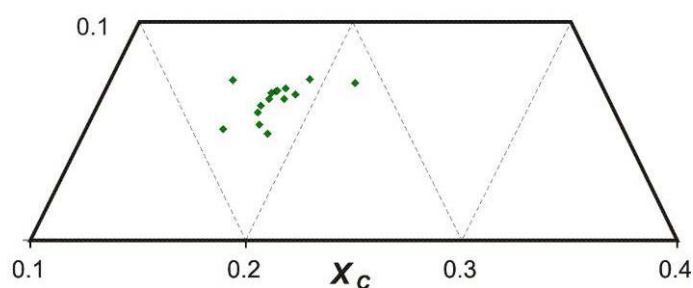
Fig. 43: Calculated compositions of garnet, plotted in the triangle pyrope, almadine+spessartine, grossular

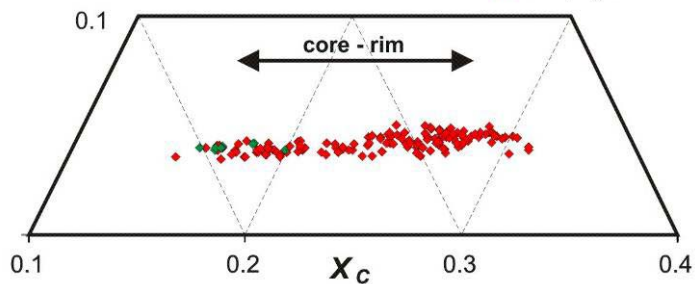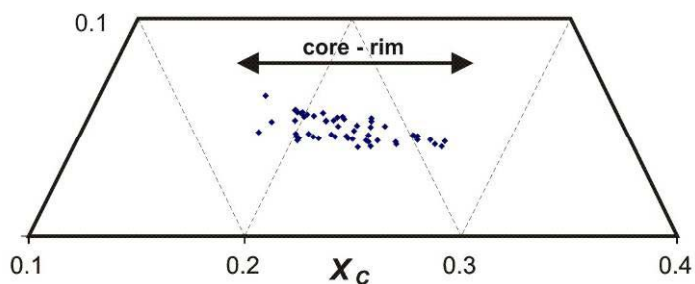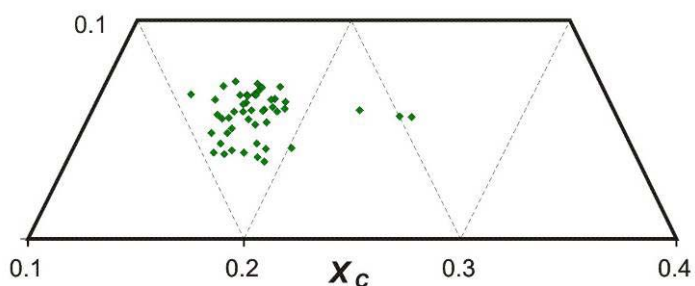| | LGG | | | blueschist | | greenschist | Ep-Ab-Chl-fels | eclogite | | |
| | relict core | core | rim | core | rim | core | | retro | rim | core |
	Mean 13pt	Mean 73pt	Mean 40pt	Mean 17pt	Mean 17pt	Mean17 pt	Mean 15pt	Mean 3pt	Mean 21pt	Mean 20pt
SiO2	37.22	37.14	37.33	37.154	37.15	37.12	37.255	37.39	37.31	37.086
TiO2	0.07	0.08	0.10	0.094	0.09	0.09	0.079	0.183	0.082	0.106
Al2O3	21.32	21.22	21.30	20.885	20.86	20.65	20.607	20.647	20.668	20.57
Fe2O3	0.19	0.156	0.281	0.379	0	1	0.812	0.76	0.726	0.718
FeO	30.729	30.570	29.722	30.779	31	29	29.987	29.703	31.835	31.534
MnO	2.027	2.408	0.876	0.993	0.993	4.035	2.721	0.85	1.389	2.124
MgO	1.037	1.018	1.119	1.099	1.099	0.635	1.581	1.413	1.584	1.153
CaO	8.114	7.818	9.781	8.475	8.475	7.766	7.099	9.113	6.73	6.802
Total	100.710	100.419	100.512	99.859	100	100	100.153	100.066	100.334	100.099
Si	2.975	2.979	2.976	2.99	2.99	2.995	2.994	2.994	2.995	2.993
Al_IV	0.025	0.021	0.024	0.01	0.010	0.005	0.006	0.006	0.005	0.007
Al_VI	1.984	1.986	1.977	1.971	1.971	1.96	1.945	1.943	1.95	1.949
Ti	0.004	0.005	0.006	0.006	0.014	0.005	0.005	0.011	0.005	0.006
Fe_3+	0.011	0.009	0.017	0.023	0.023	0.035	0.049	0.046	0.044	0.044
Fe_2+	2.054	2.051	1.981	2.072	2.072	1.976	2.015	1.989	2.137	2.128
Mn	0.137	0.164	0.059	0.068	0.068	0.276	0.185	0.058	0.094	0.145
Mg	0.124	0.122	0.133	0.132	0.132	0.076	0.189	0.169	0.19	0.139
Ca	0.695	0.672	0.835	0.731	0.731	0.672	0.611	0.782	0.579	0.588
T(3)	3.000	3.000	3.000	3.000	3.000	3.000	3.000	3.000	3.000	3.000
M(2)	2.000	2.000	2.000	2.000	2.000	2.000	2.000	2.000	2.000	2.000
C(3)	3.010	3.008	3.009	3.002	3.002	3.000	3.001	2.997	3.000	3.000
alm	0.682	0.682	0.658	0.69	0.690	0.659	0.672	0.664	0.712	0.709
sps	0.046	0.054	0.020	0.023	0.023	0.092	0.062	0.019	0.031	0.048
pyr	0.041	0.040	0.044	0.044	0.044	0.025	0.063	0.056	0.063	0.046
grs	0.223	0.216	0.266	0.229	0.229	0.204	0.176	0.232	0.168	0.171
Xmg	0.057	0.056	0.063	0.06	0.06	0.037	0.086	0.078	0.081	0.061

Tab. 2: representative microprobe analyses of Grt, formula calculation based on 12 Oxygens, Fe3+ estimated by iteration of Fe2O3/FeO-ratio until M = 2

Pyroxene

Structural formula of Pyroxene ($M1_1M2_1T_2O_6$) have been calculated based on 6 oxygens, Fe^{3+} estimated by iteration of Fe_2O_3/FeO-ratio until sum of cations = 4.

Relictic pyroxenes have been found as inclusions in Grt in BS and LGG, and as inclusions in Ep in Ep-Ab-Chl-fels. In the eclogite, the matrix is mainly composed of massive, pale green pyroxene.

In the BSE-image of the microprobe, a chemical zoning is commonly observed in these crystals, with lighter colors at the rims due to an increased Fe. There is no distinct boundary, but a gradual, undulating transition between these zones. In addition, relictic core domains can be distinguished in BSE-images due to their suspicious dark color. The calculated compositions plot in the jadeite-field. A trend of decreasing Jd-component towards the rim-domains can be observed. The relictic domains in the matrix are nearly pure Jd, while inclusions in Grt have compositions similar to those of the core-domains.

Pyroxenes of the BS and LGG plot in the Jadeite-field, while the relictic inclusions in Ep of the Ep-Ab-Chl-fels have typical Omphacite-composition.
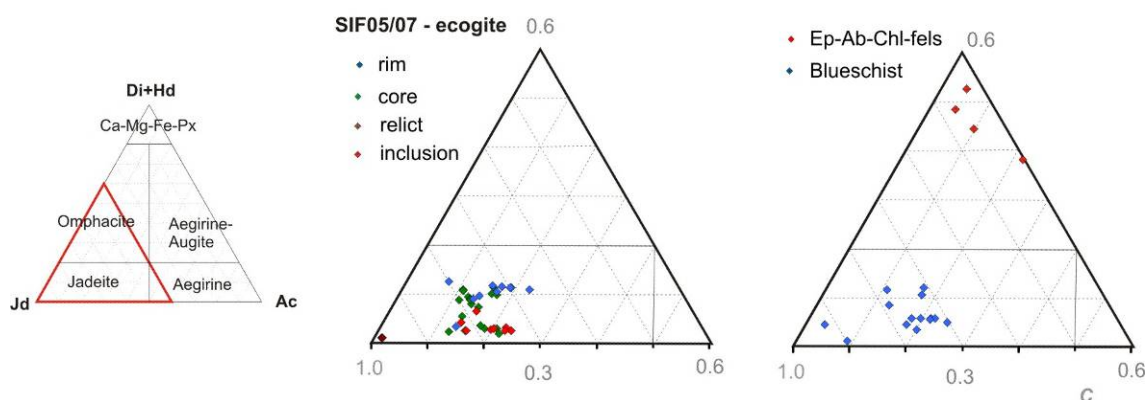
Fig. 44: Composition of pyroxene, plotted in the Morimoto (1988) diagram
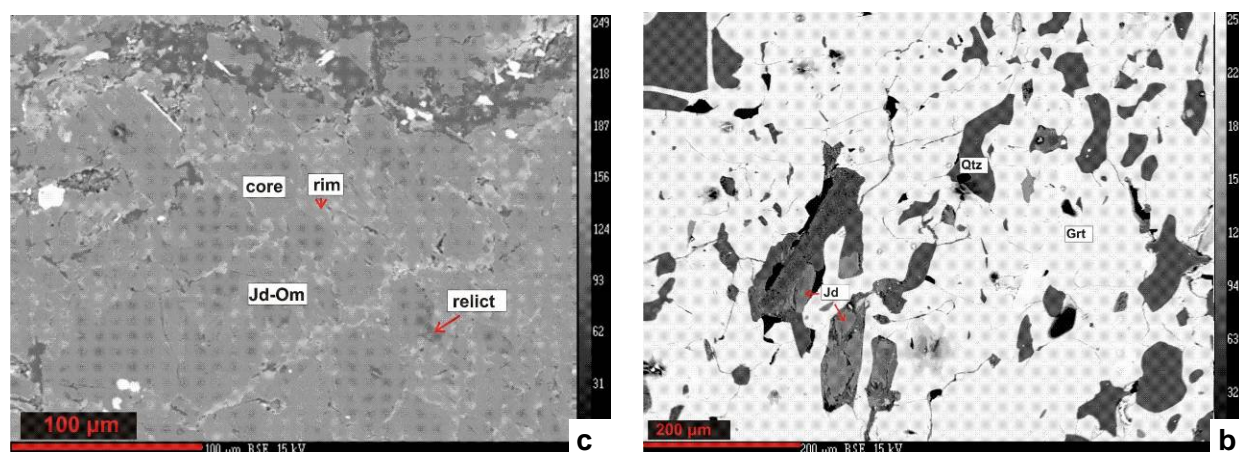
Fig. 45: BSE-images of Pyroxene,   **a)** fabric of eclogite with patchy core- and rim domains   **b)** Jd- inclusions in Grt, BS

	BS	eclogite				Ep-Ab-Chl-fels
	SIF013b	rel	inclusion	core	rim	
	Mean 14pt	Mean 2pt	Mean 8pt	Mean 18pt	Mean 10pt	Mean 4pt
SiO2	57.80	58.76	57.43	57.50	57.23	55.25
TiO2	0.05	0.40	0.03	0.02	0.02	0.04
Al2O3	18.21	21.91	17.23	17.16	16.13	11.27
FeO	8.29	3.82	9.48	8.62	9.11	7.23
MgO	0.63	0.30	0.41	0.94	1.45	6.08
CaO	11.61	0.28	0.86	1.76	2.56	11.81
Na2O	13.27	14.30	13.72	13.18	12.65	7.83
Total	99.48	99.79	99.25	99.23	99.18	99.55
Si	2.024	2.016	2.017	2.020	2.020	1.981
Al_IV	0.000	0.000	0.000	0.000	0.000	0.019
Al_VI	0.752	0.886	0.713	0.711	0.671	0.457
Fe_3+	0.098	0.013	0.186	0.146	0.154	0.103
Mg	0.033	0.015	0.021	0.049	0.076	0.325
Fe_2+	0.145	0.096	0.093	0.108	0.114	0.114
Ca	0.044	0.010	0.033	0.066	0.097	0.454
Na	0.901	0.951	0.934	0.898	0.866	0.544
T(2)	2.024	2.016	2.017	2.020	2.020	2.000
M1(1)	1.000	1.000	1.000	1.000	1.000	1.000
M2(1)	0.976	0.984	0.983	0.980	0.980	1.000
Xmg	0.184	0.137	0.186	0.313	0.399	0.741
Di+Hd	0.043	0.010	0.033	0.066	0.097	0.454
Ac	0.168	0.014	0.186	0.146	0.154	0.104
Jd	0.760	0.938	0.749	0.752	0.712	0.441

Tab. 3: representative microprobe analyses of Pyroxene, formula calculation based on 6 oxygens, Fe3+ estimated by iteration of Fe2O3/FeO-ratio until Sum of cations = 4

White mica

Structural formulas of white mica ($A_1M1_{0-1}M2_2T_4$ OH_2O_{11}) have been calculated on the base of 6 cations without Na, Ba, K, Fe_2O_3/FeO -ratio was estimated as Fe^{III+} = Fe – Si – 3 – Mg + Ti. Results for Phn are plotted in the triangle muscovite – celadonite - paragonite.

Paragonite

Pg was measured in blueschists, LGG and eclogites. Associations of intergrown Pg and Phn are common in these lithologies.

Msc component ranges from 3 to 9 mol per cent in LGG, 1 to 9 mol per cent in blueschist and 3 to 10 mol per cent in eclogite, where the larger crystals were mainly identified as Pg. A significant difference in chemical composition between structural types (large porphyroblasts and later crystals in foliation and shear zones) could not be observed.

Phengite

In all samples, Phn has 8 % or less Pg-component and 20 to 35 % Cel-component. In the eclogites, phengite can be found throughout the fabric. A difference in chemical composition between the various observed generations could not be observed. Cel- components are between 0.2 and 0.4 %, and are generally higher in BS and eclogite.
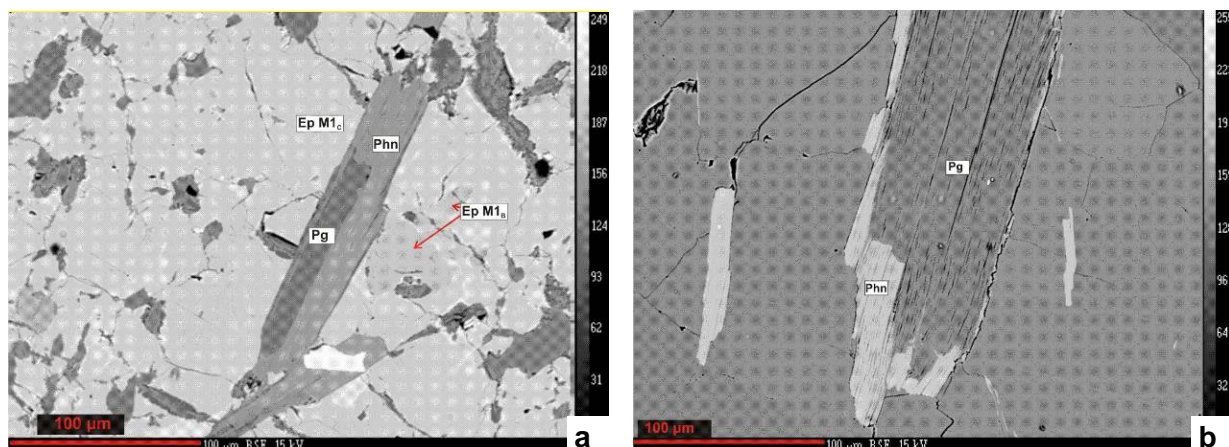
Fig. 46: BSE-images of intergrown phengite and paragonite **a)** as inclusion in Ep, Ep-Ab-Chl-fels, **b)** in LGG with Qtz

	Phengite					paragonite			
	LGG	BS	greenschist	Ep-Ab-Chl-fels	eclogite	LGG	BS	Ep-Ab-Chl-fels	eclogite
	Mean 36pt	Mean 14pt	Mean 14pt	Mean 10pt	Mean 12pt	Mean 34pt	Mean 16pt	Mean 5pt	Mean 8pt
SiO2	49.54	51.24	48.61	50.62	49.72	47.08	47.06	46.74	47.19
TiO2	0.17	0.11	0.13	0.07	0.14	0.05	0.06	0.05	0.06
Al2O3	26.38	25.41	27.30	27.35	26.38	39.85	39.25	39.38	38.98
FeO	2.72	2.04	3.93	2.53	2.58	0.71	0.84	0.50	0.79
Fe2O3	1.91	1.33	1.74	0.63	2.02				
MgO	2.68	3.72	2.08	3.32	2.68	0.12	0.13	0.16	0.15
CaO	0.02	0.02	0.01	0.05	0.01	0.12	0.10	0.23	0.09
Na2O	0.37	0.20	0.46	0.26	0.40	7.26	7.12	6.90	7.22
K2O	10.71	10.85	10.34	10.60	11	0.66	0.61	0.83	0.76
Total	95.15	94.95	94.62	95.48	94.59	95.86	95.17	94.80	95.23
Si	3.338	3.441	3.299	3.367	3.371	2.992	3.012	3.001	3.021
Al_IV	0.662	0.559	0.701	0.633	0.629	1.008	0.001	0.999	0.979
Ti	0.009	0.006	0.007	0.004	0.007	0.002	0.003	0.002	0.003
Al_VI	1.503	1.451	1.483	1.510	1.479	1.978	1.972	1.982	1.962
Fe3	0.154	0.114	0.223	0.141	0.146				
Fe2	0.097	0.067	0.089	0.032	0.103	0.008	0.014	0.000	0.022
Mg	0.245	0.372	0.210	0.329	0.271	0.011	0.012	0.016	0.014
Na	0.049	0.026	0.061	0.034	0.053	0.895	0.884	0.859	0.896
K	0.921	0.929	0.895	0.900	0.918	0.054	0.050	0.068	0.062
T(4)	4.000	4.000	4.000	4.000	4.000	4.000	4.000	4.000	4.000
M(2)	2.008	2.012	2.012	2.017	2.008	2.000	2.000	2.000	2.000
A(1)	0.971	0.957	0.957	0.937	0.972	0.030	0.032	0.027	0.021
Xmg	0.717	0.847	0.703	0.604	0.940	0.228	0.211	0.366	0.247

Tab. 4: representative microprobe analyses of white mica, formula calculated on the base of 6 cations without Na, Ba, K, Fe2O3/FeO-ratio was estimated as FeIII+ = Fe – Si – 3 – Mg + Ti.

Pg

Msc   Cel
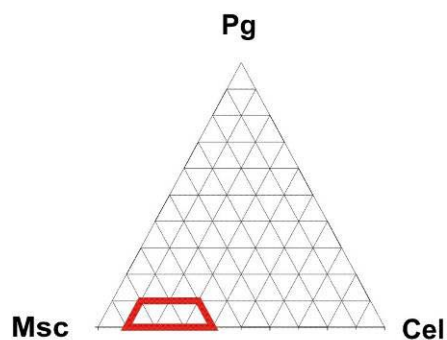
Fig. 47: Calculated compositions of phengite, plotted in the triangle paragonite, muscovite, celadonite

SIF012A - light Grt- gneiss

X_c

SIF013B - Blueschist

X_c

SIF017A - Greenschist

X_c
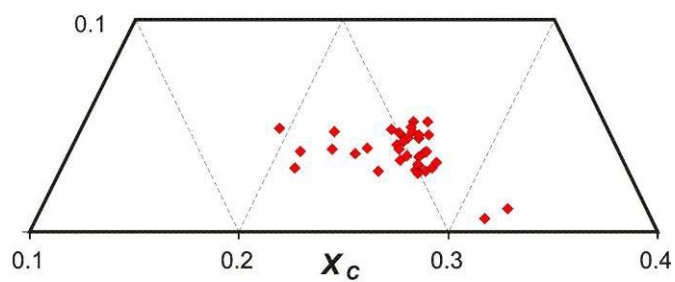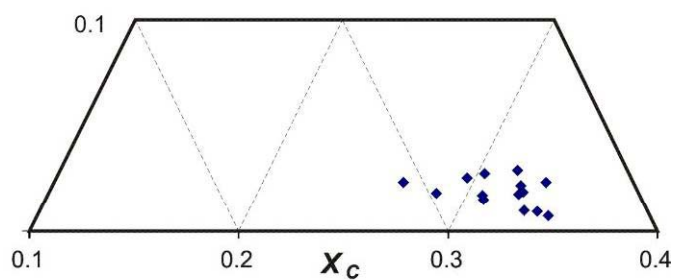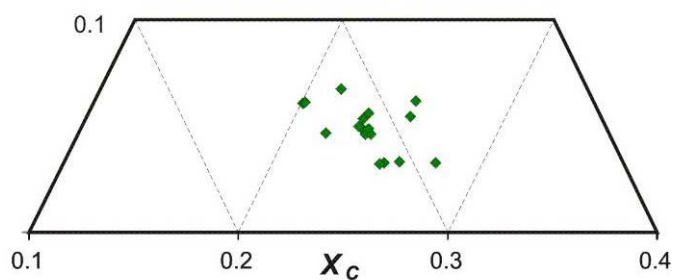
SIF05/03 - Ep-Ab-Chl-gneiss

X_c

SIF05/07 - Eclogite

X_c
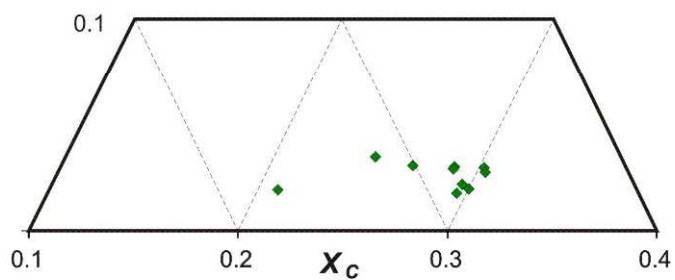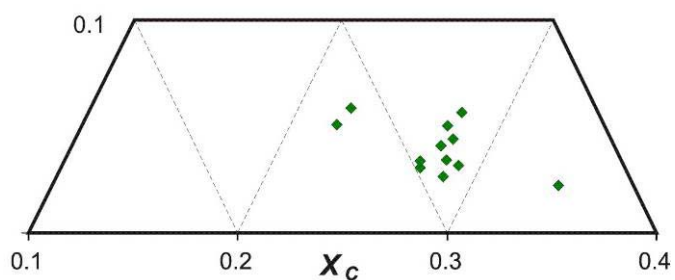
Epidote-Zoisite

Formulas of Ep were calculated on the base of 16 cations and 25 oxides, Fe^{3+} and Mn^{3+}-content was estimated by charge balance. Results are plotted in the triangle Clinozoisite (Al-VI-endmember), Pistazite (Fe^{3+}-end-member) and Piemontit (Mn^{3+}-end-member). The observed Piemontit components are between 0 and 3 % in all samples.

The compositional zoning has already been described in the previous chapter, and different structural types could be distinguished with the optical microscope. The differences in interference colors in Ep of the Ep-Ab-Chl-fels led to the assumption of a increasing Fe-content with ongoing mineral growth. This was confirmed by microprobe investigations. The opposite was observed in zoned Ep in LGG and BS: In these lithologies, a decrease of Fe-content from core to rim was measured.

Three structural types were distinguished and can be assigned to the proposed metamorphic episodes:

M_{1A}/ M_{1B}: Relictic, small grains and core domains in large porphyroblasts of Ep-Ab-Chl-fels have zoisitic compositions with about ca. 90 % or more Zo-component. The inclusions of Ep in Grt of the blueschist and Grt-gneiss have compositions between 65 and 80 % Zo-component. (see **Fig. 49 b**)

M_{1C}: large porphyroblasts and elongated crystals growing in the dominant foliation. Zo-component of the large porphyroblasts in the Ep-Ab-Chl-fels is between 75 and 90 %. In porphyroblasts of LGG, Zo-component is between 80 and 85 %, the chemical zoning is characterized mostly by an irregular, gradual transition of decreasing Fe-content (i.e. increase of Zo-component) from core to rim. In the greenschists, the Ep crystals of M_{1C} have a similar zoning, with compositions between 60 and 80% Zo-component.

M_{1D}: Rim-domains in large porphyroblasts of Ep-Ab-Chl-fels can be distinguished by the BSE-images (see **Fig. 49 b**), and are characterized by a higher Fe-content. Compositions are typically between 70 and 80% Zo- component.

Fig. 48: Calculated compositions of epidote, plotted in the triangle piemontit, clinozoisite, pistazite (plot 1, LGG: inc = inlusion in Grt
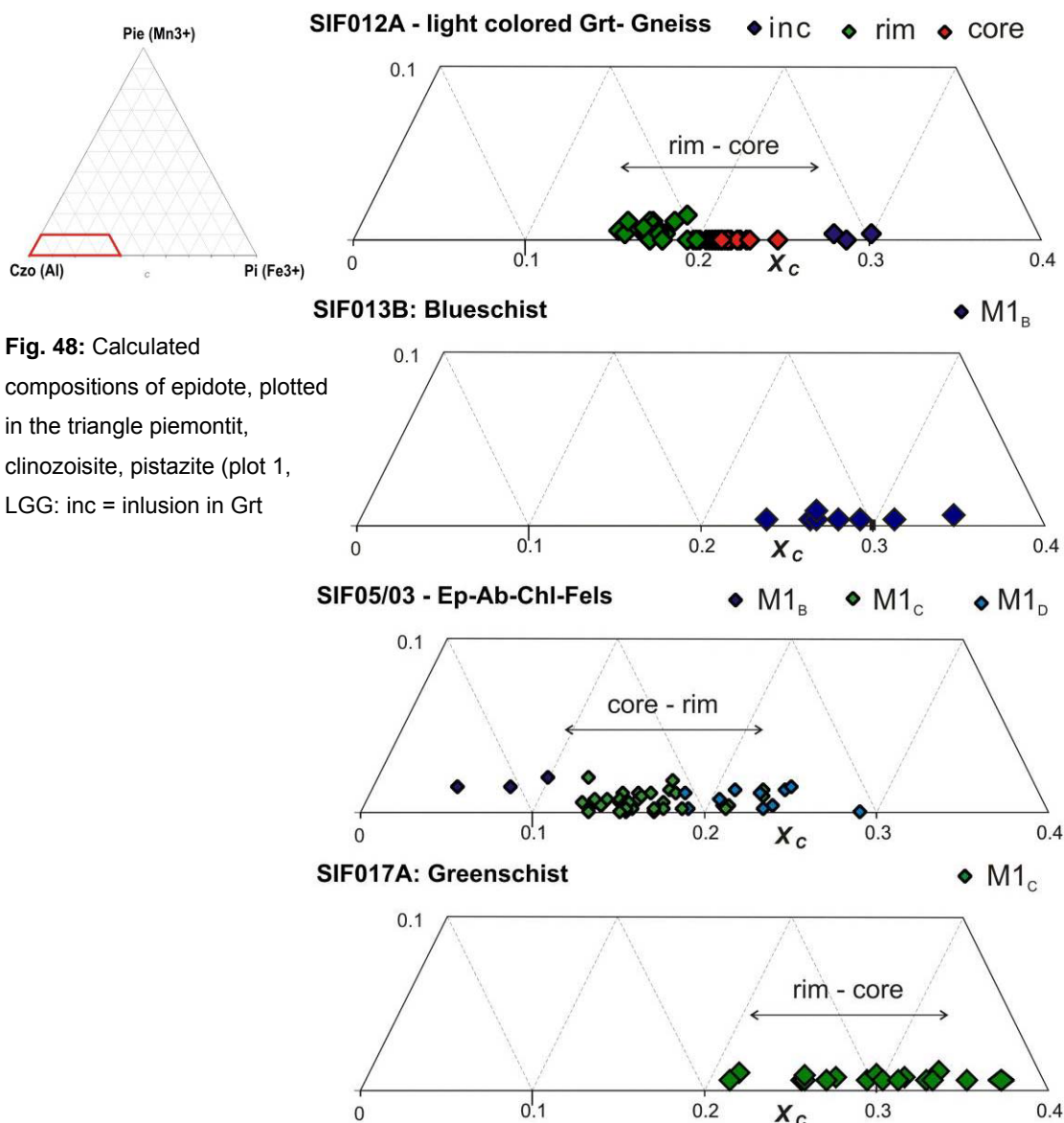
Feldspar

Structural formula of Albite ($X_1Z_4O_8$) have been calculated based on 8 oxygens, total Fe considered as Fe^{3+}. In all samples, analyzed feldspar was nearly pure albite (<99%). Representative analyses are given in **Tab. 6**.

Oxides

Magnetite was identified as inclusion in porphyroblastic Grt (BS and LGG) and Ep (Ep-Ab-Chl-fels) as well as in the matrix of all analyzed samples. Structural formula of Spinel ($R(3+)_{16}R(2+)_8O_{32}$) were calculated based on 32 oxygens, Fe^{3+} estimated by iteration of Fe_2O_3/FeO-ratio until sum of cations = 24.

	LGG			blueschist	greenschist	Eb-Ab-Chl-fels		
	rim	core	inclusion			M1B	M1C	M1D
	Mean 22pt	Mean 26 pt	Mean 3 pt	Mean 8pt	Mean	Mean 3pt	Mean 36pt	Mean 12pt
SiO2	38.24	37.94	37.32	38.17	37.56	38.94	38.41	37.92
Al2O3	26.93	25.48	22.96	26.24	24.96	30.26	27.32	24.70
Fe2O3	9.40	10.96	14.63	9.61	9.35	3.95	8.02	11.35
FeO	0.01	0.44	0.00	0.12	0.96	0.00	0.00	0.00
Mn2O3	0.00	0.00	0.14	0.00	0.00	0.95	0.33	0.48
MnO	0.17	0.06	0.07	0.23	0.14	-0.19	-0.06	-0.08
MgO	0.04	0.03	0.00	0.05	0.06	0.02	0.04	0.03
CaO	23.55	23.14	23.07	23.41	22.54	24.78	24.00	23.69
Total	9.83	9.80	9.82	9.78	9.56	98.13	97.92	98.00
Si	5.970	5.982	5.954	6.001	6.060	5.978	5.996	5.993
Al	4.955	4.735	4.318	4.862	4.746	5.025	5.475	4.602
Fe 3+	1.104	1.300	1.757	1.137	1.135	0.943	0.457	1.350
Ca	3.939	3.909	3.944	3.943	3.897	4.005	4.006	4.002
T(6)	5.970	5.982	5.954	6.001	6.060	5.978	5.996	5.993
M(6)	6.059	6.035	6.092	6.000	6.000	6.044	6.009	6.013
Ca(4)	3.970	3.982	3.954	3.999	3.940	3.998	3.996	3.993
zo	**0.830**	**0.791**	**0.725**	**0.810**	**0.783**	**0.916**	**0.838**	**0.768**
ps	**0.185**	**0.217**	**0.295**	**0.189**	**0.187**	**0.076**	**0.157**	**0.225**
pie	**0.000**	**0.000**	**0.003**	**0.000**	**0.000**	**0.019**	**0.006**	**0.010**

Tab. 5: representative microprobe analyses of Epidote, formula calculation based on16 cations and 25 oxides, Fe3-content was estimated by charge balance.

	LGG	**Greenschist**	**BS**	**Ep-Ab-Chl-fels**
	Mean 2pts	Mean 10pt	pt 126	Mean 12pt
SiO2	69.01	68.82	68.71	68.54
Al2O3	20.02	19.74	19.67	19.80
CaO	0.06	0.08	0.36	0.10
Na2O	11.85	11.44	10.80	11.44
K2O	0.02	0.04	0.03	0.08
Total	101.07	100.30	100.04	100.03
Si	2.982	2.993	2.993	2.989
Al_IV	1.020	1.012	1.010	1.018
Ca	0.003	0.004	0.017	0.005
Na	0.993	0.964	0.912	0.967
K	0.001	0.002	0.002	0.004
Z(4)	4.006	4.010	4.019	4.010
X(1)	0.997	0.971	0.931	0.977
an	0.003	0.005	0.019	0.005
ab	0.996	0.993	0.979	0.990
or	0.001	0.002	0.002	0.004

Tab. 6: representative microprobe analyses of Ab, formula calculation based on 8 oxygens, total Fe considered as Fe^{3+}.
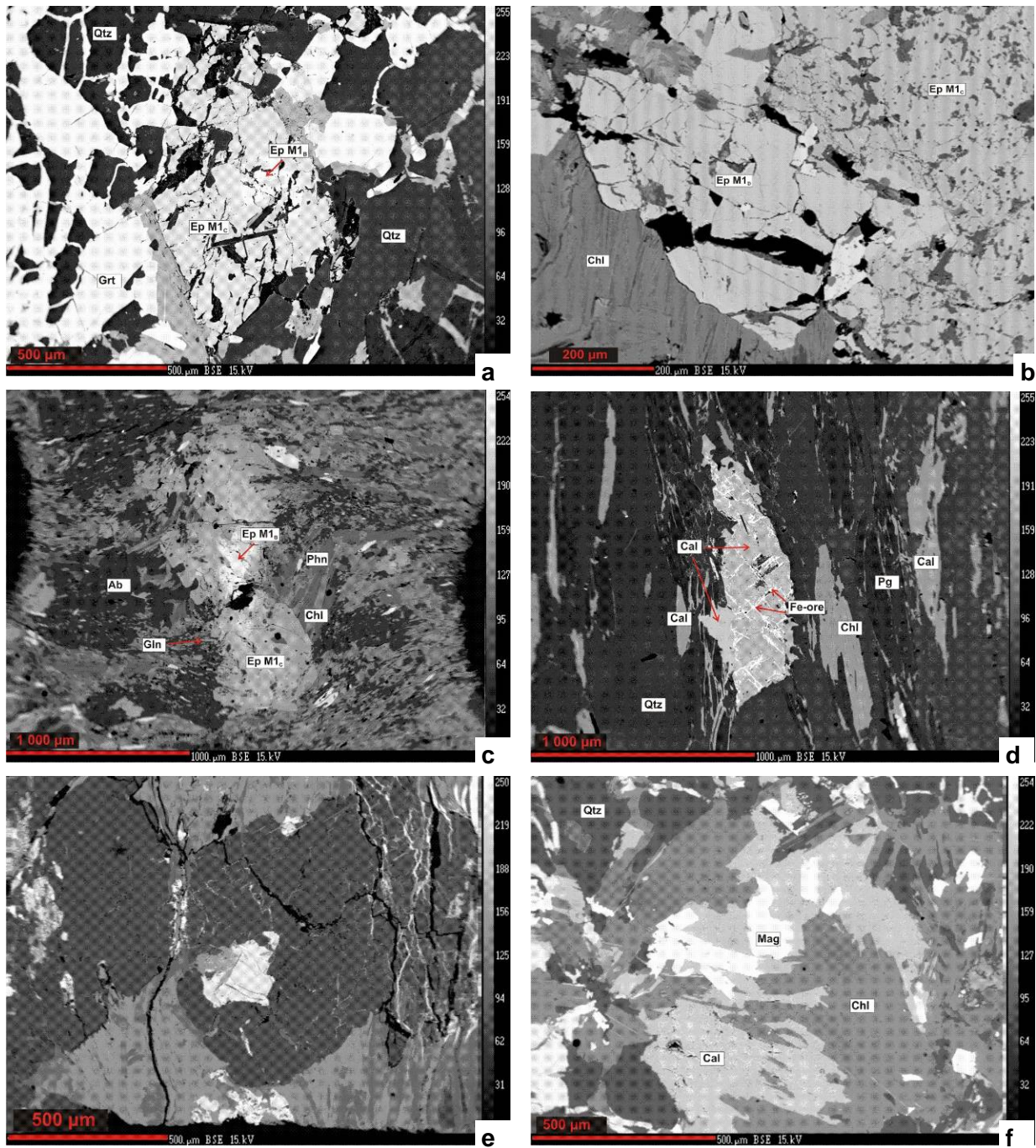
Fig. 49: BSE-images of **a)** Zoned Ep-crystal in LGG   **b)** Ep-porphyroblast and rim in Ep-Ab-Chl-fels   **c)** zoned Ep-porphyroclasts in greenschist   **d)** Arg-pseudomorphs, with Fe-hydroxide mimicking the cleavage planes   **e)** Ab-porphyroblast in Ep-Ab-Chl-fels, with inclusion of relictic Grt   **f)** Magnetite, in matrix of blueschist

8.3   Conclusion of microprobe investigations

Microstructurally distinguished types of Na-amphibole, pyroxene and epidote can also be characterized by a different chemism. Leitner (1999) measured similar compositions in his samples and described the same zoning pattern concerning Ep in LGG and Grt.

In Na-amphibole, pyroxene and epidote, irregular, gradual and patchy transitions between chemically different domains are common. This may be attributed to metasomatic processes. All these minerals have Fe^{3+} in their structure, and varying ratios of ferric to ferrous iron indicate that the fugacity of oxygen played an important role during the metamorphic history of the investigated rocks. This might also be related to the activity of fluids during these processes. The used models for formula calculation strongly depend on the estimation of Fe^{II}/Fe^{III}- ratios. Obviously, this topic needs to be addressed in more detail, which is out of the scope of this Master thesis and must be addressed in further investigations.

9 INTERPRETATION

9.1 Metamorphic and deformation history

Microscopic and chemical investigations confirm the four deformation phases inferred from field observations and show that the M1-HP metamorphism can be further subdivided. In **Tab. 7**, episodes of crystal growth and deformation are summarized, with respect to the different lithologies and the dominance of static or dynamic re-crystallization.

Static / dynamic		Event and characterisitc fabric elements						
	Episode	M1$_A$/M1$_B$	post-M1$_B$	M1$_C$	late to post-M1$_C$	M1$_D$	post - M1$_D$	post - M1$_D$
direction		?	fold axes NE-SW		relative movement top N to NE		?	NE-SW-compression, fold axes NW-SE
Lithology	Eclogite	main fabric static Jd+Grt+Gln1+Phe (+Ep?)	-	large Pg-crystals, Gln	veins of Qtz, Gln, Phn and Pg	-	-	-
	blueschist	relictic paragenesis in Grt: strong foliation Jd+Gln1+Grt+Ep1+Ph+Pg ±Cht+Qtz	folding	static growth of large porphyroblasts (Grt, Ep2, Gln2, Phn, Pg, Fe-Carbonate)	dominant foliation (matrix) Gln+Ep+Phn+Pg+Ab	static pseudomorphs of Chl after Grt	-	-
	light coloured Grt Gneiss	relictic paragenesis in Grt: strong foliation Jd+Gln1+Grt+Ep+Ph+Pg ±Cht+Qtz	folding	static growth of large porphyroblasts (Grt, Ep2, Gln2, Phn, Pg, Fe-Carbonate)	dominant foliation (matrix) Gln+Ep+Phn+Pg (+Ab)	static pseudomorphs of Chl after Grt	-	
	Ep-Ab-Chl-fels	first relictic foliation in Ep-porphyroblasts Gln1+Ep1	-	static growth of large porphyroblasts: Ep2 + Grt	second relictic foliation Gln+Phn	dominant fabric static blastic growth of Ep3, Ab and Chl	-	-
	Carbonate-rich metasediment	-	-	static growth of large porphyroblasts: Ep + Phn	dominant foliation, defined by Phn and Ep	dominant fabric static blastic growth Ab, Cal and Chl	-	-
	greenschist + Ab-gneiss	relictic fabric in Grt foliation Qtz+Ep1 (+Gln1?)	folding	static porphyroblastic growth of Ep2, Grt, Phn	foliation, defined by Phn, Ep, Gln	static pseudomorphs of Chl after Grt, Ab-blastesis	foliation, Ab as clasts, growth of Chl and Phn	asymetric crenulation cleavage, folding

Tab. 7: Summary: episodes of static and dynamic crystal growth with respect to the observed lithologies in the working area.

9.2 (Micro-) structural evolution and implications to the PT-path

Tab. 7 illustrates the alternation of deformation events and phases of widespread mineral growth under static conditions. This allows the assumption that changes in PT-conditions, obtained during substantial tectonic transport, are responsible for these observed re-equilibration processes. Especially the static dyctionitic grow of Grt and the later Ab-blastesis can be interpreted as strong indicators for re-equilibration after decompression.

No PT-estimates were obtained during this study, and therefore the results are discussed in context to similar structural observations of other authors with existing links to calculated PT-

conditions or chronological data: In **Fig. 50**, the observed episodes of Tab. Xx are plotted in the PT-diagram of published PT-paths (see chapter five, **Fig. 10**).
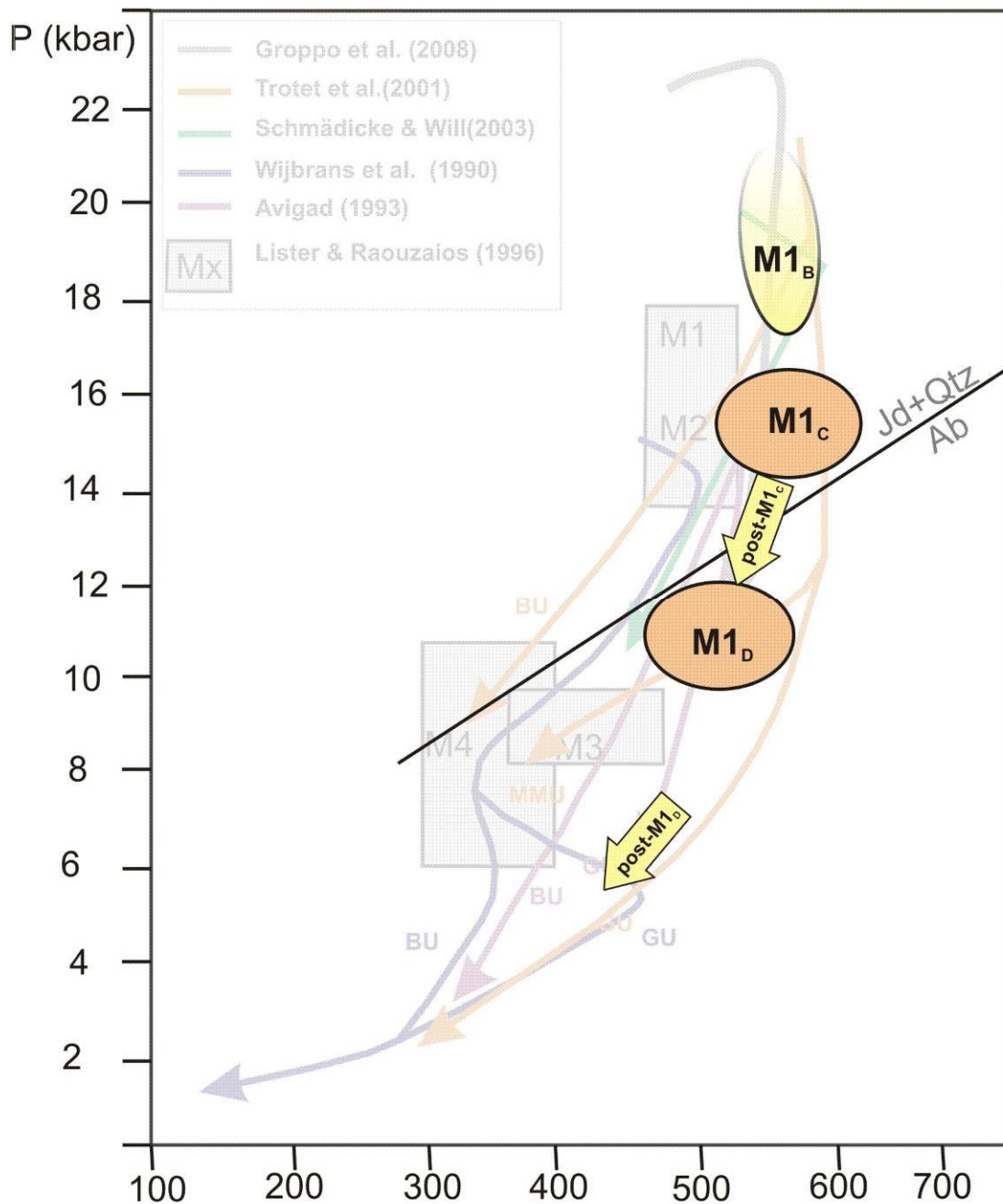
Fig. 50: Observed episodes of mineral growth of **Tab. 7**, plotted in the PT-diagram of published PT-paths

Groppo et al. (2008) applied this classification of HP-metamorphic events to the rocks of Vroulidia bay in northern Sifnos, and used P-T-pseudosections to constrain the PT-path (see chapter 4). Their results are comparable to the observations in this study.

Schmädicke and Will (2003) used samples of blueschist from Vroulidia bay in northern Sifnos to calculate petrogenetic grids (**Fig 51** shows the resulting diagram for their sample "Vrou-8"). They observed 3 to 4 stable mineral associations that are interpreted as a retrograde succession: (A) refers to the locally observed relictic prograde assemblage with Gln and Lws. The peak-assemblage Grt-Omp-Gln-Pg is represented by (B) and two re-equilibrated stages are (C) Omp replaced by Ep and (D) Grt replaced by Chl. These observations are comparable to the observations from southern Sifnos. Their derived PT-path is also given in **Fig.51**.
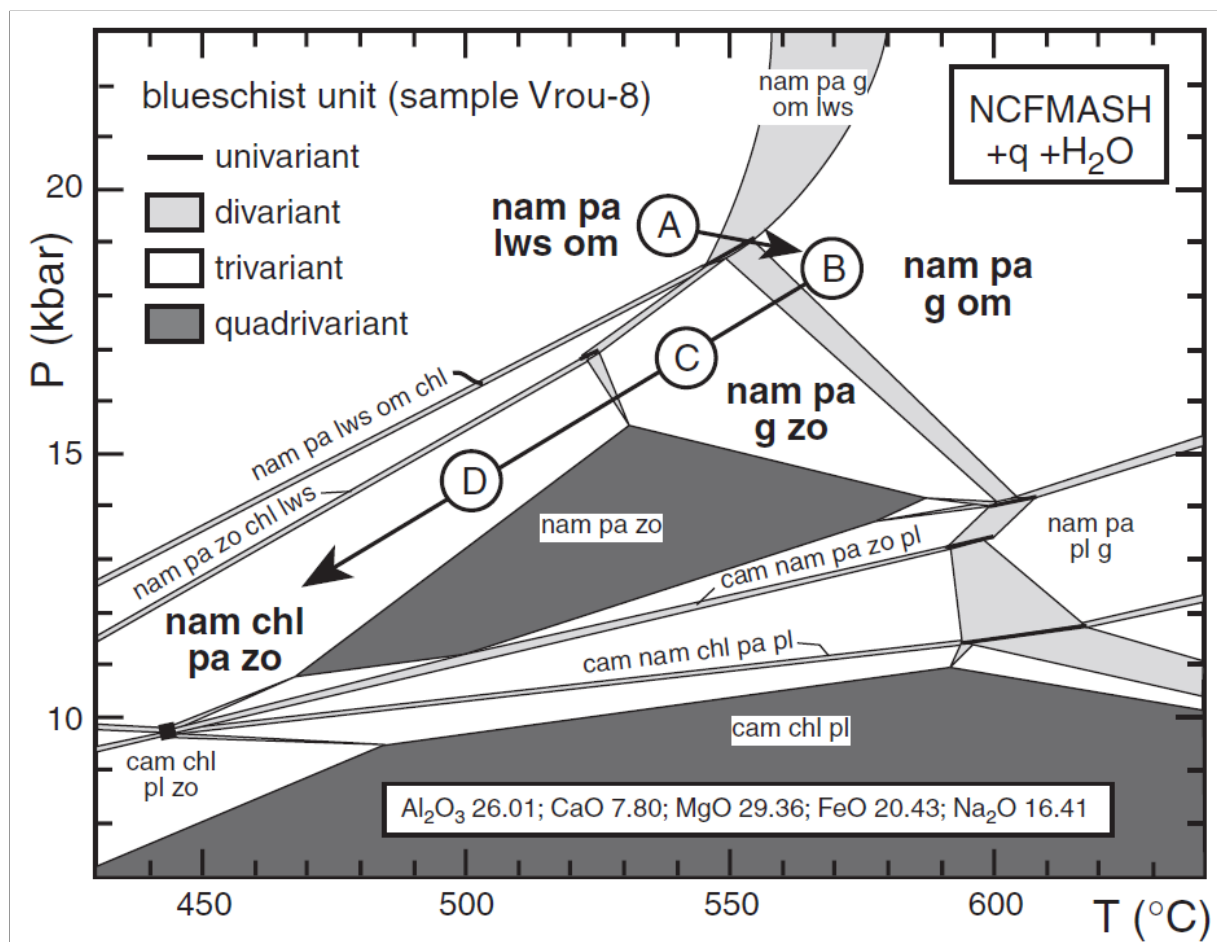
Fig. 51: From Schmädicke and Will (2003): Petrogenetic grid for blueschist-sample from Vroulidia bay, northern Sifnos, calculated on the basis of the complex phase diagram in the model system Na2O–CaO–FeO–MgO–l2O3-SiO2-H2O (NCFMASH), (Will et al., 1998),

10 DISCUSSION AND REGIONAL IMPLICATIONS

10.1 Exhumation

Forster and Lister (2005) estimated $^{40}Ar/^{39}Ar$ ages for exhumation in extensional shear zones after each of the HP events that have been correlated with the results obtained in this work. For the whole Cycladic Blueschist Unit, these data are:

post-M1$_B$ = 53–49 Ma; post-M1$_C$ = 44–38 Ma; post-M1$_D$ = 35–30 Ma

This is consistent with the age–data around 41 to 42 Ma by Altherr et al. (1979) and Wijbrans et al. (1990), assuming that K-Ar and Rb-Sr-systems were reset during the M1$_C$-event when the highest temperatures were reached.

Forster and Lister (2005) developed a geodynamic model ("tectonometamorphic slices") to explain the juxtaposition of units with different metamorphic record, assuming repeated tectonic inversion, with (in this order): Compression and thrusting during plate collision – switch into lithospheric extension, thrust becomes detachment – switch of tectonic mode to overall shortening, new thrusting – final exhumation of rocks in extensional setting.

Schmädicke and Will (2003) emphasize that extension-driven exhumation models must be excluded, because the calculated PT-paths suggest cooling during decompression. They consider buoyancy-driven models like a model proposed by Chemenda et al. (1996) to account for the exhumation of crustal material during active subduction with contemporaneous cooling. This model assumes that decoupled slivers of crustal material rise to mid-crustal levels, where buoyancy effects decline. Here, the rocks could be cooled by a) the subducting plate from below, and b) the base of the hanging wall, that has attained a low geothermal gradient due to a long period of ongoing subduction.

This transport to a mid-crustal level with a subsequent re-equilibration seems to be an explanation for observed structures of the M1$_D$–episode (porphyroblastic growth of minerals of the Ep-Ab-blueschist facies under static conditions, attributed to decompression).

Schmädicke and Will (2003), as well as Lister and Raouzaios (1996), correlate similar microstructural observations with the phases of exhumation. They state that the early stage of exhumation is "entirely unrelated to back-arc extension" (p.808). Similar conclusions are made by Ring et al. (2010). Schmädicke and Will (2003) explicate that HP units must have returned to mid-crustal levels before extension began (Oligocene-Miocene), maybe related to the start of underthrusting of the external blueschist-belt on Crete. They extrapolate their

derived PT-trajectory to the temperature of 360°C (closing temperature of Phn, Ar-Ar-ages of 42 – 29 Ma by Wijbrans et al. (1990) and state that the HP unit should have reached a depth of 15-20 km at ca. 30 Ma. Stöckhert et al (1999) suggested similar exhumation rates of > 4 mm/a for blueschists in Crete. The conclusion by Schmädicke and Will (2003), in agreement with Avigad et al. (1997) and Ring et al. (2003), is that extensional tectonics during crustal thinning and back-arc spreading is only responsible for the last part of the exhumation process. The already obtained high crustal level can be seen as a reason why the Barrovian-type metamorphism observed at other Cycladic islands at 23-15 Ma (Wijbrans & McDougall, 1988; Bröcker et al., 1993) had so little effect on Sifnos.

10.2   Greenschist-facies overprint and structural position

An overview of published interpretations concerning the varying degree of retrograde overprinting in BU and GU has already been given in chapter five.

In the studied area, the re-equilibration during exhumation is more advanced than in the rocks of northern Sifnos, for example no Jadeite-gneisses could be observed. The tectonostratigraphic base of the HP-silicate rock assemblage is not accessible, and the overprinting brittle tectonics disguise the original configuration of marbles and silicate rocks. The observed greenschist-facies overprinting and signs of fluid activity like new growth of Cal and Mag and hydration reactions are stronger towards the shear zone at the lithological contact to the marbles. Comparing the results of microstructural observations and the implications on the P-T-history of the studied rock unit, the inferred P-T-development can be best compared with those inferred from samples of blueschist-lenses in the MMU. As an example can be seen the second calculated PT-path of Trotet et al. (2001b). For these calculations, samples of similar structural positions (from the base of MMU and the top of GU) were used.

The position of the HP-rock assemblage inside the surrounding marble can be therefore be understood as a large boudin, which must have acted as a rigid body during the extensive ductile deformation associated with the exhumation. The mylonitic marbles and localized shear zones accommodated most of the strain at lower temperatures, so that the static fabrics, created in 20 to 30 km depth, could be preserved. The greenschist-facies overprint is related to ductile shear zones, which acted as fluid pathways, and later re-equilibration is controlled by the availability of fluids and deformation. Schmädicke and Will (2003) as well as Ring et al. (2010) come to similar conclusions, and propose that these deformation-related metamorphic equilibration stages do not reflect regional P-T "controlled" metamorphic events.

Matthews and Schliestedt (1984) and Schliestedt and Matthews (1987) report the infiltration of oxidized fluids with high $\delta^{18}O$, what they interpreted as one reason of retrograde overprinting. The influence of fluids and the fugacity of oxygen played an important role during retrograde metamorphic processes observed in the studied area, as the results of microprobe-investigations suggest. In all recent publications, authors agree that the influence or the availability of fluids is responsible to some extent for the more advanced retrograde re-equilibration in some rocks.

Another assumed causation is the varying influence of cooling mechanisms in the individual units, as the interpretation of Trotet et al. (2001b) suggests (the structural pile that is cooled from above, heat flow and possible fluids come from the bottom). Different duration of isothermal decompression can be explained by different crustal slices or slivers, that are decoupled from the subducting slab and juxtaposed during their exhumation to mid-crustal levels, where they formed what today is seen as the Cycladic Blueschist Unit (as described by Schmädicke and Will 2003). In their interpretation of the geological map of Sifnos, Trotet et al. (2001a) draw a low angle shear zone throughout the island (after Avigad 1993), separating the Main Marble Unit from the lower Greenschist Unit. This major shear zone could be confirmed neither during the field trip 2005 nor during the fieldwork for this study.
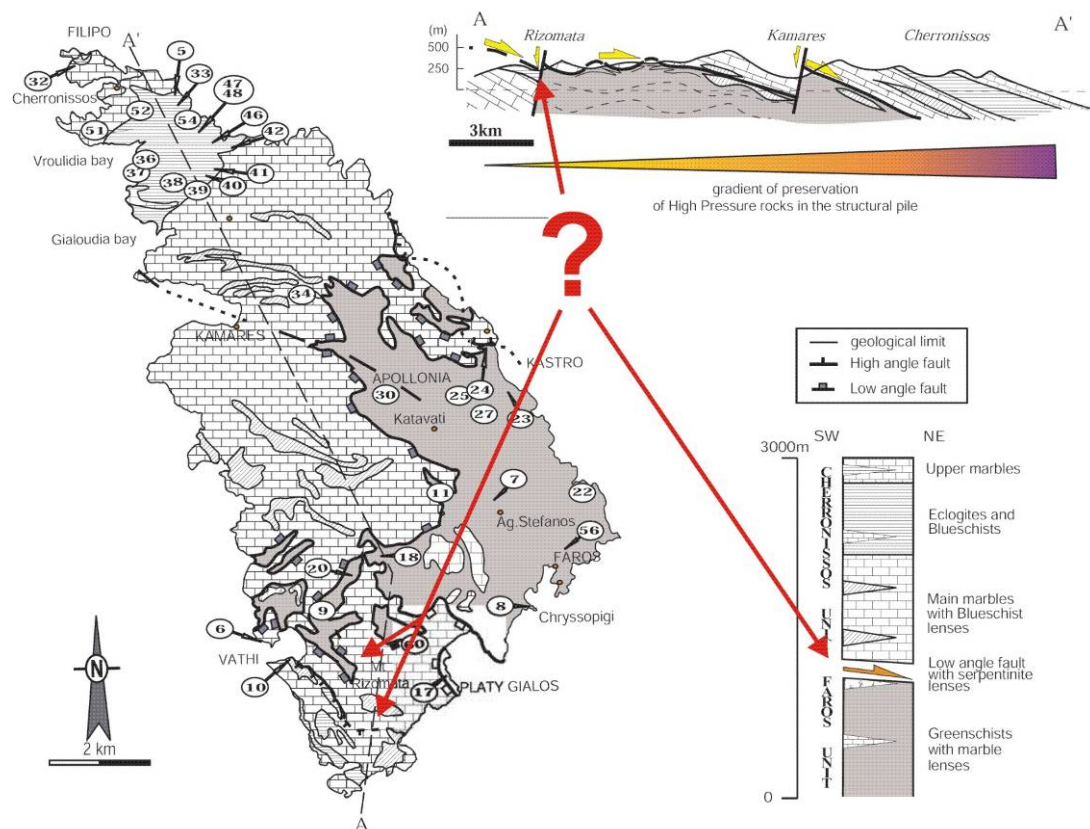
Fig. 52: Interpretation of the Geological map of Sifnos by Trotet et al. (2001a). MMU and GU separated by a low angle detachment fault, southern part of Sifnos displaced along high angle normal fault at Risomata.

Lithostratigraphically, the southern part of the island is seen as an equivalent to the marbles with lenses of blueschist further north. Trotet et al. (2001a) draw a separating high angle normal fault at *Ritsomata* Hill between Platy Gialos and Fikiada bay.

Leitner (1999) interprets the contact of marbles and micaschists north of the hill *Katsistria* as a large, south dipping normal fault, and the position of the HP-rock assemblage as he result of "down faulting" to SW of large blocks of the marble unit. He also describes the sinistral strike slip fault zone of the *Kontos*-trench as a reactivated normal fault.

No evidence of a major normal fault along *Katsistria* or *Ritsomata* Hill could be recognized in the field, and the satellite images suggest an undisturbed, coherent sequence of marble and schists between *Ritsomata* and Platy Gialos. The fault zone from *Kontos*-trench to *Tourkavlako* is corroborated by this study, and the striking direction is consistent with the NE-SW extension under brittle-ductile to brittle conditions observed in the working area. Therefore this fault zone can be interpreted as the normal fault responsible for the structurally low position of the HP-rock assemblage at Fikiada bay.

11 REFERENCES

Altherr, R., Schliestedt, M., Okrusch, M., Siedel, E., Kreuzer, H., Harre, W., Lenz, H., Wendt, I., Wagner, G.A. (1979), Geochronology of high-pressure rocks on Siphnos (Cyclades, Greece), Contributions to Mineralogy and Petrology, 70, 245–255

Altherr, R., Kreuzer, H., Wendt, I., Lenz, H., Wagner, G., Keller, J., Harre, W., Hoehndorf, A. (1982), A late Oligocene/early Miocene high temperature belt in the Attic-Cycladic crystalline complex (SE Pelagonian, Greece), Festschrift zum 75. Geburstag von Hans Closs; Festschrift for the 75th birthday of Hans Closs. Geologisches Jahrbuch, Reihe E: Geophysik, 23, 97–164

ANAVASI (2002),Topographic map of Sifnos, 1:25 000

Armijo, R., Meyer, B., Hubert, A., Barka, A. (1999), Westward propagation of the North Anatolian fault into the northern Aegean: Timing and kinematics, Geology, 27, 267-270

Armijo, R., Meyer, B., King, G., Rigo, A., Papanastassiou, D. (1996), Quaternary evolution of the Corinth rift and its implications for the late Cenozoic evolution of the Aegean, Geophysical Journal International, 126, 11–53

Avigad, D. (1993), Tectonic juxtaposition of blueschists and greenschists in Sifnos Island (Aegean Sea)—implications for the structure of the Cycladic blueschist belt, Journal of Structural Geology, 15, 1459–1469

Avigad, D., Garfunkel, Z. (1991), Uplift and exhumation of high-pressure metamorphic terrains: the example of the Cycladic blueschist belt (Aegean Sea), Tectonophysics, 188, 357-372

Avigad, D., Garfunkel, Z., Jolivet, L., Azanón, J. M. (1997), Back arc extension and denudation of Mediterranean eclogites, Tectonics, 16, 924–941

Becker, T.W. (2008), Azimuthal seismic anisotropy constrains net rotation of the Lithosphere, Geophysical Research Letters, 35, L05303. doi:10.1029/2007GL032928 (Correction:2008GL033946)

Bijwaard, H., Spakman, W., Engdahl, E.R. (1998), Closing the gap between global and regional mantle tomography, Journal of Geophysical Research, 103, 30055–30078

Bröcker, M., Kreuzer, H., Matthews, A., Okrusch, M. (1993), 40Ar∕39Ar and oxygen isotope studies of polymetamorphism from Tinos Island, Cycladic blueschist belt, Greece, Journal of Metamorphic Geology, 11, 223–240

Brun, J.P., Sokoutis, D. (2007), Kinematics of the Southern Rhodope Core Complex (North Greece), International Journal of Earth Sciences, doi:10.1007/s00531-007-0174-2

Buick, I.S. (1991), The late Alpine evolution of an extensional shear zone, Naxos, Greece, Journal of the Geological Society, London, 148, 93–103

Chéry. J. (2001), Core complex mechanics: From the Gulf of Corinth to the Snake Range, Geology, 439-442

Cloos, M., Shreve, R.L. (1988), Subduction-channel model of prism accretion, mélange formation, sediment subduction, and subduction erosion at convergent plate margins; part II, Implications and discussion, Pure and applied Geophysics, 128, 501-545

Cowan, D. S. & Silling, R. M. (1978), A dynamic scaled model of accretion at trenches and its implication for the tectonic evolution of subduction complexes, Journal of Geophysical Research, 83, 5389-5396

Davis, E. N. (1966), Der geologische Bau der Insel Siphnos (in Greek with German summary). Institute for Geology and Subsurface Research, Athens. Geological and Geophysical Research, 10, 161–220

Davis, E.N. (1972) Geological map of Kea, 1:50,000. Map of Greece. Geological Survey of Greece, Athens

De Sigoyer, J., Guillot, S., Dick, P. (2004), Exhumation of the ultrahigh-pressure Tso Morari Uni in eastern Ladakh (NW Himalaya); a case study, Tectonics, 23, 18pp

Ernst, W.G. (1993), Metamorphism of Franciscan tectonostratigraphic assemblage, Pacheco Pass area, east-central Diablo Range, California Coast Ranges; with Suppl. Data 9307, Geological Society of America Bulletin, 105, 618-636

Evans, B.W. (1986), Reactions among sodic, calcic, and ferromagnesian amphiboles, sodic pyroxene, and deerite in high-pressure metamorphosed ironstone, Sifnos, Greece, American Mineralogist, 71, 1118–1125

Forster, M. A., Lister, G. S. (1999), Detachment faults in the Aegean core complex of Ios, Cyclades, Greece. In: Exhumation Processes: Normal Faulting, Ductile Flow and Erosion (eds Ring, U., Brandon, M. T., Lister, G. S. & Willet, S. D.) Geological Society, London, Special Publications, 305-323

Forster, M. A., Lister, G. S. (2005), Several distinct tectono-metamorphic slices in the Cycladic eclogite-blueschist belt, Greece, Contributions to Mineralogy and Petrology, 150, 523-545

Forster, M.A., Lister, G. (2009), Core-complex-related extension of the Aegean lithosphere initiated at the Eocene-Oligocene transition, Journal of Geophysical Research, 114, doi:10.1029/2007JB005382

Fytikas, M., Innocenti, F., Manetti, P., Peccerillo, A., Mazzuoli, R., Villari, L. (1984), Tertiary to Quarternary evolution of volcanism in the Aegean region, Geological Society, London, Special Publications, 17, 687-699

Gautier, P., Brun, J.P. (1994), Ductile crust exhumation and extensional detachments in the central Aegean (Cyclades and Evvia islands), Geodinamica Acta, 7, 57–85

Gautier, P., Brun, J.-P., Moriceau, R., Sokoutis, D.,Martinod, J., Jolivet, L. (2001), Timing, kinematics and cause of Aegean extension: a scenario based on a comparison with simple analogue experiments, Earth and Planetary Science Letters, 187, 95-104

Gerya, T., Stoeckhert, B., Perchuk, A. (2002), Exhumation of high-pressure metamorphic rocks in a subduction channel: a numerical simulation, Tectonics, 21, 19pp

Grasemann, B., Petrakakis, K. (2007), Evolution of the Serifos Metamorphic Core Complex. In: Lister, G., Forster, M., Ring, U. (Eds.), Inside the Aegean Metamorphic Core Complexes. Journal of the Virtual Explorer, 28, 2

Groppo, C., Forster, M., Lister, G., Compagnoni, R. (2009), Glaucophane schists and associated rocks from Sifnos (Cyclades, Greece): New constraints in the P-T evolution from oxidized systems, Lithos, 109, 254-273

Huet, B., Labrousse, L. c. & Jolivet, L. (2009), Thrust or detachment? Exhumation processes in the Aegean: Insight from a field study on Ios (Cyclades, Greece), Tectonics, 28

Iglseder, C., Grasemann, B., Schneider, D., Rice, A.H.N., Lenauer, I., Müller, M., Mörtl, G., Voit, K., Petrakakis, K., Draganits, E. (2008), Low-angle normal fault mechanics and architecture in the Western Cyclades (Greece), Geophysical Research Abstracts, EGU General Assembly 2008, 10, 07793

Iglseder, C., Grasemann, B., Schneider, D.A., Petrakakis, K., Miller, C., Klötzli, U.S., Thöni, M., Zámolyi, A., Rambousek, C. (2009), I and S-type plutonism on Serifos (W-Cyclades, Greece), Tectonophysics, 473, 69-83

Jacobshagen, V. (1986), Geologie von Griechenland. Borntraeger, Berlin

Jolivet, L., Brun, J.P. (2008), Cenozoic geodynamic evolution of the Aegean region, International Journal of Earth Sciences doi:10.1007/s00531-008-0366-4

Jolivet, L., Faccenna, C., Goffé, B., Burov, E., Agard, P. (2003), Subduction tectonics and exhumation of high-pressure metamorphic rocks in the Mediterranean orogens, American Journal of Science, 303, 353-409

Jolivet, L., Faccenna, C., Goffe, B., Burov, E.,Agard, P. (2003), Subduction tectonics and exhumation of high pressure metamorphic rocks in the Mediterranean orogens, American Journal of Science, 303, 353-409

Jolivet, L., Lecomte, E., Huet, B., Denèle, Y., Lacomb, O., Labrousse, L., Le Pourhie, L., Mehl, C. (2010), The North Cycladic Detachment System, Earth and Planetary Science Letters, 289, 87-104

Katzir, Y., Matthews, A., Garfunkel, Z., Schliestedt, M. & Avigad, D. (1996), The tectono-metamorphic evolution of a dismembered ophiolite (Tinos, Cyclades, Greece), Geological Magazine, 133, 237-254

Leitner, C. (1990), Exhumation history of Blueschists: Southern Sifnos (Cyclades, Greece), Diploma Thesis, Naturwissenschaftliche Universität Salzburg

Lister, G. S., Banga, G. and Feenstra, A. (1984), Metamorphic core complexes of Cordilleran type in the Cyclades, Aegean Sea, Greece, Geology, 12, 221-225

Lister, G. S., Raouzaios, A., (1996), The tectonic significance of a porphyroblastic blueschist facies overprint during Alpine orogenesis, Sifnos, Aegean Sea, Greece, Journal of Structural Geology, 18, 1417–1435.

Matthews, A., Schliestedt, M. (1984), Evolution of the blueschist and greenschist facies rocks of Sifnos, Cyclades, Greece, Contributions to Mineralogy and Petrology, 88, 150-163

McClusky, S., Balassanian, S., Barka, A., Demir, C., Ergintav, S., Georgiev, I., Gurkan, O., Hamburger, M., Hurst, K., Kahle, H., Kastens, K., Kekelidze, G., King, R., Kotzev, V., Lenk, O., Mahmoud, S., Mishin, A., Nadariya, M., Ouzounis, A., Paradissis, D., Peter, Y., Prilepin, M., Reilinger, R., Sanli, I., Seeger, H., Tealeb, A., Toksöz, M.N., Veis, G. (2000), Global Positioning System constraints on plate kinematics and dynamics in the eastern Mediterranean and Caukasus, Journal of Geophysical Research, 105, 5695-5719

McClusky, S., Reilinger, R., Mahmoud, S., Ben Sari, D., Tealeb, A., (2003), GPS constraints on Africa (Nubia) and Arabia plate motions, Geophysical Journal International, 155, 126-138

Mocek, B. (2001), Geochemical evidence for arc-type volcanism in the Aegean Sea: the blueschist unit of Sifnos, Cyclades (Greece), Lithos, 57, 263-289

Oberhänsli, R., Partzsch, J., Candan, O., Cetinkaplan, M. (2001), First occurrence of Fe-Mg-carpholite documenting a high-pressure metamorphism in metasediments of the Lycian Nappes, SW Turkey, International Journal of Earth Sciences, 89, 867-873

Okrusch, M., Bröcker, M. (1990), Eclogites associated with high-grade blueschists in the Cyclades archipelago, Greece; a review, European Journal of Mineralogy, 2, 451–478

Okrusch, M., Seidel, E., Davis, E.N. (1978), The assemblage jadeite-quartz in the glaucophane rocks of Sifnos (Cycladic Archipelago, Greece), Neues Jahrbuch für Mineralogie Abhandlungen 132, 284–308

Papanikolaou D, Barghathi H, Dabovski C, Dimitriu R, El-Hawat A, Ioane D et al (2004), TRANSMED Transect VII: East European Craton–Scythian–Platform–Dobrogea–Balkanides–Rhodope Massif–Hellenides–East Mediterranean–Cyrenaica. In: Cavazza, W. et al. (eds) The TRANSMED Atlas—the Mediterranean region from crust to Mantle. Springer, Berlin

Papanikolaou, D. (2007), Timing of tectonic emplacement of the ophiolites and terrane paleogeography in the Hellenides, Lithos, 108, 262-280

Pelikan, A. (1902), Pseudomorphose von Magnetit und Rutil nach Ilmenit, Zeitschrift für Kristallographie, Mineralogie und Petrographie, Wien, 21, No.3

Petrakakis, K., Dietrich, H. (1985), MINSORT; a program for the processing and archivation of microprobe analyses of silicate and oxide minerals, Neues Jahrbuch fuer Mineralogie. Monatshefte, 1985(8), 379-384

Platt, J.P. (1986), Dynamics of orogenic wedges and the uplift of high-pressure metamorphic rocks, Geological Society of America Bulletin, 97, 1037–1053

Platt, J.P. (1993), Exhumation of high-pressure rocks: a review of concept and processes, Terra Nova, 5, 119–133

Ridley, J., (1984), The significance of deformation associated with blueschist facies metamorphism on the Aegean island of Syros. In: Dixon, J.E., Robertson, A.H.F., (eds.), The Geological Evolution of the Eastern Mediterranean. Geological Society Special Publications. Blackwell Scientific Publications, Boston, 545–550

Rice, A. H. N., Iglseder C., Grasemann, B., Schneider, D., Weil, J., Rockenschaub , M. (2009), Tectonic evolution of bi-directional extension in the W. Cyclades, Geophysical Research Abstracts, Vol. 11, EGU2009-9168, 2009

Ring, U., Brandon, M.T., Willett, S.D., Lister, G.S. (1999), Exhumation processes. In: Ring, U. et al (eds) Exhumation processes: normal faulting, ductile flow and erosion, 1–27, Geological Society, Special Publication, London, 154,1–27

Ring, U., Layer, P.W. (2003), High-pressure metamorphism in the Aegean, eastern Mediterranean: underplating and exhumation from the Late Cretaceous until the Miocene to Recent above the retreating Hellenic subduction zone, Tectonics, 22, doi:10.1029/2001TC001350

Ring, U., Kumerics, C. (2008), Vertical ductile thinning and its contribution to the exhumation of high-pressure rocks: the Cycladic blueschist unit in the Aegean, Journal of the Geological Society, 165, 1019-1030

Ring, U., Glodny, J. (2010), No need for lithospheric extension for exhuming (U)HP rocks by normal faulting, Journal of the Geological Society, 167, 225-228

Ring, U., Glodny, J., Will, T. & Thomson, S. (2010), The Hellenic Subduction System: High-Pressure Metamorphism, Exhumation, Normal Faulting, and Large-Scale Extension. Annual Review of Earth and Planetary Sciences, 38, 45-76

Schliestedt, M., and Matthews, A. (1987), Transformation of blueschist to greenschist facies rocks as a consequence of fluid infiltration, Sifnos (Cyclades), Greece, Contributions to Mineralogy and Petrology, 97, 237–250

Schliestedt, M., Okrusch, M. (1988), Meta-acidites and silicic meta-sediments related to eclogites and glaucophanites in northern Sifnos, Cycladic Archipelago,Greece. In "Eclogites and eclogite-facies rocks. Developments in Petrology", D. C. Smith, (ed) Elsevier, Amsterdam, 291-334

Schmädicke, E., Will, T.M. (2003), Pressure–temperature evolution of blueschist facies rocks from Sifnos, Greece, and implications for the exhumation of high-pressure rocks in the Central Aegean, Journal of Metamorphic Geology, 21, 799-811

Sengör, A.M.C., (1985), Die Alpiden und die Kimmeriden: die verdoppelte Geschichte der Tethys. Geologische Rundschau, 74, 181–213

Skourtsos, E., Kranis, H. (2009), Structure and evolution of the western Corinth Rift, through new field data from the Northern Peloponnesus, Geological Society, London, Special Publications, 321, 119-138

Stampfli, G.M., Borel, G.D. (2002), A plate tectonic model for the Paleozoic and Mesozoic constrained by dynamic plate boundaries and restored synthetic oceanic isochrons, Earth and Planetary Science Letters, 196, 17-33

Stöckhert, B., Wachmann, M., Küster, M., Bimmermann, S. (1999), Low effective viscosity during high pressure metamorphism due to dissolution precipitation creep: the record of HP-LT metamorphic carbonates and siliciclastic rocks from Crete, Tectonophysics, 303, 299–319

Tirel, C., Gueydan, F., Tiberi, C., Brun, J.P. (2004), Aegean crustal thickness inferred from gravity inversion. Geodynamical implications, Earth Planet Science Letters, 228, 267–280

Trotet, F., Jolivet, L., Vidal, O. (2001a), Tectono-metamorphic evolution of Syros and Sifnos islands (Cyclades, Greece), Tectonophysics, 338,179–206

Trotet, F., Vidal, O., Jolivet, L. (2001b), Exhumation of Syros and Sifnos metamorphic rocks (Cyclades, Greece). New constraints on the P-T paths, European Journal of Mineralogy, 13, 901–920

Tschegg, C. and Grasemann, B. (2009), Deformation and alteration of a granodiorite during low-angle normal faulting (Serifos, Greece), Lithosphere, 3, 139-154

van der Maar, P.A., Jansen, J.B.H. (1983), The geology of the polymetamorphic complex of Ios, Cyclades, Greece and its significance for the Cycladic Massif, Geologische Rundschau, 72, 283-299

van Hinsbergen, D. J. J., Hafkenscheid, E., Spakman, W., Meulenkamp, J. E. & Wortel, R. (2005), Nappe stacking resulting from subduction of oceanic and continental lithosphere below Greece, Geology, 33, 325-328

Vigner, A., (2002), Images sismiques par réflexions verticales et grandangle de la croute en contexte extensif: les Cyclades et le Fossé Nord-Egéen. Thèse de doctorat, Institut de Physique du Globe, Paris, pp 269

Villa, I.M. (1998), Isotopic closure, Terra Nova, 10, 42-47

Wernicke, B. (1981), Low-angle normal faults in the Basin and Range province: nappe tectonics in an extending orogen, Nature, 291, 645–648

Wernicke, B. (1992), Cenozoic extensional tectonics of the US cordillera. In: Burchfiel, B.C. et al (eds) The Cordilleran Orogen: conterminous US G3. Geological Society of America, Boulder, 553–581

Wijbrans. J. R., van Wees. J. D.. Steohenson. R. A. & Cloetingh, S. A., Lister, G. S. and Baldwin, S. L. (1996), Modelling the effect of arbitrary P-T-t histories on argon diffusion in minerals using the MacArgon P. L. (1993), Pressur+temperatur&me evolution of the high pressure program for the Apple Macintosh, Tectonophysics, 53, 83-109

Wijbrans, J. R., McDougall, I. (1986), 40Ar/39A dating of white micas from an Alpine high-pressure metamorphic belt on Naxos (Greece); the resetting of the argon isotopic system, Contributions to Mineralogy and Petrology, 93, 187-194

Wijbrans, J. R., McDougall, I. (1988), Metamorphic evolution of the Attic Cycladic metamorphic belt on Naxos (Cyclades, Greece) utilising 40Ar/39Ar age spectrum measurements, Journal of Metamorphic Geology, 6, 571-594

Wijbrans, J. R., Schliestedt, M., York, D. (1990), Single grain argon laser probe dating of phengites from the blueschist to greenschist transition on Sifnos (Cyclades, Greece), Contributions to Mineralogy and Petrology, 104, 582-594

Yamato, P., Agard, P., Burov, E., Le Pourhiet, L., Jolivet, L., Tiberi, C. (2007), Burial and exhumation in a subduction wedge: mutual constraints from thermomechanical modeling and natural P-T-t data (Sch. Lustre´s, W. Alps), Journal of Geophysical Research, 112, B07410. doi:07410.01029/02006JB004441

12   APPENDIX

12.1   Geological map of southern Sifnos, regional

## 12.2   Geological map of the working area around Fikiada bay

12.3   Sample list

Sample No.	Lithology	Coordinates (UTM zone 34)		Orientation			Thin sections		
		North	East	Foliation	Lineation	Joint	20µm	45µm, pol.	sample No.
SIF05/03	Ep-Ab-Chl-fels	4086905	295473	-			1	1	SIF05/03
SIF05/04	volc. Dyke	4086941	295539	-			1		SIF05/04
SIF05/05	BS	4086898	295451	-			1		SIF05/05
SIF05/06	LGG	4086901	295445	-			1		SIF05/06
SIF05/07	Eclogite	4086902	295422	-			1	1	SIF05/07
SIF05/08	Marble	4087212	295356	-			1		SIF05/08
SIF009	Ep-boudin (BS)	4086895	295424	-			1		SIF009/1+2 R
SIF010A	LGG	4086932	295498	-			2		SIF010A/1+2 R
SIF010B	LGG	4086932	295498	-			1		SIF010B R
SIF010C	LGG	4086932	295498	-			1		SIF010C R
SIF011	BS overprinted	4086932	295498	-			1		SIF011 R
SIF012A	LGG	4086909	295432	134/20			4	2	SIF012A/1+2+3+4
SIF012B	LGG	4086909	295432	134/20			2		SIF 012B/1+2
SIF013A	BS	4086895	295424	182/20			2	1	SIF013A1+2
SIF013B	BS	4086895	295424	178/27				2	SIF013B1+2+3+4+5
SIF014	LGG	4087078	295366	032/35		238/53	1		SIF014
SIF015A	Carbonated-bearing	4087088	295433	-			1		SIF015A R
SIF015B	Metasediment	4087088	295433	-			1		SIF015B R
SIF016	Ep-Ab-Chl-fels shear zone	4086783	295786	274/14	290/12				SIF016
SIF017A	Greenschist/Ab-gneiss	4088308	296938	034/5x			1	2	SIF017A
SIF017B	Greenschist	4088308	296938	036/45					
SIF017C	Greenschist/Ab-gneiss	4088308	296938	034/50			2		SIF017C/1+2
SIF018	Metaconglomerate	4088373	297016	050/30	072/31		1		SIF018
SIF019	mylonitic Marble	4087120	295386	040/34					SIF019
SIF020	Ep-Ab-Chl-fels	4086909	295432	120/30			1	1	SIF020
SIF021A	Ep-Ab-Chl-fels	4086909	295432	-			1		SIF021A R
SIF021B	Ep-Ab-Chl-fels	4086909	295432	-					
SIF022A	Metabasit	4086834	295845			144/68	1		SIF022A
SIF022B	Marble	4086834	295845	122/15			1		
SIF023	Quartzite	4086729	595678	182/52	130/57	067/52	1		SIF023
SIF024	LGG	4086729	595678	183/56			1		SIF024
SIF025	Qtz-vein (BS)	4086904	295432	062/21	358/09		1		SIF025
SIF026	Dol-Cataklasite	4086829	295236				1		SIF026
SIF027	Quaternary Cal-cement	4086748	295173	-			1		SIF027
SIF028A	Qtz-vein with Mag	4086407	295417	-					
SIF028B	Qtz-vein with Mag	4086407	295417	-					
SIF029	Dol-Cataklasite	4086645	295553			270/72	2		SIF029/1+2
SIF030	mylonitic Marble, dolomitised	4086953	295569		025/80		2		SIF 030
DOL1	Dolomite	4086840	295789	-					
DOL2	mylonitic Marble, dolomitised	4087096	295592	-					
DOL3	Dolomite			-					
DOL4	Dolomite			-					
DOL5	mylonitic Marble, dolomitised	4086892	295880	-			1		DOL5
DOL6	mylonitic Dolomite	4086830	295769	-			1		DOL6
DOL7	mylonitic Marble, dolomitised	4087065	295199	-					
DOL8	mylonitic Marble, dolomitised	4087095	295191	-					
DOL9	mylonitic Marble, dolomitised	4087102	295210	-					
DOL10	mylonitic Marble, dolomitised	4087259	294864	-			1		DOL10

Tab. A1: List of samples and thin sections from southern Sifnos, taken in the course of this study

12.4   Map sample localities
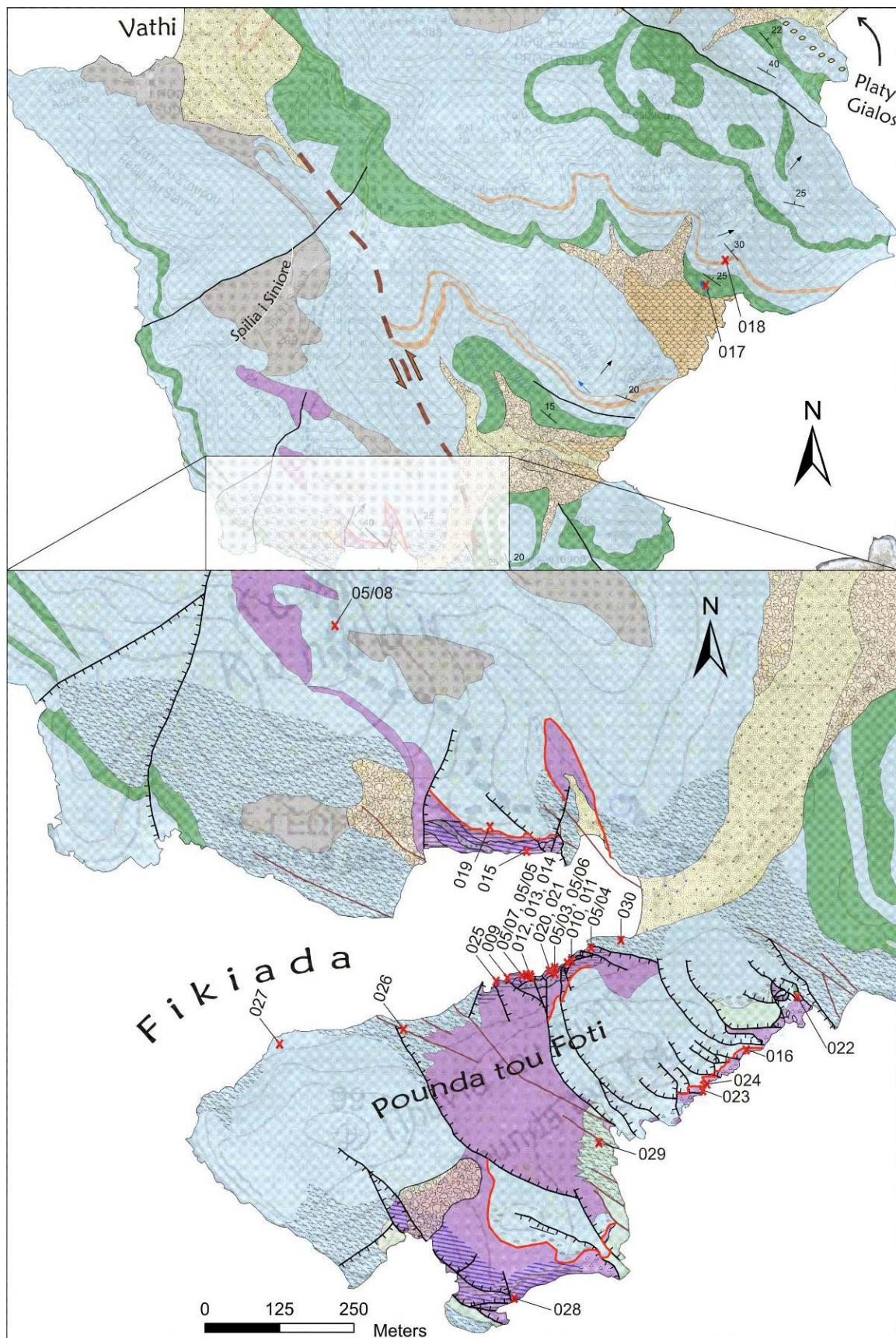
Fig. A1: Locations of samples in geological map (SIF+number in map). Coordinates are listed in **Tab. A1**

LEBENSLAUF

Persönliche Daten

Name	Jonas Weil
Anschrift	Lorbeergasse 2/8a,
	1030 Wien
	Österreich
Geburtsdatum	29.08.1983 in Frankfurt/Main
Familienstand	ledig
Staatsangehörigkeit	deutsch

Berufserfahrung

Seit Januar 2007
(Unterbrechung wegen
Auslandsaufenthalt von Februar
bis Juni 2008)

IBF Faustmann KG,
Freier Mitarbeiter

Lorystraße 134/1/20, 1110 Wien, Österreich
Tel: 0043 19434959

Flache Geothermie/Grundwasserwärme,
Brunnenbau, Hydrogeologische und Thermische
Grundwassermodellierung,
Altlastensanierung

März 2008 bis April 2008

CBH Resources Limited
Mining geologist

2 Elizabeth Plaza
North Sydney NSW 2060, Australia
eingesetzt bei

Endeavor Operations Pty Ltd,
via Louth Road, Cobar NSW 2835, Australia

Undergound mapping. core logging, Interpretation
von Levelplänen und Profilen, Datenverarbeitung
mit VULCAN 3D

September 2003 – Juni 2004	**Lebenshilfe Limburg gGmbH,** Zivildienst Wiesbadener Straße 15, 65549 Limburg

Ausbildung

Seit März 2008	**Masterstudium Erdwissenschaften** Universität Wien, Österreich, Studienrichtung Geologie Voraussichtlicher Abschluss: Juni 2010
September 2005 – Januar 2008	**Bakkalaureatsstudium Erdwissenschaften** Universität Wien Mit Auszeichnung bestanden am 29.01.2008
September 2004 – Juli 2005	**Bachelorstudium Geowissenschaften** Ruhr Universität Bochum
Juni 2003	**Abitur** an der Taunusschule in Bad Camberg, Abschlussnote: 1,5

Weitere Qualifikationen

Sprachen

- Englisch verhandlungssicher
- Französisch Grundkenntnisse
- Spanisch Grundkenntnisse

Führerschein Klasse B

Software

- Sicherer Umgang
- AutoCAD,
- ArcGIS,M
- MS Office
- GoCAD
-
- Numerische Modellierung
- MODFLOW
- FeFLOW,
- SHEMAT
- EED (Dimensionierung von Erdwärmeanlagen)

- Grundkenntisse
- PhreeqC
- MatLab

Wien, 08.06.2010